Hydrokinetic Turbine Systems for Remote River Applications in Cold Climates

By

John Woods

A Thesis submitted to the Faculty of Graduate Studies of
The University of Manitoba
In partial fulfilment of the requirement of the degree of

Doctor of Philosophy

Department of Mechanical and Manufacturing Engineering
The University of Manitoba
Winnipeg, Manitoba

Abstract

In-situ testing of hydrokinetic river turbines demonstrates the feasibility of installing these turbines in cold climates and at remote communities without significant infrastructure requirements. Complete water-to-wire systems are deployed, tested in winter conditions and retrieved with major aspects of the technology investigated. A robust river-bottom anchoring system is developed and tested suitable for remote community applications with minimal infrastructure. Vertical-axis 5-kW and 25-kW hydrokinetic turbines are deployed and tested in the Winnipeg River, under various climatic and flow conditions: -36ºC to 30ºC and 2.0 m/s to 2.6 m/s. Winter testing reveals that frazil ice accumulates on devices near the water surface, ice forms at the air-water interface, and ice sheets flowing with the stream can impact near-surface components. These factors lead to the conclusion that for low-maintenance and reliable year-round deployment in cold climates, systems must be fully submerged and removed if major ice floes occur. Hydrokinetic turbine generated power is delivered to a utility 12.47-kV overhead distribution line through pole-top transformers and bi-directional electricity meters, establishing a remote community water-to-wire system for the first time. Commercially available rectifier/inverters, developed for use in wind and solar energy capture, are successfully integrated into the power conversion system for the 5-kW and 25-kW units, simplifying development and reducing costs. A power conversion design is developed and tested. Concurrent measurement of river flow and turbulence with electrical power output from the permanent magnet generator are obtained in-situ. This data is used to investigate power production fluctuations resulting from turbulence in the flow. Turbulence is evaluated in detail, using time domain and frequency domain analysis. Calculated turbulence length scales varied from 0.7 m to 1.2 m, which are in the order of magnitude for the physical rotor elements. The results show that power extraction is maintained in the presence of moderate to high levels of turbulence in the range of 4% to 5% and that such level can improve energy capture. These studies indicate that hydrokinetic turbine systems can provide reliable power for both micro-grids and base-load applications in remote communities located in cold climates if placed below the water surface and not impacted by river ice floes.

Acknowledgement

Many thanks to Dr. Bibeau. Without his drive and dedication to renewable energy, this thesis and many others, would not have been possible. The other committee members: Dr. Gole, Dr. Kuhn and Dr. Rajapakse deserve thanks for their patience and oversight. Thanks also to Dr. Birjandi and Dr. Mossalat for their collaboration and willingness to share their knowledge. The technicians at the University of Manitoba, and in particular Mr. Erwin Dirks, assisted greatly in building the necessary hardware. Manitoba Hydro provided the initial funding for this endeavor and specific thanks are due to Tom Molinski and Randy Wachal for their support and guidance. Equipment operators at Point du Bois assisted in moving heavy loads on site. Many thanks are also due to New Energy Corporation Inc. and their capable field staff, all of whom contributed greatly to this research. Additional funding was provided by NSERC, Western Economic Development, and CEATI. Finally, special thanks to my dear family, Catherine and Wolf, for their patience and support.

Table of Contents

List of tables

List of figures

1. Introduction

Whereas traditional hydroelectric generation on rivers require dams or lengthy penstocks to develop or access sufficient potential energy, hydrokinetic turbines covert the existing kinetic energy in the flowing water directly without additional containment or re-direction structures.

1.1 Research needs in marine energy

In-situ tests are required to support the emerging marine renewable industry to demonstrate the deployment and operations of hydrokinetic turbine systems water-to-wire, particularly those applications related to rivers in cold climates.

The relevancy of in-situ testing of hydrokinetic turbines is to improve the capture of energy from naturally occurring renewable sources and de-risk this industry. However, other reasons for developing cost-effective hydrokinetic power systems include their immediate use for off-grid applications for mining and remote and/or less privileged communities. In addition, there is the growing interest in distributed generation of electricity to supply expanding markets, reduce losses in transmission and assist in the modernization of the electricity "grid" to make it less vulnerable to large-scale blackouts [1]. Other than the issue of icing addressed in this thesis, results are applicable to remote community electrification programs worldwide.

1.2 Hydrokinetic energy

The mass flow in moving water, with practical velocities of 2 to 3 m/s, results in energy intensities of 4 to 13.5 kW/m^2 suitable for base load generation applications. The two main sources of flowing water for marine hydrokinetic turbine power production are rivers and ocean tidal.

Canada has the longest coastline of any country in the world, and river drainage basins of more than 10 million square kilometers [2]. An estimated 2 GW of hydrokinetic energy is

available from these sources [3]. More than half of the rivers drain to the Arctic or far north, therefore an understanding of the cold-weather aspects is essential to harnessing significant amounts of this energy resource. The physical devices used to capture energy and convert power to a suitable electrical supply are conceptually similar for both river and marine flows. Figure 1 shows the installation of a 25-kW vertical-axis hydrokinetic turbine in a Canadian river, connected to the Manitoba Hydro grid as part of the in-situ testing requirements to achieve research objectives.

(a) (b)

Figure 1: Testing a 25-kW New Energy vertical-axis turbine at Point du Bois at flow velocity of 2.4 m/s: (a) system deployed and grid connected, and (b) rotor shown pivoted out of the water pre-deployment.

However, the following differences result in different operational requirements and deployment strategies:

- Marine environment relies on the tide, which creates flow in two directions, cycling twice per day.
- At suitable locations, river applications represent a nearly consistent flow 24 hours a day, with variation from season to season.
- The physical depth of most in-land rivers is considerably less than the marine energy locations, resulting in devices of different scale.
- Deployment methods are dependent on locations, scales and available infrastructure.

- Ice issues are prevalent for river applications while for ocean applications storms and high waves affect the technology.
- Deployment in rivers must be performed at full flow unlike tidal applications that may have as long as one hour of slack tide to perform deployment operations.

1.3 Hydrokinetic research requirements

Although there are efforts to optimize turbine components like the rotor efficiency [4], [5], [6], such research has little impact on the implementation of this emerging renewable energy technology in remote communities in cold climates. A 25-kW unit operating at a capacity factor of 60% will generate $19,710 per year with a $0.15 per kWh power purchase agreement so efficiency improvements of a few percent have minimal impact on the levelized cost of electricity. Research needs to be focused instead on reducing water-to-wire costs and increased turbine availability over the lifetime of the turbine to counteract low yearly revenues. There is a strong need expressed by marine energy stakeholders to demonstrate if these devices can operate successfully in river environments in cold climates and compete with alternatives [7], [8]. There is limited water-to-wire testing reported in the literature and none in cold climates to assist in understanding the impact of ice formation.

Moreover, there are limited measurements reported in the literature on turbines tested water-to-wire while measuring the flow variations simultaneously with the output of the turbine generator. As there are yet no valid procedures to scale highly-energetic turbine river sites' turbulence and length scales in water tunnels to perform such experiments; in-situ testing remains the best approach. Such data is required to assist in the design of turbines water-to-wire to reduce costs, more accurately specify power electronic requirements, contribute to turbine sighting, and predict the effects of turbulence on turbine power conversion.

1.4 Research objectives

The research seeks to demonstrate hydrokinetic turbines water-to-wire in cold weather river environments to provide evidence that this is a suitable technology for renewable energy distributed applications in remote communities. Specific objectives are to:

1. Evaluate the suitability for this technology for cold Canadian river applications
    - Assess how this technology could be implemented for remote communities using local and low cost infrastructure.
    - Develop an understanding how best to grid connect these devices in remote locations.
    - Document how winter conditions impact this technology.

2. Measure and document the interaction between flow variations and turbine electrical components including the power converters
    - Measure the length scales of the flow and their relative sizes with respect to the turbine physical dimensions.
    - Analyze the impact of flow variation on power output and any potential impact of the choice of power conversion technologies or flow parameters.

1.5 Research methodology

To achieve the research objectives, the methodology employed was to develop, water-to-wire, four river hydrokinetic turbine generators in the 5 kW to 60 kW range, install them on the Winnipeg River in winter and summer, and perform power and flow tests. The Pointe du Bois hydrokinetic turbine testing facility was developed for this purpose and turbines were supplied by research partners for testing. All aspects of the test facility had to be developed, as this was the first test facility of this kind. Moreover, operating in winter months at temperatures below -30^{o}C on open water requires an approach that is safe, well planned and follows operational health and safety codes. The test facility had unique design features that permitted working on the Winnipeg River in winter months to achieve program objectives.

1.6 Contributions

This research includes development and implementation of water-to-wire hydrokinetic turbine-generation and power conversion systems; including electrical design and grid connection of hydrokinetic devices to the provincial power utility as contributions to the marine energy effort. These contributions are directly in-line with marine energy stakeholders research needs seeking to understand if such systems can be installed and operated in winter.

Systems are developed to measure three-dimensional river velocities in-situ up to 2.4 m/s with concurrent measurement of electrical power generation. The author's specific contributions include technology application in cold climates, electrical connection design, high-resolution measurements and effects on power conversion, direction of deployment and retrieval, safety planning, and water-to-wire river testing of the following hydrokinetic turbines systems:

- 5-kW vertical-axis turbine with a 5-kW, 36-pole permanent magnet generator and stand-alone 5-kW power converter, adapted from a commercially available solar solution, with battery storage.
- 5-kW vertical-axis turbine with a 5-kW, 36-pole permanent magnet generator and adapted wind/solar 6-kW power converter with grid connection.
- 25-kW vertical-axis turbine with a 12-kW, 36-pole permanent magnet generator and adapted wind/solar 12-kW power converter with grid connection.
- Shrouded horizontal turbine with 60-kVA, 24-pole permanent magnet generator with a custom design 155-kW power electronics converter; also with grid connection and battery storage potential. The deployed unit could not be tested adequately due to excessively low river velocities during the test period.

1.6.1 Emerging hydrokinetic turbine milestones

There are four main milestones achieved in support of emerging marine energy in cold climates:

1. The safe and successful delivery of power to a rural utility grid in summer 2008 using a hydrokinetic turbine, achieved as part of the in-situ tests performed herein, was the first of its kind in North America this century. A similar project achieved this only once in early 1980 on the Ottawa River.
2. Winter deployment, retrieval and operational experience in -20°C weather are critical milestones for this emerging technology to be able to generate revenue year-round.
3. The river flow data collected as part of in-situ testing in summer 2008 is the first ever reported.
4. Turbine deployment in winter and testing through the winter of a surface mounted turbine remains the only one ever performed to date.

1.6.2 Test setup and deployment for remote communities

All four of the test scenarios used a pontoon-based research platform. The platform was not connected or supported by any existing man-made structure, and therefore the deployment method is suitable for remote and natural locations. This includes the main anchoring to the rock at the river bottom as well as device deployments under normal river velocities of 2.5 m/s or greater.

A site plan was developed using aircraft-based photographs of the site. Bathymetric and boat-measured acoustic Doppler current profile data were overlaid to allow selection of the optimum location. The test location was chosen so that the velocity and depth of the water was suitable for efficient operation of the turbine year-round. In addition, the selected location allowed for moving the platform laterally to several locations across the stream, providing a range of flow velocities and turbulence levels for observation of mechanical-electrical interactions.

A test site that replicates remote communities was selected and developed. At a nominal velocity of 2.5 m/s, people accidentally falling in the water would be in contact with the power station within minutes. Therefore, deployment and safety plans were prepared and

submitted showing detailed drawings of the site, cabling and mechanical connection details, safety ropes and safety boat positions. Safety protocols developed throughout the research can be applied at other sites.

1.6.3 Site impacts

The pontoon-based test platform was used for all test setups. The deployment of the test platform into the test position, and its retrieval was required for each setup. During the first winter season test, it became apparent that frazil ice quickly formed on and around the pontoons and ultimately caused instability, making sinking the turbine assembly a definite possibility. The on-board monitoring of vibration, flow, power and temperature documented a nearly catastrophic occurrence. The support for the 25-kW unit was redesigned by New Energy Corporation Inc. and tested at the site with the connections to the mooring cable at mid-ship and below the water level. This improved the deployment by considerable reducing the moment on the platform, making an important contribution to surface mounted turbines.

For the horizontal-axis turbine with a shroud, a safe deployment system was required. This required the design and construction of an “A” arm, and hydraulic pistons allowing the turbine to be lifted entirely out of the water for transportation from shore to the test position in the flow. When the test platform was in place, it could be lowered into the water. The hydraulic motors, and all on-board winches and electrical supplies were powered with a 12-VDC battery cabinet, so that no AC power from the shore was required. Other systems developed and installed in the 60-kW system included a closed loop circulating cooling system for the generator and gearbox, a lubricating oil system for the drive chain with an on-board oil/water separation system, temperature and vibration monitoring. With the help of technicians, these systems were installed and tested as part of the research. Worker’s abilities were impaired by cold weather and additional safety precautions were developed and implemented to minimize the risk of falling in the water.

1.6.4 Electrical grid connection

The test site required various electrical connections for setup, measurement and control as well as *grid connect* or interconnection to deliver power from the hydrokinetic turbines under test to Manitoba Hydro's local 12.47-kV rural overhead distribution system. Electrical design, planning and drawings were required for each stage of the testing, and an electrical permit was required for installation of bi-directional metering. On-site adjustments to the power conversion systems were required to accommodate over-voltage during high water flow incidences. Implementation of ballast resistors to allow for voltage regulation/stabilization on the DC bus ahead of the inverter was achieved. Other aspects of grid interconnection, such as anti-islanding and synchronization requirements were investigated and the specific implementations are summarized in this thesis.

1.6.5 Long-term test operation

The operation of hydrokinetic turbines in cold weather climates was not previously documented. At the test site, a 5-kW vertical-axis turbine and inverter was deployed at sustained temperatures below -20°C. The hydrokinetic turbine was successfully operated in -20°C and -30°C temperatures for weeks at a time, and electrical parameters, water velocity and a video feeds were continuously monitored. During this test period, many cold weather operational adjustments were required, such as heating of the gearbox oil and removal of ice formations from the test platform. Several icing mitigation techniques were tried and are documented. While the requirement for de-icing was substantial, turbine operation in extreme cold weather was confirmed. The test platform was removed before the breakup of ice in the spring. Any component that pierces the water interface will accumulate ice through direct splashing and freezing, or buildups through frazil ice process. Failure to mitigate these ice formations will result in catastrophic system failure.

Operation was confirmed for the 5-kW vertical-axis turbine and a 25-kW vertical-axis turbine. The larger unit delivered over 9 kW continuously to the Manitoba Hydro local electrical distribution line through two parallel connected 6-kW rectifier-inverter units repurposed for hydrokinetic energy use as part of this project. Load power and water

velocity were continually monitored. These observations identified a potential line frequency resonance problem between the 80 m long power feeder cable to the shore and the capacitance inherent to the commercially available inverter adapted from wind power applications. This information was used to incorporate the necessary filtering system for the connection of the 155-kVA power electronic converter developed for the 60-kW generator; supplied for the horizontal axial flow turbine described herein. Development of the power electronic converter was accomplished by fellow researcher, Farid Mosallat and is documented in his thesis [9].

1.6.6 Velocity and turbulence effect on electrical output

The water-to-wire setup for the 25-kW vertical-axis turbine made use of diode-based rectifiers and two 6-kW solid-state power converters using insulated gate bipolar transistor (IGBT) based inverters. These inverters were connected to the 100A 120/240V electrical panel in the test facility trailer and, when in operation, provided power to the test site and exported the excess power to the grid through a bi-directional meter. The power converters operated on a table-based maximum power point tracking system (MPPT), which varied the output load to suit the rotational speed. For this generator, voltage is a linear function of the speed and therefore output voltage was used as the control signal [9].

The operation of the solid-state power converters on the system makes it impractical to observe the effects of flow variation or turbulence intensity on the electrical power output of the system. This relationship is important for site evaluation and for understanding the nature of power fluctuations within the power conversion system. Therefore, a test set up was developed to deliver generated power directly to independent resistive-only loads. An acoustic Doppler velocimeter was used to measure water velocity and turbulence at 200 Hz sampling rate concurrently with electrical power output measured at a 20-kHz sampling rate. Time domain and frequency domain analyses were performed on both data sets and a correlation between the two was evaluated. The results show that power output increases with moderate level of turbulence intensity in the 4% to 5% range. In addition, for the vertical-axis turbine studied, the operation of the turbine increased turbulence intensity

significantly within one rotor radius upstream and a reduction in average velocity was measured. For cross-stream vertical-axis turbines, a significant amount of momentum is transferred to smaller eddies at higher frequencies as a result of the shear effects of the wake produced when the turbine passes across the in-stream flow. Additional details on this work can be found in the journal Renewable Energy [10].

Unlike previous literature highlighting cavitation and turbine instabilities of Darrius turbines blade rotors, such phenomenon where not observed in-situ. In addition, once turbine and system efficiency issues were addressed, turbines were sometimes self-starting; demonstrating that with additional reduction in internal friction, a 4-blade Darrius rotor can self-start, in river conditions.

1.7 Published materials

The following papers and conferences were published form this research.

Journal papers

1. Birjandi A.H., Woods J. and Bibeau E.L. (2012), "Investigation of effect of macro-turbulent flow structures in a fast-flowing river on a vertical hydrokinetic turbine," Renewable Energy, 48, December, p. 183-192.
2. Bibeau E.L., Kassam S., Woods J., Molinski M. and Bear C (2009), "Operating a 5-kW grid-connected hydro kinetic turbine in a river in cold climates," Canadian Journal of Ocean Engineering, 35, p 67-79.

Conferences

1. Birjandi A.H., Woods J. and Bibeau E.L. (2011), "High frequency velocity measurement upstream of a 25-kW vertical river kinetic turbine," International Conference Energy & Meteorology 2011, 8- 11 November 2011, Gold Coast, Australia.
2. Mosallat F., Gole A. M., Wachal R. W., Bibeau E. L. and Woods J. (2007), "Harnessing kinetic energy of Canadian rivers: Opportunities and challenges,"

CIGRE Canada Conference on Power Systems, Calgary, Alberta, Canada, 27-28 August.

3. Birjandi A.H., Woods J., Shahsavarifard M., Bibeau E. L., Molinski, T. (2011), “Kinetic turbine research, demonstration and development in Manitoba rivers," CSBE /SCGAB Annual General Meeting and Technical Conference, Winnipeg, Canada, 2011.
4. Birjandi A.H., Woods J., Shahsavarifard M., Bibeau E.L. and Molinski T. (2011) “Kinetic turbine research, demonstrations and development in Manitoba rivers,” CSBE/SCGAB 2011 Annual Conference, Inn at the Forks, Winnipeg, Manitoba, 10-13 July.

2. Literature review and theory

This thesis investigates the application of hydrokinetic turbines in cold climates, mainly at the electrical utility distribution level, as a distributed generation concept. The literature review is focused on site selection, deployment and observation of flows and on-site operation, especially in cold climates. The literature review covers the published knowledge related to research objectives: (i) evaluating the suitability of this technology for use in remote locations in cold climates and (ii) measurement and documentation of device operation in-situ. These topics overlap within the broad field of river flow dynamics. As such, this chapter also provides background information to show how the present work adds to previous knowledge obtained and advances the understanding of how this emerging technology, at the distributed level, can be applied in cold climates.

2.1 Hydrokinetic power generation

Kinetic turbines generate power by immersing turbines in flowing water to produce torque that turns a shaft connected to a generator. This principal is the same as that used in wind power extraction, with the main differences being that water is incompressible and significantly denser. In 1919, Albert Betz applied the concepts of conservation of mass and momentum to an idealized rotor or actuator disc to derive a maximum limit for energy extraction of 16/27 or 59.3 % of the available kinetic energy [11]. The amount of power available P_A in the flow depends on the fluid velocity V, fluid density ρ, rotor area A, and power coefficient in the relations:

$$P_A = \frac{1}{2}\rho A V^3 \tag{1}$$

$$C_p = \frac{P}{P_A} = \frac{P}{\frac{1}{2}\rho A V^3} \tag{2}$$

The power coefficient C_p represents an efficiency term, including mechanical and electrical losses within the energy conversion system. In a 2012 article [12], Ross Vennell suggests

that the Betz limit is not strictly applicable to hydrokinetic turbines, particularly when they are included in an array. Not all of the assumptions made to actuator disc theory are intact. Firstly, in theory, the fluid in which the device operates is assumed unbounded. For wind turbines operating at an 80 m height within a 100 km thick atmosphere of air, this assumption is reasonable. However, for river applications, the air-water surface boundary and the riverbed are much closer to the operating turbine. The effects of operation near the surface are reported on by Birjandi [13], and were evident in operation during our site tests. Secondly, the fluid by-passing the rotor-swept area is assumed not to interact with the fluid within the stream, and the velocities within the rotor are assumed to be uniform. Neither of these can be valid for vertical-axis turbines due to their low solidity ratio and their rotation in the plane of flow. Moreover, to this we can add the effect of ice growing on turbine structures and penetrating below the water surface as reported for the first time by the present work in Chapter 5. Ferrer and Willden provide a detailed analysis of blade–wake interactions [14] and show that the flow in the interstitial space is complex and variable within the rotor cross section. Nonetheless, except for applications with multiple turbines which are close enough to react with each other, Equations (1) and (2) are universally used as a basis for comparing efficiencies and maximum values. When a hydrokinetic device extracts energy from a fluid stream, it is not immediately restored by the elevation gradient at the river bottom or an instantaneous rise of the tide, but by transfer of momentum from the surrounding flow creating shear forces and causing turbulence. For turbine 'farms' having multiple devices in the same stream vicinity the number and spacing of devices requires optimization [15], [16].

Equation (1) shows that the power is proportional to the swept area of the turbine facing the mean flow, and proportional to the cube of the velocity. Since the power is also proportional to the density, and water is 815 times denser than air (at 4º C) a hydrokinetic turbine is significantly smaller than its wind counterpart for a given kW output and fluid velocity. For riverine hydrokinetic turbines, this is fortunate, as river depth is typically a limiting factor and mean velocities are lower. For tidal streams, the range of physical size is larger.

Figure 2 shows the relative size of hydrokinetic turbines versus wind turbines and an example hydroelectric turbine and the relative dimensions of the turbines tested in this thesis.

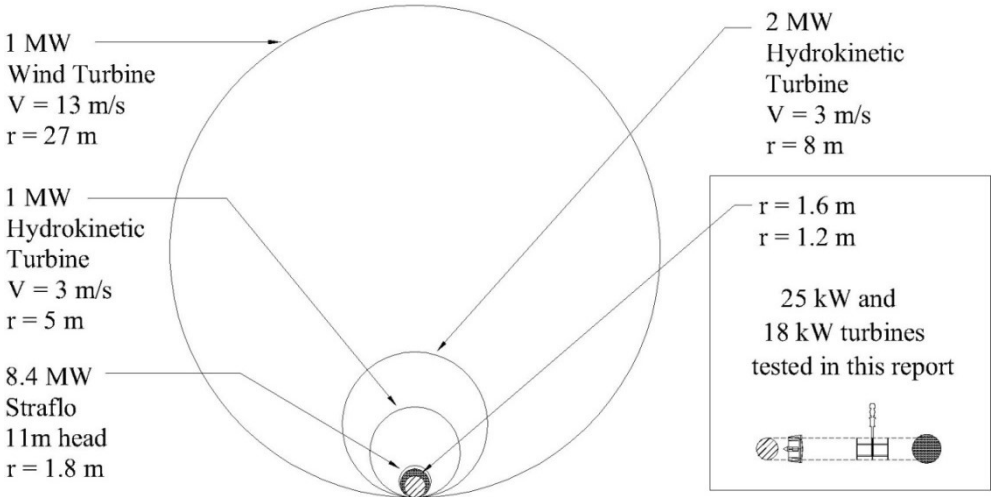

Figure 2: Relative sizes of swept area of 1 MW wind, 1 and 2 MW marine (tidal stream) hydrokinetic turbines, 8.4 MW straight flow hydroelectric turbine, and turbines tested in this research with radius of 1.2 m and effective rotor area of 1.6 m for the 25-kW vertical-axis Darrius.

Considering Equation (1) at a high level, and taking the Betz limit and water density as fixed values; power is increased by making the swept area larger, improving the efficiency, C_p, or increasing the velocity.

Turbine dimensions are site specific and constrained by river depth, flow velocity profile, and ice thickness. The mean velocity in Equation (1) often denoted V_∞ relates to the average in-stream velocity away from the influence of the turbine and does not consider the more complex turbulent flows in which hydrokinetic devices are typically employed. Turbulence is an inherently three-dimensional phenomenon [17] and contains kinetic energy beyond what is apparent in mean flow measurement; therefore, it should not be neglected when considering details of energy conversion. The effects of turbulence on the mechanical-fluid interface, such a cavitation, are significant and are a part of the system efficiency and practical operating range. The C_p efficiency term includes electrical losses

including cable and generator “copper” or thermal losses, as well as losses in the power conversion devices.

Electrical power can be produced on many different scales: from household levels, such as roof-mounted solar panels; to hydroelectric and thermal/nuclear plants. For discussion, the National Research Council of Canada [18] uses the classifications for hydro electrical generation listed in Table 1.

Table 1: Power generation classifications

Classification	**Power Level**
Large	50 MW and greater
Small	1 MW to 50 MW
Mini	100 kW to 1 MW
Micro	Less than 100 kW

Most of the hydrokinetic turbine systems developed or studied to date fall into the mini-hydro or micro-hydro category, though Open Hydro and Marine Current Technologies have developed single-rotor systems as large as 2 MW for tidal stream use. As a point of reference, there are six hydroelectric generating stations on the Winnipeg River, with a combined capacity of 579 MW. Stations range from 55 MW to 165 MW, and individual generators range from 4.7 MW to 27.5 MW. Vertical drop, or head, at the stations range from 10 m to 18 m, with a total drop in elevation, from Point du Bois to Lake Winnipeg of approximately 77 m.

Hydrokinetic energy is a small but growing source of renewable energy, which plays a part in the more general grouping of sustainable energy. It is important to place hydrokinetic energy production in context. Generating capacity from renewables is expected to increase worldwide from 13% to 18% by 2040, or 75 GW [19]. To put this in perspective, the largest river hydrokinetic turbine generator considered in this work was in the order of 60 kW.

Open Hydro is completing a project, for late 2016, which includes two 2 MW marine tidal energy turbines [20].

In order for hydrokinetic turbines to supply a significant part of the new demand for low-carbon emission electricity, especially in remote communities that are not served by the grid, they must achieve a levelized cost of electricity that is comparable to alternatives. Canada's Marine Renewable Energy Technology Roadmap [3] estimated that wave energy could be as much as 27.5 GW. They estimate that river-current extraction, where this research is focused, could add an additional 2 GW in a relatively short term. Much of the technology developed for river flow conditions is also applicable to in-stream tidal energy capture, where the resource is estimated to be 6.3 GW. All together, these sources could add another 35.7 GW to the hydro related generation capacity. Canada's water-based renewable energy production is estimated at 87 GW by 2040 [21]. The National Research Council of Canada is completing Phase III of its report titled Canada's Hydrokinetic Power Potential [18]. The assessment indicates in the order of 700 GW of extractable power, though this does not include restrictions on location or device efficiencies, and has a 300 GW uncertainty level.

2.2 Vertical-axis and horizontal-axis turbine arrangements

There are two main types of turbines used to harness the power of the water's kinetic energy at the distributed scale: horizontal and vertical-axis turbines. An example of each is shown in Figure 3. There are many other styles of turbines used, such as vertical and horizontally oriented Gorolov rotors and three-bladed propeller type rotors which are similar to wind turbine designs. A review paper by Khan, Bhuyan, Iqbal and Quaicoe [23] and the Assessment of Canada's Hydrokinetic Power Potential [18] provide information on these other styles.

The basic design of turbines has existed for many years and has been used for extracting power from wind and water. The principles of operation are the same in both fluids. The fluid flows over the airfoils or hydrofoils, inducing aero/hydrodynamic forces that generate

a torque with respect to the axis of rotation. The horizontal-axis turbine has its axis in line with the flow while the vertical-axis turbine has its axis of rotation orthogonal to the flow. Turbine efficiencies are higher for horizontal-axis turbines. The horizontal-axis of rotation allows each blade to produce a continuous torque throughout one rotation, producing a smooth and constant power with less vibration and potential fatigue. The relative fluid velocity of vertical-axis blades changes in magnitude and direction throughout each rotation leading to an oscillating torque and power output [24], [13]. The horizontal-axis turbine can self-start in lower flow velocities than the vertical-axis turbine. This is mainly due to its higher solidity ratio [13].

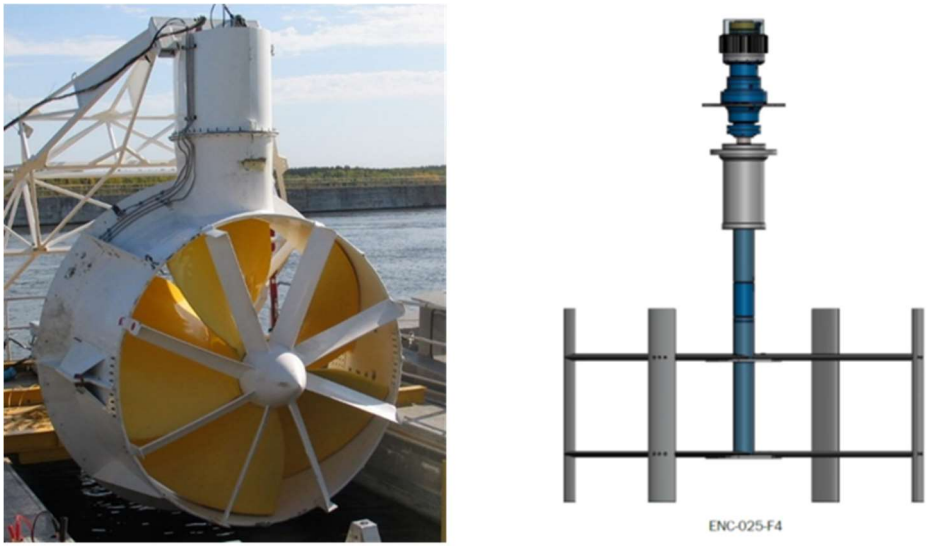

Figure 3: (a) Horizontal-axis shrouded turbine (photo taken with permission), and (b) vertical-axis, H-Style Darrius turbine by New Energy Corporation Inc. tested in-situ in this research.

When starting, these devices, as with all rotating machines, must overcome powertrain friction from gears, linkages and inertia. The vertical-axis configuration has some advantage over the horizontal-axis turbine such as flexibility of blade and rotor dimensions, and the location of the generator and bearings above the water line. In cold climates, however, equipment above the waterline causes disruptions due to the formation of ice as reported in Chapter 5.

The hydrofoils in an H-style vertical-axis turbine do not have a twist or taper. Some studies identify rotor instability as an issue for these turbines for water applications and recommend a helix configuration to smooth out torque [25]. Such studies disregard the lower efficiency achieved at higher flow velocities due to a vertical velocity components created by twisted blades. New Energy Corporation Inc.'s concept uses hydrofoils and support arms manufactured in one two-dimensional extrusion, with lengths cut to suit. This simplistic design can reduce the manufacturing cost compared to the horizontal-axis turbine that requires detailed manufacturing in three-dimensions. For smaller ratings and testing, rotors are constructed from aluminum or fiberglass. In larger designs, more advanced composite materials are used [26]. Horizontal-axis rotors for hydrokinetic turbines are very similar in shape to rotors used in more traditional straight flow (or Straflo) hydroelectric turbines as shown in Figure 4(a).

(a) (b)

Figure 4: (a) 8.4 MW, 3.6 m diameter steel rotor for straight flow hydroelectric plant, and (b) 2.4 m diameter hydrokinetic rotor constructed of fiberglass (photo with permission).

Note also that with the Straflo-type device, the rotor blades or vanes are connected to the outer rim, which rotates with the axial shaft. In the hydrokinetic turbine shown in Figure 4(b) the rotor turns within the shroud. In larger tidal stream turbines, such as those by Open

Hydro, the concept of rotating the rim with the rotor vanes is used, with permanent magnets installed on the outside of the rim and the stator coils in the support housing around the rotor. Tight clearances must be maintained throughout the turbine life.

The vertical-axis rotor can operate with the free stream entering from any direction while typical horizontal-axis turbines need to yaw to be directly perpendicular to the flow for maximum energy conversion. Horizontal-axis turbines with no yaw control system lose efficiency due to the flow direction variation [27].

To increase the power density, designs can incorporate a shroud to draw more flow through the rotor area. The turbine in Figure 3(a) and 4(b) show such a device. Some designs claim that the total extractable power exceeds the Betz limit. However, this type of calculation uses the rotor diameter and not the shroud dimension, and once this is considered, the Betz limit is respected [28]. The shroud does increase the velocity through the rotor using a Venturi effect and thus increases power. However, the increase in drag can make deployment and retrieval costlier and more difficult, requiring additional safety considerations. The basic design of a vertical axis hydrokinetic turbine consists of a rotor with hydrofoil blades. In operation, the blades rotate around the shaft at 2 to 8 times the speed of the free stream. The relative velocity between the blade and the free stream induces hydrodynamic forces of lift and drag along the hydrofoil. The ratio between the velocity of the end or tip of the blade with respect to the free stream velocity V_∞ is known as the Tip Speed Ratio (TSR). It is typically designated as λ, and is used to quantify operating points of the turbine system. Varying the rotor speed, and hence the tip speed changes the power coefficient, C_p from Equation (2), because the hydrodynamic efficiencies of the rotor change with flow velocity. For comparison to other turbines and for selection of optimum operating points, the power coefficient versus TSR is plotted as shown in Figure 5.

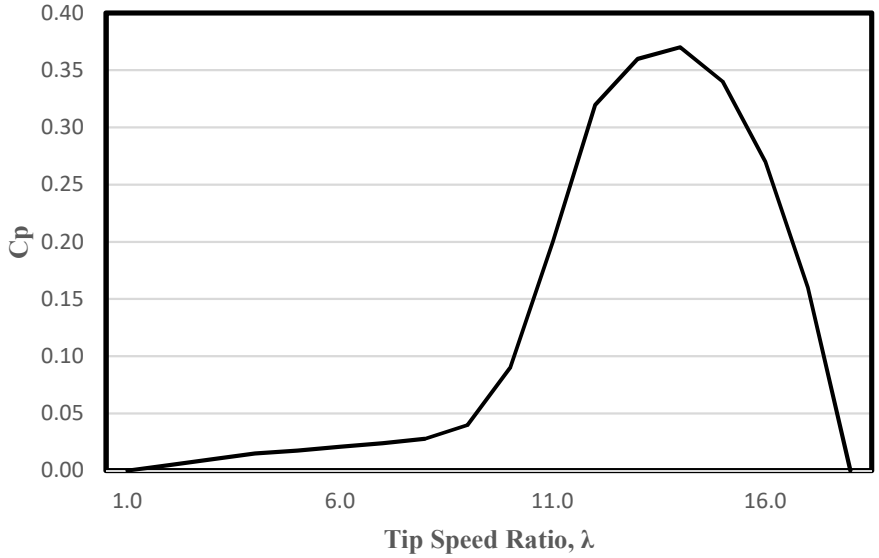

Figure 5: Typical power coefficient C_p, versus tip speed ratio λ, or TSR curve, for a horizontal-axis-type turbine as tested in this research.

The C_p curve shown in Figure 5 has relatively low efficiency in the start-up range from λ values from 0 to 1.5 indicating limited low-speed start up capability. In this case, for a Darrius "H" type cross-flow turbine the blades produce positive torque greater than the drag force and other retarding forces only in a portion of the rotation [13]. Other turbines have better capabilities at low speeds, and therefore more gradual slopes on the low-speed side of the C_p curves. For example, Figure 6 shows the associated power versus the rotational speed curve for a horizontal-axis machine. With a more conventional horizontal-axis propeller type rotor, positive torque is provided by all segments of the rotor blades during the entire rotation cycle. Self-starting in cold climates is crucial, as accessing turbines in cold weather is very difficult and not recommended based on in-situ testing experience, documented in Chapter 5.

For river hydrokinetic turbines, rectifiers are used to convert the variable frequency Alternating Current (AC) power to Direct Current (DC) and then an inverter is used to produce the appropriate AC to match grid requirements. In this way, the overall turbine system design is much less constrained with respect to rotor speeds. The rotor speed in a

hydroelectric power station is tightly controlled to ensure that the electricity produced will match the frequency of the grid [29]. In hydrokinetic systems and newer wind turbine systems, power converters are used to allow the rotor to be turned at variable speeds while maintaining suitable voltage and frequency levels [30]. For such systems, a relatively simple maximum power point tracking algorithm is practical to implement.

2.3 Generation and power conversion

The conversion of rotor torque is efficiently achieved through electrical machines to produce electricity and a grid system allows the generated electricity to be used locally or transmitted [31]. When a magnetic field is moved in the proximity of a closed electrical circuit path, a current is induced. Conversion of rotating mechanical energy into electricity, therefore, requires intermediate magnetic or electromagnetic equipment to produce a magnetic field. In a more traditional hydroelectric generating plant, and in larger wind turbines, synchronous generators are used to produce alternating voltage and current [32]. The speed of their generator shaft is controlled to produce a specific frequency of 60 Hz in North America. Using the number of poles (counting magnetic north and south) of a device, P, and the revolutions per second, N, of the shaft allows the frequency of the electrical output to be calculated as:

$$f = \frac{P}{2} N$$

Therefore, to produce a 60 Hz power frequency, a two-pole device would have to rotate at 3,600 RPM; with 24 poles, the rotational frequency drops to 300 RPM. The optimization of rotational frequency varies with the mechanical prime mover used to drive the shaft rotation. For example, a steam turbine is designed to rotate at relatively high RPM as the high-pressure vapour is applied to the first row of turbines at velocities in the order of 45 m/s, achieving a rotational speed in the order of 3,600 RPM [32]. A rotor in a hydroelectric station is much larger in diameter, and has a rotational speed in the order of 100 RPM. Hydrokinetic turbines, such as those used in the present research, rotate in the 30 to 60 RPM range. Larger tidal stream turbines turn 10 to 16 RPM. To improve efficiencies, hydrokinetic turbine manufacturers, such as New Energy Corporation Inc., have eliminated

the gearbox by increasing the number of poles in the generator, thereby achieving the same frequency range at a slower rotational speed.

To maximize power output from rivers and tidal stream flows which vary day to day and season to season and interact with large-scale eddies larger than the rotor blade, hydrokinetic turbines need to be designed to be independent from the limitations of grid power frequencies. Conversion of the turbine's rotational energy to AC is found to be the most effective first stage, with conversion to DC either in the power converter on shore or in some cases within the device itself using passive rectification circuits [33]. Once DC power is produced, a second stage of electrical conversion is generally necessary, to produce distributable AC power. DC power can be used directly for passive heating and battery charging. Therefore, a multi-level optimization is required between (a) the flow which changes continually but cannot be controlled, (b) the turbine/rotor configuration and dimensions of fixed design, and (c) the electrical conversion process including generator speed and mechanical speed increasers. Some larger rotors can use active pitch control. For river hydrokinetic turbines, a low levelized cost of electricity leads to designs with minimal moving parts and therefore most use fixed pitch hydrofoils. For a given configuration, the resulting machine needs to react to the flow and address the variable frequency generated by the turbine. Due to the countering forces of lift and drag on the rotor, and the counter torque of the electromagnetic generator reaction for a given electrical load, the output power for a given rotation velocity will increase to some maximum value and then drop off. This is generally depicted by a set of power curves as shown in Figure 6.

Figure 6 shows the maximum power on each flow velocity curve. Typical Maximum Power Point Tracking (MPPT) control systems evaluate the average velocity and adjusts the load output so that the maximum power is achieved. For basic MPPT operations a look up table is used to match water velocity to relative peak output power. Because there is more than one speed for a given power output, MPPT tracking algorithms determine which side of a curve the device is operating on, and therefore anticipate if additional load can be added [24]. In general, operation on the right-hand side of the tip-speed curves is

considered more stable. Increasing the load while operating on the left-hand side can reduce the speed to a point at which the lift force is overcome by drag causing stall on blades.

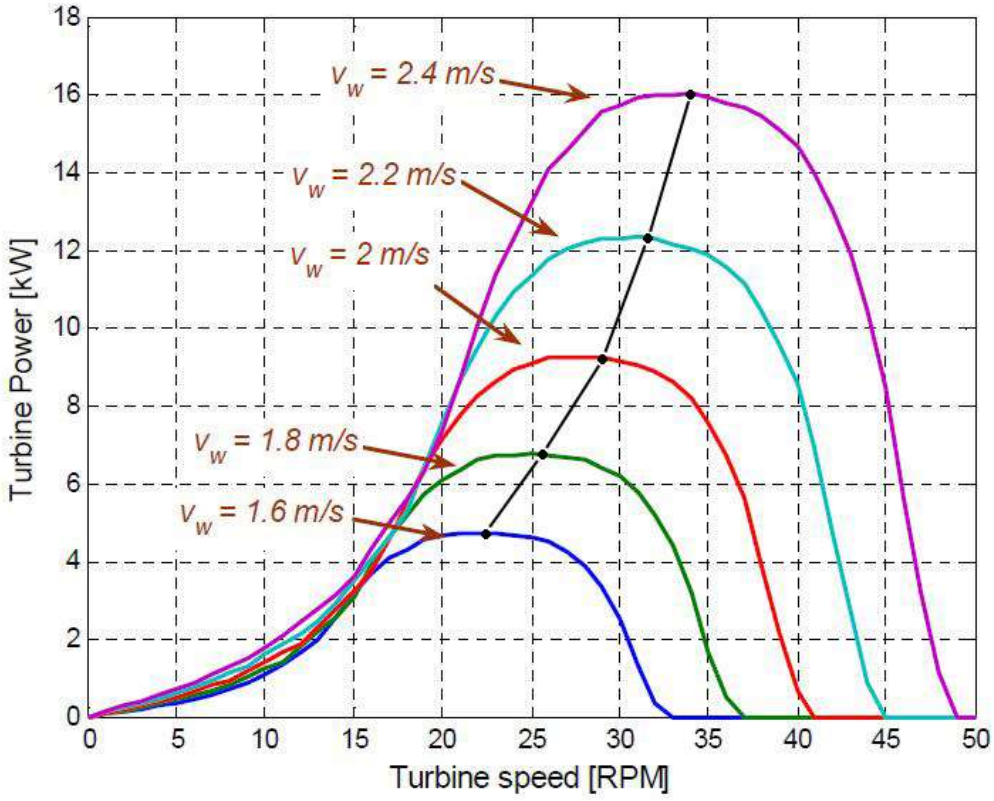

Figure 6: Family of output power versus turbine speed curves for a representative hydrokinetic turbine adapted from [9]. Black line and dots represent maximum power point tracking curve used for electrical output control.

2.4 Hydrokinetics: flow dynamics and measurements

As noted above, the essential concepts of hydrokinetic energy capture and wind energy capture are the same. Some differences, and observations related to river flows are described in the following sections.

2.4.1 Wind power

The use of rotating machines to capture the kinetic energy of flowing water is documented to 300 BC, pre-dating similar wind devices by hundreds of years [34]. However, wind occurs in all geographical areas of the world. Land accessibility is much simpler than water accessibility, resulting in wind energy being the fastest growing renewable resource. According to the US Department of Energy, wind power was the largest contributor of new electrical generation in the United States in 2012 [35]. Both China and the USA added close to 13 GW of wind powered generation in that year. The Canadian Wind Energy Atlas uses weather data to produce a weighted average wind velocity at different elevations to develop the best wind energy capture locations [36]. Since its main driver is the sun, its flows have diurnal peak and trough effects, and in most regions, significant seasonal variations. Furthermore, wind is difficult to predict [37], and its sub-hourly fluctuations during a given day are significant; thus, creating dispatching challenges for the utilities. Such fluctuations also require structural analysis, to ensure that both the rotating components and support structure can withstand the stresses. The characterization of hydrokinetic energy and the industry to efficiently capture this energy is not yet established.

Potential river-hydrokinetic turbine sites being tested in-situ as part of this research are not subject to significant hourly fluctuations in average velocity. However, seasonal variations remain in most cases [38], [39], [40]. Evidently, the use of hydrokinetic turbines for use in a tidal resource would be subject to daily tide effects and seasonal variations. Given the higher density of water and cost of accessing devices compared to wind, significant challenges remain to make marine energy a robust industry.

2.4.2 River flow

Oak Ridge National Laboratory [38] reviewed the literature on characterization of river flows and developed a reference model for use in analyzing hydrokinetic and tidal resources. Rivers of study included the Mississippi, Missouri, and Rio Grande in the US, and the Severn in England. They conducted an analysis for a near-surface mounted vertical-

axis turbine denoted as RM2. The study focused on rivers where the depth was a minimum of one meter and the flows were greater than one meter per second. The data set included 39 velocity profiles, which contained flows with Reynolds numbers above 400,000 and Froude numbers less than one indicating subcritical flow [41]. A summary of various river properties, taken from the R2M study by Neary, [38] is shown in Table 2.

Table 2: Representative river flow characteristics

Site	**Investigators**	**Depth (m)**	**W (m)**	**Re (10^6)**	**Fr**
Mississippi	McQuivey (1973)	7.4 - 16	570 - 890	3 - 9	0.06 - 0.17
Missouri	McQuivey (1973)	2.9 - 3.1	200 - 210	4 - 38	0.19 - 0.35
Missouri	Holmes & Garcia (2008)	4.9	350 - 400	5 - 9	0.13 - 0.17
Rio Grande	McQuivey (1973)	0.85 - 0.91	21 - 22	0.8 - 1.3	0.36 - 0.49
Hurunui	Nikora & Smart (1997)	1 - 2	85 - 90	1 - 5	0.70 - 0.79
Severn	Carling et al. (2002)	NR	NR	3 - 6	0.10 - 0.16
CSU flume	McQuivey (1973)	0.33 - 0.53	2.44	0.4 - 0.8	0.69 - 0.74

The Reynolds number for open channel flow is given by $R_e = \frac{UL\rho}{\mu}$ where U is average channel velocity, ρ is density and μ is viscosity. The Froude number is considered a more important dimensionless number for describing open channel flow with $\mathrm{Fr} = \frac{U^2}{gL}$ where g is the acceleration due to gravity and L is a characteristic length normally taken as river depth [41]. A Froude number less than one defines a flow that is subcritical. In such flows, devices like hydrokinetic turbines can influence upstream and downstream features.

The velocity profiles used in the RM2 study were used to calculate the shear velocity, given by u_* using:

$$\frac{\bar{U}}{u_*} = \frac{1}{\kappa} ln\left(\frac{z}{k_s}\right) + C$$

where k_s is a function of the roughness of the river bottom, κ is the Von Karman's constant set to 0.41 and z is vertical distance from the river bottom. In general, for fully rough

conditions, the constant *C* is set to 8.5. The RM2 study also used the collected river data to evaluate the more general velocity profile described by the power law equation:

$$\frac{\overline{U}}{\overline{U}_{max}} = \left(\frac{z}{D}\right)^{1/\alpha} \tag{3}$$

where again z is the distance from the bottom and *D* is the depth of the river. The exponent α fits the flow data, varying from 3 to 12, with a best-fit value of 5.4. Using ADCP on the ocean floor, Ruopp and Ruprecht documented a similar power law equation in 3.6 m of water for their testing of a 2.8 m diameter horizontal turbine [42].

Phillip Lucas-Picher studied the average velocities for North American river basins based on annual flows [40]. Average velocities are shown in Table 3. Locations in rivers which are of interest to hydrokinetic development have velocities in the 2 to 3 m/s range with energy density in the 4 to 13.5 kW/m2 range. As such, selected sites will be in locations of higher than average velocity, corresponding to natural structures like narrows or rapids, which also give rise to higher turbulence levels. Our study found that open water in winter was a suitable site selection criterion.

Using the Reynolds number based on the hydraulic radius R_h for wide channels as approximately equal to the river depth, this study on the Winnipeg River has a Re = 20 x 10^6, comparable to rivers modeled in the R2M study, summarized in Table 2.

Table 3: Average velocities for representative Canadian rivers

River Basin	Velocity m/s
Mackenzie River	0.92
St. Lawrence River	0.75
Yukon	1.65
Columbia	0.94
Fraser	1.73
Nelson	1.05
Churchill	1.22

2.4.3 Open channel flow

In open channel flow, the surface of the water is bounded by the atmosphere. The presence of wind can affect velocity and shear measurements [43]. Also, waves can affect the operation of both surface mounted and submerged equipment. However, the optimum location for energy capture is not precisely at the surface.

In fully turbulent open channel flows, the maximum velocity is near the surface where there is nominal shear force [43]. In practical measurement of such a flow, the actual maximum is somewhat below the surface due to secondary circulating currents at the surface [41]. Therefore, for rivers in cold climates, the optimum location for kinetic energy capture is below the surface and below the level where ice may flow during spring break-up, but near the top of the water column outside of the viscous effects near the river bottom.

Figure 7 shows five representative velocity profiles *a* to *e*. Profiles *b* and *d* show examples of in-stream velocity profiles for laminar and fully turbulent flow, respectively. In-stream measurements by Grabbe, Yuen and Goude of Uppsala University, Sweden confirmed such velocity profiles over a five-year measurement period in the Dal river, one km downstream of a hydroelectric plant [44]. Profile *a* is representative of the Pointe du Bois site [45]. Profile *d* includes a nearly vertical segment of fully turbulent flow near the surface, which is optimal for turbines located in this region of the water column because it is at or near the

maximum velocity, and is a relatively constant value over the span of the turbine. For less ideal profiles, such as *b*, *c* and *e* this factor must be considered in design of the rotor bearings and overall structure of the rotor [46]. Modern tidal energy conversion devices, such as the three-bladed axial flow device designed by Marine Current Technologies, may adjust the pitch of each hydrofoil as it rotates through the different velocity zones [47]. This is expected to complicate control aspects, and requires additional moving parts. However, due to the significant cost of deploying and removing turbines for maintenance, this trade-off is expected to extend the mean time between failures of crucial components such as thrust bearings. Looking at profiles *b* then *a*, as a progression from laminar to turbulent flow, the relative increase in velocity closer to the river bottom results from the net dispersal of momentum from higher faster flows to the lower slower flows as a natural and well known property of turbulence [17], [41].

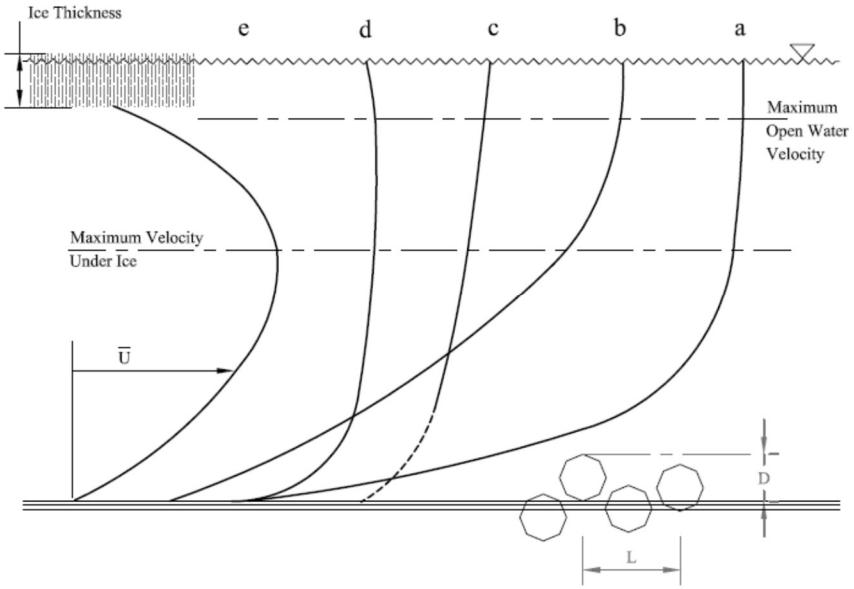

Figure 7: Idealized open channel in-stream velocity profiles *a* to *e*: *a* representative velocity profile measured at the Pointe du Bois test site, *b* a laminar flow profile, *c* typical power-law profile for fully developed turbulent flow, *d* idealized fully developed turbulent flow profile, with free surface, and *e* flow profile under ice. Parameter D represents the diameter of an obstruction on the bottom and L the spacing between obstructions.

To be cost effective, river hydrokinetic turbines should be suitable for winter use as well. Many rivers in Canada freeze over and create a closed channel for much of the flow, as represented in profiles *e* of Figure 7 adapted from reference [48]. Flow volumes on inland rivers are lower in the winter, reflecting normal precipitation climatology [39], [49]. The development of fully turbulent flow would be in constant flux as the flow volumes change with thickening ice impinging further on the height of the channel. The resultant reduction of channel height lowers the maximum flow position in the water column as indicated in Figure 7.

The under-surface of ice developing on rivers with high flow are not flat, but undulate based on unsteady flow conditions [48]. Therefore, both the upper surface and lower river bottom of the channel are "rough", leading to additional turbulent production. Ice cover on the rivers changes the vertical transport of temperature and sediment, as well as the distribution of shear stress at boundaries [48]. However, due to its buoyancy, it is safe to assume that ice is always floating and therefore the ice cover of a channel does not lead to pressurization of the flow. Slush at the river edge, and stress cracks and ridges on formed ice are evidence of ongoing readjustment. During the siting of the test facility described in Chapter 3 it became apparent that capture of hydrokinetic power from rivers would be conducted in river areas where the water surface does not freeze over during winter as velocities are above 2 m/s. However, hydrokinetic sites remain vulnerable to frazil ice formation.

2.4.4 Turbulence

An understanding of turbulence is required as the main purpose of this research is to measure the power produced by a hydrokinetic turbine generator in-situ. The testing site selected would represent a typical site for hydrokinetic devices with flow velocities in the order of 2 to 3 m/s year-round and fully turbulent. The placement of the turbine in the water column needs to be properly understood from a power production point of view and the effects of turbulence, ice and debris are required for deployment in remote areas. Moreover, the first ever detailed velocity measurements presented in Chapter 6

demonstrate that there is a significant increase in turbulence intensity ahead of hydrokinetic turbines, due to increased shear from the cross-stream rotation of the vertical-axis turbine. Additional results from this study regarding macro-turbulent flow structures are presented in Reference [10].

The detailed understanding and analysis of turbulent flows has been the focus of considerable work over nearly 100 years, starting with the work of Osborne Reynolds, and later, more detailed mathematical treatment by Prandtl and Taylor in the 1930's. Theoretical and applied studies by Batchelor, Townsend and Kolmogorov in the 1940s and 1950s provided new insights in the field. More current work in this field, by Nobach, Tummers, Tropea and others is also applicable to the present work. Seminal engineering textbooks, such as "Turbulence," by J.O. Hinze and more recently "An Introduction to Turbulent Flow," by Jean Mathieu and Julian Scott [17] continue to deliver the basic and complex underlying concepts of turbulent flow analysis. Nevertheless, exact analytical solutions for all but the simplest cases remain impractical. Thus, measurement, and post-process computational methods are required to produce specific results from the study of turbulence in fluids. Starting with a most basic description, following what is known as Reynolds decomposition, the momentary velocity $U = U(x_i,t)$ of a turbulent flow of fluid can be written as:

$$U = \overline{U} + u \tag{4}$$

where turbulent intensity is defined as

$$u' = \sqrt{\overline{u^2}} \tag{5}$$

Averaging over three velocity components, we estimate turbulent intensity as:

$$u'^2 = \frac{1}{3}(\overline{u_1^2} + \overline{u_2^2} + \overline{u_3^2}) \tag{6}$$

Here, the relative turbulent intensity $\frac{u'}{\overline{U}}$ is a characterization of the turbulence in a given flow. Given that the kinetic energy of a fluid flow with velocity U is:

$$KE = \frac{1}{2}mU^2 \tag{7}$$

and using Equation (4), we can express the average kinetic energy per unit mass as:

$$\frac{1}{2}\overline{U_\iota U_\iota} = \frac{1}{2}\overline{U}_\iota\overline{U}_\iota + \frac{1}{2}\overline{u_\iota u_\iota} \tag{8}$$

with the over score representing a time averaging. Therefore, $\overline{U}$ is the average (mean) velocity and *u* is the fluctuating component, representing the turbulent portion of the flow. Therefore, the total kinetic energy can be thought of as being carried by both the mean flow and the turbulent portion. River velocities are measured with 3-D devices and noted with U, V and W representing the stream-wise, cross-stream and vertical components of velocity, respectively.

Following the work of Kolmogorov, the transfer of energy from the "mean" flow to the smallest turbulence scales results from physical aspects of the fluid in a continuous and cascading process from large-scale turbulence, down to the smallest dissipative scales where kinetic energy is ultimately converted into heat. Furthermore, turbulence is understood to operate through a continuum of vortice-like structures. Mathieu demonstrates this to be true in experiments in both gas and liquids [17]. Analytical solutions are not, in general, possible due to the complex nature of the interactions within the fluid and the sensitivity to initial and boundary conditions, which are evidently changing from moment to moment in most real cases. Nevertheless, from an application standpoint, statistics can be used to establish broad characterizations of flows, so that comparisons between different flows and the reactions of different designs and devices can be measured, compared and considered. For river applications, large-scale fluid motions manifesting as boils and bursts create turbulence and eddies that are significantly larger than what can typically be studied under controlled laboratory environments. It is difficult to find literature that documents how to scale the turbulence characteristics experienced by river hydrokinetic turbines in controlled conditions in a water tunnel. However, it remains pertinent to review how turbulence is understood to help anticipate how it will affect power production and the coupling between the rotor immersed in the water and the electric machine.

Following a traditional approach, there are three types of averaging used in turbulence evaluation:

$$\text{Time Average:} \quad \bar{U}(t) = \lim_{T\to\infty} \frac{1}{2T} \int_{-T}^{T} U(x_0, t)dt$$

$$\text{Spatial Average:} \quad \bar{U}(x) = \lim_{x\to\infty} \frac{1}{2X} \int_{-X}^{X} U(x, t_0)dx \tag{9}$$

$$\text{Ensemble Average:} \quad \bar{U}(x_0, t_0) = \frac{1}{N} \sum_{1}^{N} n\, U_n(x_0, t_0)$$

In the equation for time averaging, it is assumed that the time average is independent of the time interval used, and the turbulence can be classified as *stationary or steady*. In the spatial average, the average value is independent of physical location, and turbulence is further classified as homogeneous. In the last, ensemble average, the value is calculated as an average taken over many different measurement sets, with the same initial conditions, but where the turbulence may be neither homogeneous or stationary. Where turbulence is considered both homogeneous and stationary—all three techniques are assumed lead to the same value—leading to the ergodic flow hypothesis [17].

Based on turbulent measurements at the hydrokinetic turbine-testing site considered in this study, there are too many variables to expect complete homogeneity within the turbulence before and after the turbine. Variability in the mean flow, and therefore in the total flow are known to exist, however, homogeneity in the mean flow is not implied nor required [17] in the analysis of how turbulence affects the rotor and interacts with the electrical machine.

One of the primary reasons to consider homogenous turbulence is that it yields a more exact result from spectral analysis. In his 1938 paper "The Spectrum of Turbulence" [50] Taylor hypothesized that if the mean velocity $\bar{U}$ of the flow is sufficiently large when compared to the turbulence intensity u', then to a first approximation, the turbulence can be considered as 'frozen', and carried along with the mean flow. Therefore, using this hypothesis, one can evaluate the spatial structure of the turbulence by measuring the river flow in one location over a period of time; assuming that the measurements at two times intervals on the river represent the flow at two different locations at the same time.

The objectives given in Chapter 1 do not set out to resolve and model turbulence ahead of the turbine. Only the effects on power production are of interest. Following Kolmogorov's hypothesis of turbulence cascading to smaller and smaller eddies, it is expected that turbulence in the dissipation range will not contribute significantly to electrical power production. However, the momentum carried in the large eddies may contribute along with the mean flow, particularly where their length scales are larger than rotor dimensions. It is expected that each turbine's axis orientation, shape and size will affect its efficiency in a given flow regime.

Referring again to Taylor's 1938 paper, if one considers a turbulent velocity measurement as a signal, one can model the total signal as a composition of many sinusoidal signals of different wavelengths, with more signals resulting in a better model. In this decomposition, referred to as Fourier analysis, each wavelength and frequency is thought to represent a scale of turbulence, and the results can provide insight into how the energy contained in the signal is distributed within the turbulence. Note that common use of spectral analysis in communication theory is based on signals that are a function of time. In the case of turbulence, time is a secondary consideration, and we are looking at the signal for spatial components. Nevertheless, the mathematics are the same. As a matter of convention, and considering the concept of frozen turbulence again, where u/U<<1, one can substitute u(t) for $u(x_i)$.

From the velocity model given in Equation (4), a correlation function can be defined as a velocity correlation function:

$$R_{ij}(x, x', t) = \overline{u_i(x, t)u_j(x', t)} \tag{10}$$

with x' being a slightly different location than x. For an assumed homogeneous turbulence, this correlation can be considered a function of the displacement between x and x', denoted by r. For an infinite displacement, the correlation between the two points trend to zero. However, at some distance, there remains a significant correlation between the velocities

measured at two points in space, and this value estimates the largest scales of turbulence as follows [17].

Using Equation (10) and non-dimensionalizing it by the turbulence intensity u_i' using Equation (5), correlation coefficients are defined as:

$$\rho_{ij}(r,t) = \frac{R_{ij}(r,t)}{u_i' u_j'} \tag{11}$$

For $i = j = 1$ this results in self-correlation, and for r = 0, there is complete correlation of the signal with itself, therefore, the value is normalized and equal to 1. As noted above, the value drops off to zero at some large distance between measurements. The correlation length scale, or integral length scale, in a given direction is determined by integrating the correlation coefficient over the range of r_1:

$$L_{ij}^{(1)} = \int_{-\infty}^{\infty} \rho_{ij}(r_1, r_2 = r_3 = 0) dr_1 \tag{12}$$

This provides a quantitative value of the largest spatial scales of turbulence in r_1 direction (similar for r_2 and r_3). In some cases, for river turbulence measurements in this research, the autocorrelation does not diminish monotonically, and in fact crosses zero at one or more places. O'Neill, Nicolaides, Honnery, and Soria [52] investigated this phenomenon. They recommend that the length scale be evaluated as the area under the correlation coefficient curve and *up to the first zero crossing*. This is the method used in this study.

Evaluating time scales of turbulence, at a fixed point x with a time separation $\tau = t - t'$ taking the place of r in Equations (11) and (12):

$$T_{ij} = \int_{-\infty}^{\infty} \rho_{ij}^{(t)}(x,t) d\tau \tag{13}$$

Going back to Equation (10) and using the time variable τ, then one can write:

$$R_{ij}(\tau) = \overline{u_\iota(x,t) u_J(x,t')} \tag{14}$$

as an autocorrelation, and define the Fourier transform pair as:

$$R_{ij}(\tau) = \int_{-\infty}^{\infty} \psi e^{i\omega\tau}(\omega) d\omega \quad (15)$$

$$\psi_{ij}(\omega) = \frac{1}{2\pi} \int_{-\infty}^{\infty} e^{-i\omega\tau} R_{ij}(\tau) d\tau \quad (16)$$

This transform pair allows use of the autocorrelation of a river velocity signal to evaluate the time correlation of the turbulent components [17]. The autocorrelation can be calculated in accordance with Equation (15) using built-in functions in Matlab® or DADiSP®. To look in some detail at the energy spectrum as a function of frequency, the power spectral density (PSD) can also be calculated from the velocity signal, with built-in functions performing calculations based on Equation (16).

At one end of the spectrum, the largest structures superimposed on the mean flow are the large eddies, to which energy is transferred from the mean flow. The eddies are stretched in the stream-wise direction and through a process of interaction between other eddies (presumably large and small). These breakdown into smaller eddies at a rate equal to the dissipation since at the smallest scales kinetic energy is lost to thermal energy through viscous dissipation [17].

In between these two ranges is known as the inertial range, where energy is transferred to smaller scales of turbulence. With respect to the spectrum in this range, there is interest in determining what scales of turbulence as considered by wave number or frequency effect the performance of a river hydrokinetic turbine.

For river flows, the non-compressible and fully turbulent equations of motion are the Navier-Stokes equations written as:

$$\frac{\partial U_i}{\partial t} + U_j \frac{\partial U_i}{\partial x_j} = -\frac{1}{\rho} \frac{\partial P}{\partial x_i} + \nu \frac{\partial^2 U_i}{\partial x_j x_j} \quad (17)$$

$$\frac{\partial U_i}{\partial x_i} = 0$$

Using Equation (1) to replace U in Equation (17) we get the Reynolds time average equation:

$$\frac{\partial \overline{U}_i}{\partial t} + \overline{U}_J \frac{\partial \overline{U_i}}{\partial x_j} = -\frac{1}{\rho}\frac{\partial \bar{P}}{\partial x_i} + \nu \frac{\partial^2 \overline{U}_i}{\partial x_j x_j} - \frac{\partial \overline{u_i u_j}}{\partial x_j} \qquad (18)$$

which describes the flow experienced by the turbine. The evaluation of the stress tensor subject to the appropriate boundary conditions is beyond the scope of this study. The objective is to provide a dataset that quantifies the velocity fluctuations in the vicinity of an operating hydrokinetic turbine.

2.5 Environmental considerations

In 2010, the Alaskan Center for Energy and Power studied the use of hydrokinetic turbines in remote communities [52] with an update in 2011 [53]. The concept was to determine if a hydrokinetic turbine could be used to displace existing diesel fired generation for remote communities along the waterways in Alaska. An example of such a community is the town of Igiugig, which operates three diesel generators with capacities of 60 to 100 kW. Electrical demand on the system range from 40 to 95 kW, peaking during the winter months. In the first test a 5-kW vertical-axis rotor/generator combination was suspended from a pontoon boat. The system was set up at the site by New Energy Corporation Inc., and was nearly identical to the 5-kW unit used in our research at Point du Bois. While the rotor and test platform operated as expected, the slow speed of the water near the shore inhibited significant power from being generated. The pontoon was then moved and anchored out further into the stream of the Ruby River. In this location, debris quickly accumulated on the front of the pontoon boat and required continuous maintenance. The power cable brought to shore was abraded by being in contact with rocks at the river bottom and failed within four days of operation.

Similar results on the Yukon River near Eagle Alaska, with New Energy's 25-kW vertical-axis rotor occurred with floating debris and power cable failures inhibiting long-term operation. The same study also included a horizontal-axis, cross-flow dual Gorolov rotor turbine, built by Ocean Renewable Power Company and placed in the Cook Inlet on

Alaska's south-east shoreline. This location allowed for the testing of hydrokinetic turbines for tidal energy capture. The use of Gorolov-style turbines allows for energy capture of both incoming and outgoing tide flows. Data provided demonstrate that the design power of 30 kW could be achieved at flows of approximately 2.5 m/s, and that power is produced in a range of flows, from 0.5 to 2.5 m/s in both ebb and flood stages. Some of the conclusions of this study include:

- Flows may be reduced in the winter months to below operational minimums of 1.5 m/s.
- Frazil ice is capable of forming from initial freeze up to spring thaw. This frazil ice forms as small flakes in super-cooled water, and will gather downstream on almost any obstruction or surface, confirming our own results. Tests were done on various materials, including Teflon, ABS plastic, stainless steel and steel and all accumulated frazil ice.
- Floating debris is a significant factor, particularly in spring and flooding events, where larger logs and brush are dislodged and can accumulate to a catastrophic failure.
- Underwater cables bringing the generated power to the shoreline are also vulnerable to floating and submerged debris, as well as chafing against rocks.

In 2011, further studies were performed at the Tanama River in Alaska by the University of Alaska Fairbanks and reported on by Fochesatto and Toniolo [53]. In this study, detailed acoustic Doppler current profiler, ADCP, measurements were taken at 12 locations along an 1,100 m stretch of the Tanana River. Samples were taken at 200 m intervals along the river with a vertical resolution of 0.25 m, down to within 1 m of the river bottom. The goal was to capture the details of both the mean flow kinetic energy and the turbulence kinetic energy in the column of flowing water. The authors determined that recording intervals of 15 minutes were necessary to capture the larger eddies based on timescales equivalent to 1.5 times the river depth, which was 15 m. In their analysis, the authors followed a method developed for atmospheric studies where the airflow direction is constantly changing. In

the case of the Tanama River, the segment of river under study was not straight. They used a streamline coordinate rotation, to project the 3D coordinate system of the ACDP into the flow direction at the various depths, before processing the turbulent kinetic energy data. The results of this study provide a good understanding of how the river bottom morphology can affect the maximum flows within the cross section of a natural and varying river. The maximum horizontal flow angles from north direction were generally located away from the greatest river depth. In the vertical direction, a location in the river was identified where a helical cork-screw rotation of the main flow reflected a change in the momentum from one side of the river to the other.

With respect to the average kinetic energy and the turbulent kinetic energy, the study concluded that turbulent kinetic energy within the bulk flow of the river were accentuated in areas of river bottom depressions and made up as much as 30% of the overall kinetic energy of the flow. In locations where the river bottom is more flat, the percentage was an average of 5%. While the authors do not draw this conclusion, it is likely that the change in river depth results in transport of momentum, and therefore kinetic energy in the form of turbulence, to the additional water volume below. Further discussion related to the Point du Bois test site specifics is included in Chapter 3.

For river site selection, 3-D studies of fluid structures may be necessary where devices are located in meandering rivers. According to Open Hydro [55], due to the overall regularity of tidal stream flows, a 24-hour sample of the velocity profile at a site may be sufficient to evaluate a tidal resource.

2.6 Turbine deployment factors

Hydrokinetic turbines are often supported on the surface of the river using a vessel, or from the river bottom using a gravity base. Other possibilities are to provide support from an existing structure, such as a weir, a bridge, or water output structure. There remains no deployment yet of a flow-supported turbine which can sustain itself within the vertical column of the water; like the way a kite remains aloft in the wind. The horizontal turbine

testing in this project was developed as a stepping-stone to evaluate this kite concept. Cost of deployment and retrieval varies with the turbine design and the site. Parameters that affect deployment include river depth and width, road access, and shore ice in winter. Table 4 summarizes the deployment methods and their associated benefits and challenges.

Table 4: Summary of hydrokinetic turbine testing facilities

Method	Benefits	Challenges
Floating	Easy access for maintenance Access to the highest flow Low deployment cost	Surface traffic interference Ice jamming Debris, logs and ice impact
River Bottom	No surface traffic interference	Low energy zone Costly maintenance Alignment challenges
Pillar	Easy access for maintenance Easy height control	Surface traffic interference Expensive
Kiting	No surface traffic interference Access to the high-energy zone Potential to adjust operating depth	Stability issues

For hydrokinetic power generation to be viable in Canada, the technology must be able to operate during winter conditions. There are many issues related to cold conditions that influence performance and pose risks to equipment and personnel. Moreover, frazil ice, described as sticky ice particles suspended within a flow, can have a serious impact on any device operating in super cooled water [48]. The seasonal cycles of northern climates also introduce a variety of floating debris in the form of icebergs and logs [52]. The ability to operate at different depths to avoid expected ice and debris and to adjust to the variable depth of peak velocity (as shown in Figure 7) is an important advantage of a kiting deployment method. Traditional hydroelectric structures are designed to withstand the forces of impacting debris and keep them from entering the turbine. However, it requires ongoing maintenance to clear trash racks and log flumes. Hydrokinetic systems are more vulnerable to these hazards because they are constructed with minimal protection to keep infrastructure costs reasonable and to minimize the impact on the local ecology. Costs will have a more significant effect on river hydrokinetic power generation because it is harder

to justify the operational costs when revenue magnitudes are smaller for hydrokinetic compared to traditional hydro. To determine if river hydrokinetic power can be a reliable renewable technology in the future, ice issues, operational issues, and cost issues need to be investigated further.

For frazil ice to develop, three main factors must be present: super cooled water, low ambient temperature, and turbulence [48]. In areas of fast flowing water without ice cover, heat transfer between the fluid and the air enable the fluid to become super cooled. The US Army Corps of Engineers states that flows greater than 0.6 m/s are fast enough to produce frazil ice [56]. Nucleation is the mechanism through which ice initially forms. For pure water, super cooled to -40°C, spontaneous nucleation known as homogeneous nucleation may occur. This is an unlikely mechanism in nature, since river water of interest is not in a pure state. More common is heterogeneous nucleation resulting from nucleation of super cooled water onto a foreign particle or surface. Supercooled drops, re-entering the stream from splashing, crystals from condensing vapor just above the surface and dust particles are more likely sources. Secondary nucleation is the shearing of potential crystals from their parent crystals when the parent crystals collided with a hard surface or other crystals, resulting in an increase in particles and further frazil ice development. Turbulence is required to generate the shearing and collisions between parent crystals as well as mixing the coldest surface water in to the flow reducing the temperature.

Although frazil ice formation is associated with turbulent flows, turbulence does not guarantee the presence of frazil ice. Sufficient density of nucleated particles must exist for the growth of frazil ice. The presence of frazil ice in a flow adversely effects power generation by blocking intake areas [56] or changing channel hydrodynamics. In addition to natural sources, the presence of hydroelectric dams and their operation create open areas with high flow and turbulence, and therefore frazil ice conditions. For river kinetic turbine applications in cold climates, hydrokinetic sites are found in areas that do not form ice cover, and are therefore turbulent and high flow areas, subject to frazil ice.

Anchor ice is another phenomenon, which occurs when active frazil ice attaches to the river bottom or other surfaces below water level. Development of anchor ice affects the hydraulic characteristics of the flow by displacing normal flow patterns. Layers of frazil ice increase the drag force on the anchor and mooring lines and adds buoyancy forces. These factors must be considered in force calculations for cable and anchor sizing. Anchor ice is also known to attach itself to rocks at the riverbed and transport them hundreds of meters downstream of their initial position. These may float to the surface or contact mooring lines or the hydrokinetic turbines. Anchor ice formations on a mooring line may also restrict the flexibility and change the orientation of the system.

3. Site assessment

To achieve project objectives, the development of a water-to-wire turbine-testing site for cold weather operations was required. This section describes the site assessment and regulatory framework required as part of the scientific methodology.

3.1 General location

One of the primary considerations of this research is to test hydrokinetic devices in summer and winter conditions, and simulate deployments typical of remote northern communities. For remote communities, the potential turbine site characteristics include:

- Close proximity to the electrical load to be supplied reducing cable costs, parasitic losses, and minimizing response time for maintenance.
- Water depth suitable for deployment of the turbine near the surface, in the highest velocity ranges, but below any ice floes.
- Water velocities nominally 2 to 3 m/s.
- An understanding of ice thickness, ice floes, and normal frazil ice phenomenon in the area.

The use of satellite imagery, such as the Moderate Resolution Imaging Spectroradiometer operated by NASA [57] allows for a high-level view of possible hydrokinetic site locations. Images taken in the winter which show where open water exists may be indicative of velocities greater than 1.5 m/s. Figure 8 shows an example of river open water near the St. Lawrence River where the river upstream and downstream of the location are frozen over, indicative of higher flow levels.

The Point du Bois, Manitoba site was chosen as the test site for several reasons. To test the devices in the winter months and maintain access, open water was available in winter months at this site. The turbines included in our testing were optimized for 2.5 to 3 m/s velocities which are available most of the time at this site. Moreover, access to the utility electrical grid at distribution voltage level was nearby. The test site also included road

access, a fire hall and hospital in close proximity. Given the cold climate and fast moving water, this was deemed important for safety for the research project. In a less developed area, shore ice would be expected to impede access to the water and therefore reduce safety when moving near open water. The existing footbridge provided a suitable access point, lowering testing costs by reducing the number of procedures required by boat. The bridge piers also provided an opportunity to measure flow velocities and turbulence, which develops around such obstacles. Bridges are probable locations for hydrokinetic turbines since they are often located at river narrows, access is available and the roadways are good pathways for power lines to follow [52], [58].

Figure 8: MRIS image of St. Lawrence River by NASA. Magnified inset area shows open water (black color) on an inland where river ice has not formed, indicative of sustained water flow near Saguenay, Que. NASA image credit to Jeff Schmaltz [46].

Initially, three site candidates test sites were found on the Winnipeg River, which are shown in Figure 9: Pointe du Bois, Seven Sisters, and Whitemud Cut. All three sites had

suitable water velocities, but Pointe du Bois was selected based on its overall advantages such as proximity to the hydro plant for safety personnel, access roads, distribution lines, enclosed protected areas, and access to heavy lifting equipment.

Figure 9: Three potential sites: (a) Pointe du Bois generating station, views upstream of footbridge, (b) Seven Sisters generating station tailrace channel, present site of the Canadian Hydrokinetic Turbine Testing Center, and (c) Whitemouth Cut, where flow velocities are higher, but high turbulence and standing waves increase personnel hazards.

At the selected site shown in Figure 10, the walkway bridge provides access to the research platform located just beneath to allow safe winter access to the turbine. A control center and grid connection facility was established inside a trailer located near an existing

overhead line near the shore. A 240 V split-phase (two phases plus grounded conductor) grid connection as well as a 600 V three phase grid connection were established with bi-directional metering. The proximity of the control center trailer to the bridge kept control and monitoring cable lengths to a minimum. However, approximately 80 m of cable allowed for the effects of cable lengths to be studied. Power (120/240 VAC) was supplied to the working area of the research vessel from the opposite shore. Ethernet data cables and video camera cables were established to link the site trailer to the test platform.

(a) (b)

Figure 10: Point du Bois test site: (a) powerhouse at the bottom and spillway on the right-hand side and up to the right, (b) is magnification of the footbridge/test area. Note the pontoon test platform at the left-hand side of the bridge, near shore before deployment.

Manitoba Hydro operates a 16 unit 78 MW hydroelectric dam located in the town of Pointe du Bois near the border between the provinces of Manitoba and Ontario on the Winnipeg River. This location is part of the Canadian Shield geomorphology and presents large areas of exposed igneous and metamorphic rock [59]. In this area of the Winnipeg River, the rock is near the surface of the riverbed and is suitable for a drilled anchor. In Figure 10(a),

to the right and downstream side of the spillway, the exposed rock is typical for this area. Figure 11 shows the test site and open water conditions in mid-winter.

(a)

(b)

Figure 11: Aerial views of test site at the Point du Bois generating station in winter, photo (a) from the north-west, photo (b) from the south-west. Arrow indicates test location. Open water shown remains open all year due to spillway operation and water flowing through the powerhouse or spilling. The upstream eastern reach of the Winnipeg River to Ontario is up and to the right in photo (b).

Flow velocities in the forebay test location vary between 2.1 to 2.5 m/s except in occasional drought conditions. The flow is regulated by Lake of the Woods Control Board, which can change the upstream flow from Ontario at any time. However, Manitoba Hydro controls

the forebay to suit the power production requirements by bypassing excess flow through the spillway.

3.2 River, bathymetrics and flow

An acoustic Doppler current profiler, ADCP, was used to measure the mean flow characteristics, and identify the locations with maximum velocity. The ADCP profiler was mounted on a jet boat, allowing shallow areas with unknown rocks to be included in the survey. Bathymetric profiles and flow measurements throughout the channel were recorded. ADCP measurements from a boat are effective for recording the hydrodynamics of a river, and are routinely performed by hydro electric utilities such as Manitoba Hydro in this case. The model used was a Rio Grande manufactured by Teledyne. The device nameplate indicates an accuracy of ±0.25% of water velocity relative to the ADCP or ±2 mm/s and includes a GPS for 3D positioning. According to the USGS manual for Measuring Discharge with Acoustic Doppler Current Profilers from a Moving Boat, for velocities greater than 0.24 m/s, the velocity measured has an average coefficient of variation of 2.5% (standard deviation divided by the mean). For detailed results, four transects are recommended, two in each direction. Figure 12 shows the boat paths taken and geomatic survey markers 05PBDU and 05PDB8 on the left were used for reference. Four cross-stream passes were included in the test area between piers 2 and 3 near the bridge, three in the immediate downstream area and at least two in the upstream (outer) forebay.

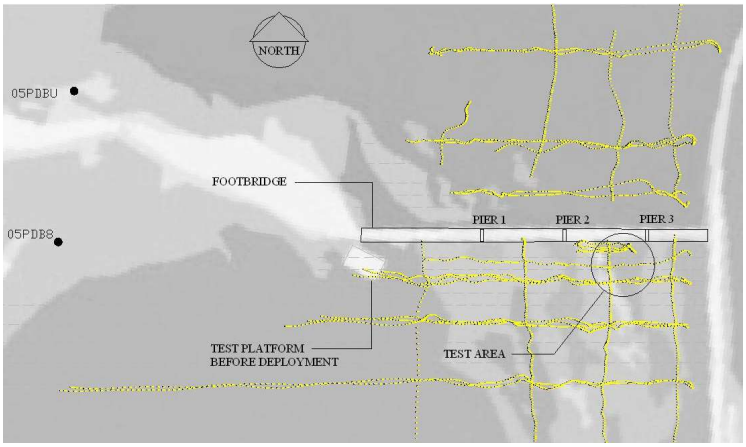

Figure 12: GPS coordinated bathymetric and ADCP measurement trails overlaid on site image from Figure 10, with surface wakes and undulations in the channel flow shown in grey, and the test platform in docked position before deployment.

The ADCP data was compiled and velocity profiles were created. Figure 13 indicates average velocity. The highest velocities indicated in dark orange color and representing velocities in the order of 2.1 m/s are just downstream of the footbridge where bridge piers create a wake and on a shoal of shallow depth. Approximately 100 m downstream of the footbridge, the newest turbine generator of the 16 located in the Point du Bois powerhouse draws significantly more water that the others, and therefore the velocity is consistently higher at that location.

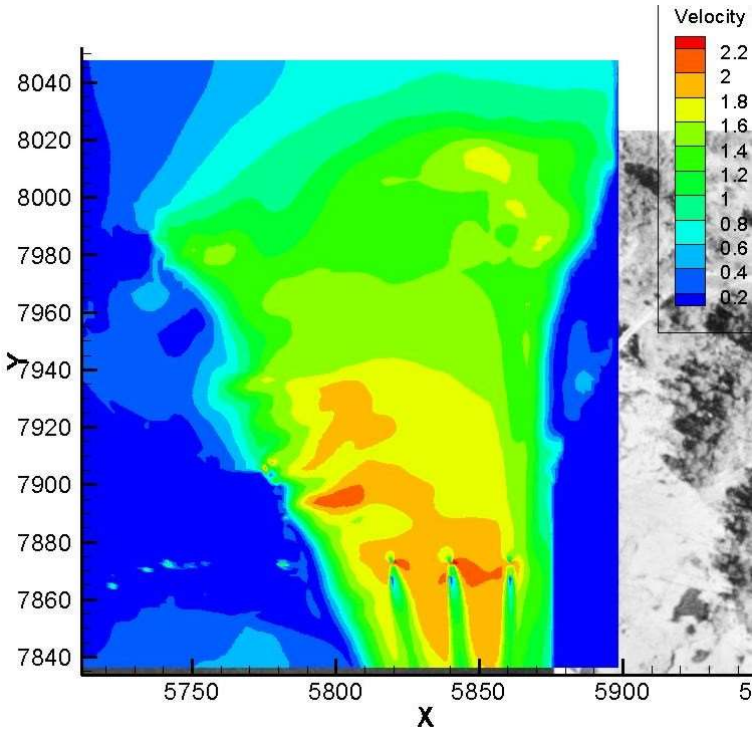

Figure 13: Average velocity for the test area near the footbridge, overlaid on an aerial photo of the site, compiled from ADCP data.

In addition to ADCP measurements, two calibrated turbine flow meters were lowered into the flow downstream of the bridge, using a large weight, to validate the ADCP measurements. These two meters measured flow velocities comparable to the ADCP, and are shown in Figure 14.

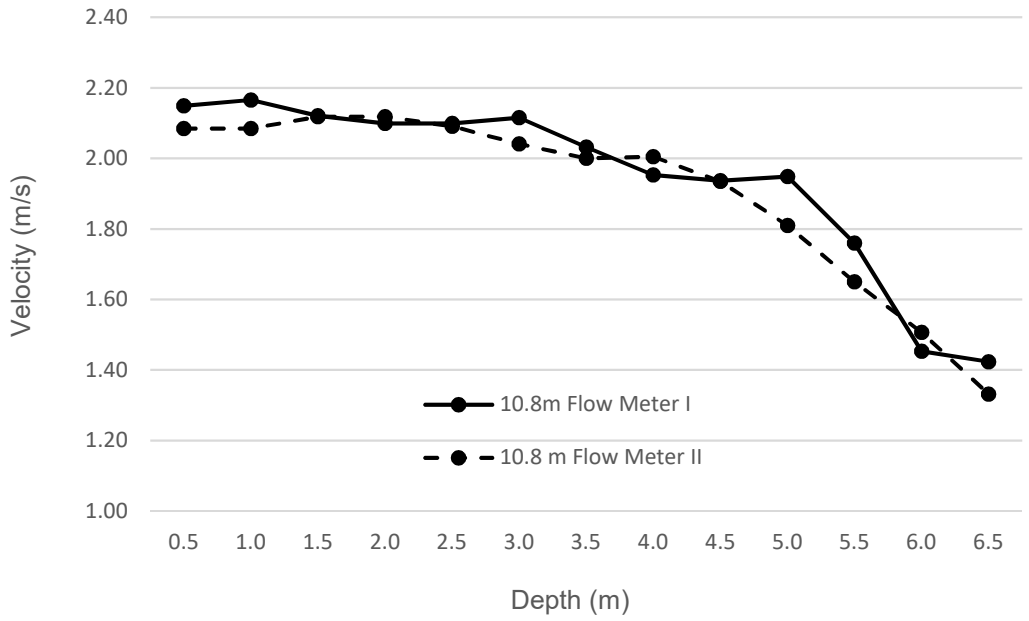

Figure 14: Verification of ADCP measurements using two turbine flow meters on the downstream side of the walkway bridge.

The detailed ADCP measurement allowed for a comparison of measured flows to those predicted by Manitoba Hydro as part of their spillway redevelopment project [45]. Figure 15 shows a plot of velocity profiles measured (grey and black) and those predicted by a 3-D flow model developed by Manitoba Hydro. This model uses a 'power law' similar to Equation (3) to estimate the velocity profile. The Flow-3D® modeling is outside of the scope of this project, and requires expensive software which was not available. However, in addition to the data provided for Figure 15, Manitoba Hydro shared some of the renderings from the model which are included in Appendix 3. These are useful to visualize the nature of the flow in the region of the test site, but are not considered essential to selection of a suitable site.

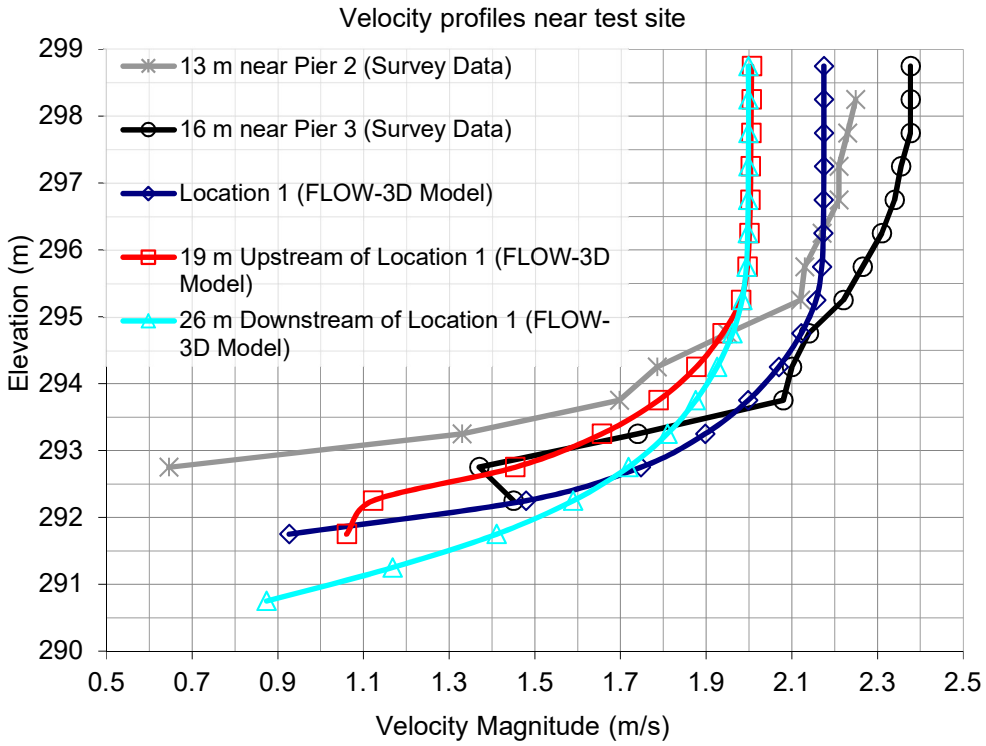

Figure 15: Measured velocity profiles and predicted velocity profiles based on data provided by Manitoba Hydro from a Flow-3D® model of the site. Additional graphical outputs from the model are included in Appendix 3 for reference. 13 m and 16 m indicate measurement position, offset from Pier 2.

Figure 16 shows the calculated velocity profile for the test position at Point du Bois and the relationship to the horizontal and vertical-axis turbines studies in this project. For an ideal fully-developed turbulent flow velocity profile the average velocity is relatively constant across the turbine. In the zone near the river bottom, where shear forces are developing turbulence, this is not the case. As discussed in Section 2.4.3, below the turbulent boundary layer the velocity gradient is significant and influences both performance and design for hydrokinetic turbines.

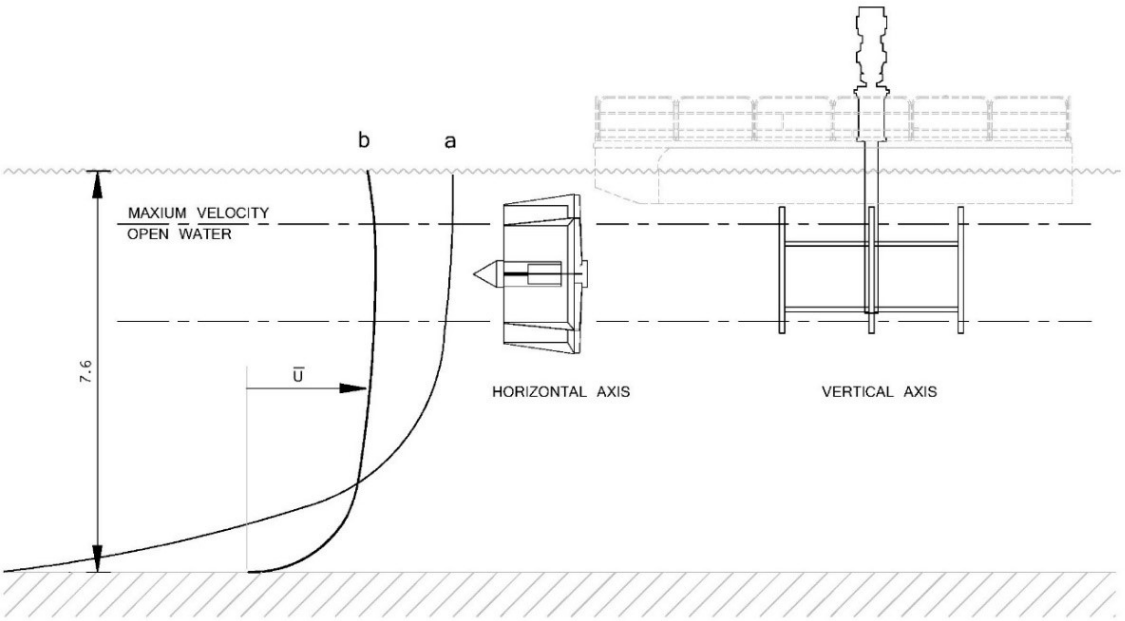

Figure 16: Representative water average velocity profiles: (a) calculated by FLOW 3D® model "Location 1" from Manitoba Hydro study [45], and (b) idealized fully developed flow. Shown with relative position in the water column to the horizontal and vertical-axis turbines tested in this project.

3.3 Permits and approvals

The permitting process for the installation of hydroelectric generation stations on a river can take five or ten years. At the time of the permit application for the research test facility, there were no established protocols for operating a river hydrokinetic turbine in Canada. For this first project, all relevant authorities were contacted and informed. The responses and comments for permits from each agency are summarized below. The list is included to assist other marine energy projects in identifying the challenges of the permitting process early in the development process. Permitting is part of the research methodology and cannot be overlooked.

3.3.1 Manitoba Conservation and Water Stewardship Branch

This permit regulates environmental assessment in Manitoba. However, a permit is only necessary for permanent installations, and hence was not required for this project.

Nevertheless, the Conservation branch's role is to inform the applicant of all Federal and Provincial permits required, and is therefore the starting point. Currently, if a provincial environmental assessment is completed, a federal assessment is not required. For this project, only a provincial assessment application was completed.

3.3.2 Manitoba Parks

The Manitoba Parks permit regulates and issues permits for use on Manitoba crown land. A parkland permit was not required for this project as the research lab was located on property already controlled by Manitoba Hydro. However, a scientific permit was required, applied for, and issued. This permit required a yearly renewal.

3.3.3 Manitoba Water Resource Branch

The Water Resources Branch of the Manitoba Department of Natural Resources administers the Manitoba Power Act and grants licenses for the development and operation of water power facilities, such as the generating station at Pointe du Bois. Temporary installations to gather data do not require a permit from this governing body; however, formal clearance was obtained. It is anticipated that the installation of a hydrokinetic turbine systems installed for generating power would require a license.

3.3.4 Fisheries & Oceans Canada

The primary objectives of this agency are for regulation of the fishing industry. A legal authorization is required where the Fisheries Act applies and this department provides advice where the act does not specifically apply. Consideration of drilling sediments and the potential impact on fish spawning-time restrictions were the primary concerns of this group. Fish mortality was not considered an issue due to the temporary nature of the installation. Furthermore, there is no scientific evidence of interference of fish from slow rotating equipment (such as hydrokinetic turbines).

3.3.5 Navigable Waters Protection Program

The Navigation Protection Act is administered by Transport Canada. As this project pertained to a research and development platform, the main issue was maintaining public access and ensuring that mooring lines do not obstruct other water traffic. Proper signage was required to alert the public of any obstruction imposed by the project. Application to Navigable Waters also triggered a First Nation consultation process.

3.3.6 Manitoba Hydro Land Permit

For this project a secondary land use permit could have been obtained. Manitoba Hydro staff and generating station operations crews were aware of the project and kept up to date on the project status. The project did not affect operation of the hydro plant. Therefore, a land permit was not deemed necessary.

3.3.7 Provincial Land Permit

The bottom of the river is owned and regulated by the Province, under the Crown Land Act. This project required two anchors to be installed on the river bottom, in the forebay of the hydroelectric development. These areas are controlled by Manitoba Hydro and did not require a special land permit at this location for this project.

4. Anchoring and turbine deployment

The development of a reliable low-cost anchoring method is an important contribution to water-to-wire installation, as this emerging industry requires innovative ways to perform tasks in fast moving waters; safely and affordably. Implementation of a new low-cost anchoring system addressing research objectives is described in this Chapter.

4.1 Anchorage

Rivers on the Canadian Shield offer a solid rock riverbed that can secure a drilled anchor reliably. However, inexpensive installation techniques to drill and install anchors in rock 10 m below the surface in 3 m/s flows were unknown. Most installations of this type use a barge with legs secured to the bottom, also known as a "spuds". The cost to mobilize such a barge to the site or retrofitting an existing barge exceeded our $35,000 anchoring budget. Unlike tidal installations that have slack tides, suitable river hydrokinetic turbine sites have uninterrupted flows. Figure 17 shows relevant locations used to deploy riverbed anchors.

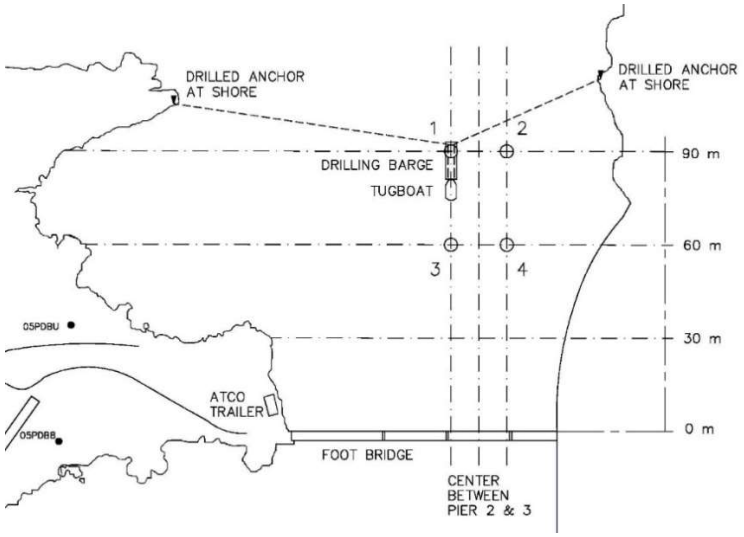

Figure 17: Anchoring plan showing selected anchor locations numbered 1 to 4, two shore anchor points for positioning winch connections and relationship to the footbridge and test site, located between Piers 2 and 3.

Note that for turbine farm applications, the method proposed is even more cost effective, as most of the cost is due to mobilization and de-mobilization of equipment. Based on the experience gained in this project, two or more anchors could easily be drilled and set in one day, and two anchors were adequate for each hydrokinetic turbine tested. As shown in Figure 17, a broad range of drill locations across and down the river can be reached with this method using only two on-shore anchors. Additional pairs of anchors, up or down stream would provide a complete range for a turbine array – without having to redeploy the vessel.

4.1.1 Drilling rig

The turbine anchoring method developed was to equip a flattop barge with a diesel-fired air compressor to power a pneumatic drill and two 1.8-tonne drum-type winches for positioning the barge over the anchor point. A tugboat transported the barge from its landing dock, to the upstream channel. Figure 17 shows where steel cables connect to pre-installed anchors drilled into the shore rock. Using slow payout of the winches on either side of the barge, and with the tugboat applying a stabilizing upstream force, the barge was moved to each anchoring locations and held stationary at each location. This arrangement provided a stationary platform so that rock anchors could be drilled into the river bottom. Figure 18 shows a simplified diagram of the equipment for installing river anchors using a floating barge. Figure 19 are photos of the drilling barge in position. In the final setup, the positioning winches were placed at the downstream end of the barge, with sheaves on the outboard sides near the bow. This provided a necessary degree of freedom for the alignment of the cables with the fixed anchor positions on the shoreline. Without the sheaves, the cables would bind against the side of the spool when the angle from craft to shore increased, as the barge moved away from shore and downstream.

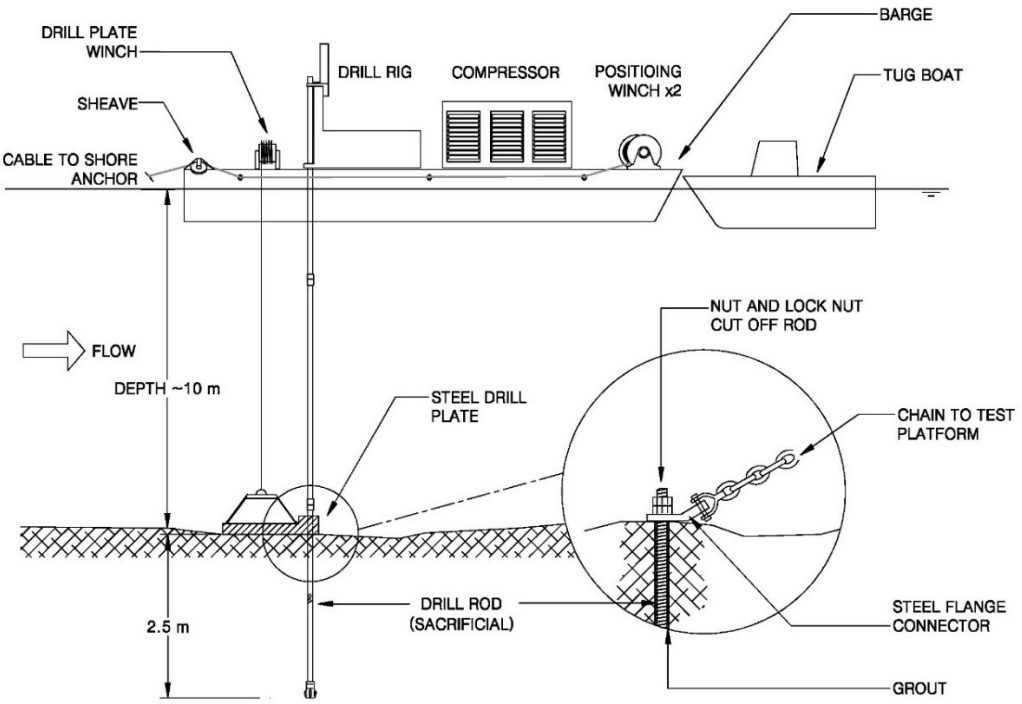

Figure 18: Simplified diagram for drilling barge showing essential rented equipment: two 2-ton positioning winches, drill plate winch, drill rig, compressor, tugboat for initial positioning and stability.

(a) (b)

Figure 19: Drill rig barge in anchor position: (a) the tugboat, compressor with the drill rig extending above, and (b) looking downstream at the compressor and front of the tugboat, the footbridge and pier 3 test area in the distance. A red safety boat is shown tethered to the barge. All procedures adhere to labor codes, including staff with valid CPR training.

Once the drilling barge was moved into place, the lever brakes on each winch were engaged, providing a temporary but secure mooring for the drilling procedure. The drill rig was a track mounted, pneumatic operated drill rig for hard rock uses, employed for drilling holes for rock blasting, as shown in Figure 20.

The river anchors are made of hollow steel drill rods drilled in the riverbed and cement grouted to the bedrock. These types of anchors are used for mining applications and rock wall stabilization. Figure 20 shows the drilling set up and a typical 38-mm diameter threaded drill rod with the cutting head welded on. Welding of the cutting head allowed the drill bit to be reversed if necessary without coming loose.

(a) (b)

Figure 20: Drilling rig setup for river bottom anchor drilling at the dock: (a) cutting bit welded onto the end of the rod with holes in the cutting tool to allow grout to be pumped through the rod and out into the cut hole, and (b) red winch in the foreground used to lower the drill plate.

The drill rig was suitable for boring 30 m deep holes. However, the hard granite rock and the 10 m of unsupported rod in the water column inhibited the drill bit from getting started into the rock. To address this issue, a steel drilling plate was fabricated, and included a 150-mm diameter collar at one end, as shown in
Figure 21(c) and in Figure 18.

Figure 21: Clockwise from left: (a) barge in place at drilling location 2, buoy marker in water and yellow marker on shore provide alignment, (b) rock anchor on shore for 9.5 mm (3/8”) positioning cable from winch on the barge, and (c) the drill plate on shore showing collar for drill pipe on right and lowering brace with adjustable balance points.

The drill plate and rod were lowered to the bottom simultaneously, with the collar acting to hold the drill bit in place at the bottom. To ensure that the drill plate would remain level during the lowering procedure, each of four connection points was provided with a welded bracket with several adjustment holes, and short lengths of chain connected to a spreader beam. The proper balance was achieved on shore by lifting at the center of the spreader bar and adjusting the four connection locations to suit. Once the anchor rod was in place and filled with cement grout, a tethered diver was lowered to the bottom to cut off the excess rod. A steel connecting plate was placed over rod, and two nuts were threaded on, one acting as a lock nut. Figure 22 shows underwater photos of the final anchors and Figure 23 shows the connection plate and yoke-style main chain shackles.

Figure 22: Three still shots of the on-board video display from underwater camera of final anchor points showing where rod was cut-off underwater using a torch. Overexposure in these photos is due to highly reflective yellow paint on chain shackles and the light source from underwater camera.

Figure 23: One of the 13 mm (1/2”) thick steel rock anchor connection plate and shackle showing master link and chain assembly before deployment. For a permanent connection, the plate would be hot-dip galvanized or otherwise coated to resist corrosion.

4.1.2 Underwater work

The initial design criteria for installing these anchors was not to use divers. Ultimately, underwater work was required as we could not leave the barge in the forebay for long enough to allow the cement to set properly before decoupling the drill rod from the anchor. An additional mechanism to allow the nuts to be threaded down from the water surface and cut-off the excess rod was conceived, but was too complicated to construct on site. The simplest solution was to employ divers to make the final connection. This included cutting off the excess rod with an underwater cutting torch, placing the connection plate over the rod and threading on and tightening the nut and lock nut. The chains were secured to the connection plate, with a heavy rope and two marker buoys attached for subsequent retrieval.

Workplace Safety and Health regulations in Manitoba require the employers of commercial divers to ensure that the divers meet the requirements of CSA Standard Z275.4-97 Competency Standard for Diving Operations. Although there are exceptions for scientific work, due to the significant flows in the generating station forebay, Manitoba Hydro allows only surface-supplied, or tethered, diving in the area. This method requires more equipment, with breathable-air compressors, helmets and hoses, but is significantly safer. The diver is constantly monitored from the surface craft with video and audio and harness-connected to a strong cord or tether; which can be used to stabilize the diver or pull them to the surface, as shown in Figure 24. In addition to air supplied from the surface, the diver also wears a portable air tank for backup. A minimum team is four, with one person monitoring the diver, a person to assist the diver in-and-out and manipulate the tether/hoses, and a backup diver who remains geared-up and ready to assist the diver in the water. Note that for the sites considered for kinetic turbines in this project, the divers would generally not exceed the 10 m (35 ft.) non-decompression depth. Therefore, there is no danger of decompression sickness should the diver need to be brought to the surface in an emergency. In general, it is not safe to dive in velocities above 1.5 m/s, therefore the anchors are located well upstream of the test site. As previously noted, the drilling procedure described can be modified to eliminate the need for divers by developing a

mechanism, fit onto the drill rod or drill plate, to terminate the lock-nuts and cut the drill rod.

(a) (b)

Figure 24: Surface-supplied tethered diver entering water to perform final cut-off of drill rods and install connecting plate and nuts. Back-up diver (red suit) provides assistance and is geared-up for quick response.

4.1.3 Rock anchors and mooring

Minimum design strength for the anchoring system was determined by considering the maximum drag of the largest turbine expected to be tested at the site. Using drag versus water velocity calculations supplied by turbine manufacturers and the expected maximum flow velocity of 2.6 m/s, the maximum force applied to the main cable by the turbine was estimated to be 64 kN. The manufacturer's published data on the rock anchors gives a yield strength of 400 kN each, which is one half of the anchor's tensile strength. This is generally a conservative estimate for ductile materials, where the generally acceptable ratio of shear yield strength versus tensile strength for ductile materials per the von Mises calculations is 0.577 [61]. For design purposes, the shear stress between the rock and cement was assumed to be 1,380 kN/m^2 (200 PSI), and between the rod and the cement 2,760 kN/m^2 (400 PSI). The main support cable was connected to a main link, which was shackled to each of the two anchor points using 19 mm (3/4") steel chains, forming a 60° angle. The chains are rated for 126 kN (14 tons) each, not including a 4 to 1 safety margin. According to the

manufacturer's published data when two chains are connected in 60° angle configuration the resultant strength is 218 kN (49,000 lb). Therefore, the safety factor is 218/64 = 3.4, not including the four times working load versus yield strength of the chains. This allows for the added drag of the pontoon boat, additional loads such as the anticipated ice buildup, the dynamic loads when the turbine is started, and an allowance for corrosion.

4.2 Test platform deployment

Deployment of the research platform into a 2.2 to 2.5 m/s flow requires detailed planning and safety precautions. Four different deployments were carried out using the two main anchors, wire rope cables, nylon ropes, winches and an outboard motor. With the exception of the roadways, all of the equipment was brought to the site, assembled and launched with minimal reliance on existing infrastructure. The initial planning was based on the 2.4 m diameter horizontal-axis turbine mounted to the downstream side of a flat-bottom aluminum boat. However, due to delays in delivery, three alternative turbine generator sets were tested ahead of its arrival.

The research vessel, referred to as the test platform when moored, was an aluminum pontoon boat with a deck measuring 9.1 m by 5.5 m (30 ft. by 18 ft.), the width extended for this project to accommodate the 25-kW turbine. The pontoons are 0.9 m (3 ft.) wide and 1.1 m (3½ ft.) deep allowing for a maximum payload of 4.5 tonnes. The deck consists of five panels, 2.4 m by 1.2 m (8 ft. by 4 ft.) on two main struts running the length of the vessel. The total weight with the 225 HP outboard motor was approximately 3,630 kg (8,000 lb.). The deck panels were removable, with steel bolt-down clips. This allowed for re-configuration of the openings to suit the various turbines tested at the site. Figure 26 shows several views of the vessel and deployment.

4.2.1 Winter deployment

New Energy Corporation provided an aluminum pontoon boat with a 225 HP outboard motor and used as the test platform for all three of New Energy's turbines. Use of the outboard motor on the pontoon boat simplified deployment by eliminating the need for the

onboard winches and cable connections to the shore. One of the shore anchors was used as a safety cable point. The pontoon boat could traverse the river to the main anchoring point buoys, for connection of the support cables. Figure 25 shows the overall plan, and vessel deployment details follow. New Energy transported the research vessel and turbine via a flatbed trailer from Calgary to the Pointe du Bois test site. The pontoon research vessel required assembly on site that took place the week of December 10, 2007. For those days, the average temperature was -15°C with a low of -29°C. The upstream river was completely frozen except for a 200 m area upstream of the dam.

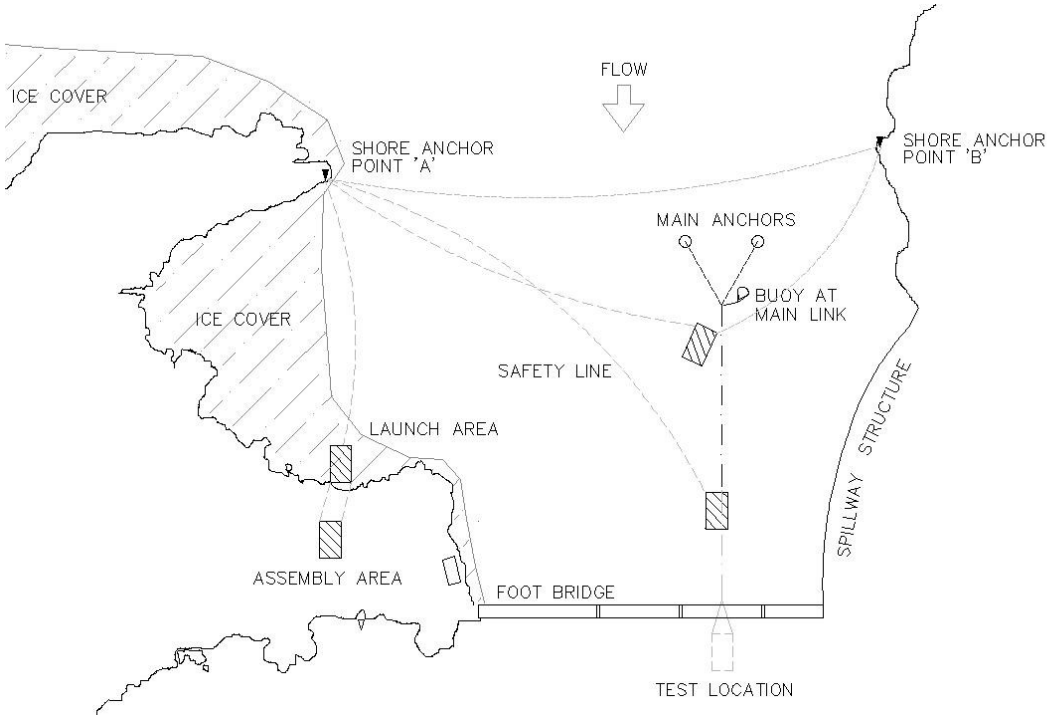

Figure 25: Overall view of deployment plan for initial test setup. Once assembled, the test platform was pushed onto the ice and winched into open water using the safety cable from Point 'A'. Then the outboard motor was used to traverse the river to the main link location where the wire rope cable was connected.

Initial deployment required that the vessel be launched upstream of the walkway bridge. Once assembled, the vessel was moved to the shore and positioned to be pushed down onto the ice on a ramp of snow. All large components of the turbine, along with the 32 mm

(1¼") main anchoring cable, were loaded onto the research platform prior to launch. Once in the launch position, a steel cable line was taken from the front winch to anchor Point 'A'.

Figure 26: Clockwise from top left: Pontoon test platform assembled on shore. Vessel on snow ramp with front of pontoons digging into surface ice. 32 mm (1-1/4") main mooring cables (underfoot) and typical marker buoys on deck of vessel. At point 'A' after maneuvering across the bay to the north and west of the main anchor points. Inset: hammer-lock style connection for main cable to the chain main link.

As shown in the top right photo of Figure 26, the ice was not sufficiently thick at the entry point to support the vessel. Thus, the pontoons dug into the ice and halted progress. The snow ramp was removed from under the rear of the pontoons to level the vessel with respect to the ice surface. Then, using the winch line and a vehicle from the shore behind, the research vessel was moved into the open waters and then placed at Point A using the outboard engine and a cable winch line as a backup.

During all on-water procedures, at least one backup system was included so that that failure of one component would not cause the vessel to be uncontrolled. The outboard motor was the primary means of transit across the flow with at least one safety cable, typically a winch line, used as the backup measure. A second safety line was installed using a zodiac boat and a two-man crew from the vessel to Point 'B'. During deployment, one of the safety anchor cables had unknowingly become wedged under a rock in the forebay and released unexpectedly later. The use of 25 mm polyolefin floating ropes for safety lines is recommended to avoid such situation. Large rocks and unknown river bottom surfaces can be expected in natural river bottom, and it is best to avoid cables on the river bottom. This is particularly the case for any cables crossing the stream at any angle to the flow. Moreover, working with wire rope across channels is difficult for operators or smaller boats to handle.

The research vessel was brought cross-stream under outboard motor power to the buoys marking the master link location. Winches onboard the vessel took up slack in the safety cables to ensure that stall or failure of the outboard motor would not result in loss of control in the flow. The buoys were installed on the main support chains when the riverbed anchors were installed. Once the buoys were reached, the master link was raised to the surface. The main cable was shackled to the master link using a hammer-lock connection, as shown in Figure 26. The research vessel was allowed to move downstream by reducing motor power and paying out the main cable from the bow of the vessel to reach the position just downstream of the walkway bridge between piers 2 and 3. Care was taken to restrain the main cable on the boat deck, as the weight of the cable in the water would otherwise drag the entire cable into the water. It was important not to walk on the bridge deck near these cables. Figure 27 shows the various steps to position the research vessel under the footbridge in winter conditions. A full-sized copy of this drawing, and the related cable and shackle configurations are included in Appendix 1.

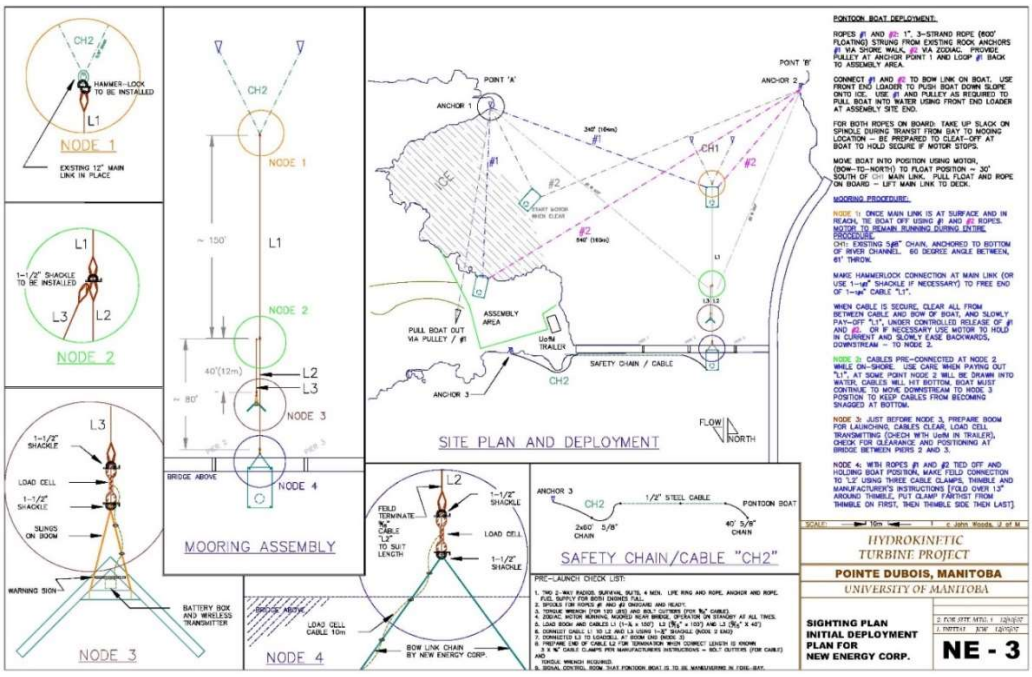

Figure 27: Deployment Plan for initial test platform winter deployment. Detailed cabling plans and complete safety plan were developed and are included in the Appendix 1 and 2.

The main cables, denoted L1 and L2 in Figure 27 and shown on the deck in Figure 26 were 32 mm diameter (1-1/4") steel wire rope cables, 'DYPAC 6' 6x19 with carbon steel end thimbles and a breaking strength of over 800 kN (90 tons). The cables were significantly over-sized for the expected loads. The additional capacity was warranted due to corrosion and expected abrasion resulting from vibration (due to flowing water) of the cables in contact with rocks on the river bottom.

The initial plan was to install a floating debris deflection boom upstream of the vessel using a common connection at Node 2. To ensure the main cable and anchor system upstream was not overloaded, should the boom retain significant debris, the cable L3 was reduced to a 15 mm (9/16") steel cable with a capacity of 17,000 kg (19 tons). The final connection from the cable to the boom was to be a nylon covered polyester sling, with a capacity of 7,700 kg (17,000 lb.). The deflection system proved to be a safety hazard and was removed from the project. Figure 28 shows cross sections of the test platform in place at the bridge

and the relative location of the river-bottom anchors. Figure 29 shows photos of the launch and the test platform in the final test location.

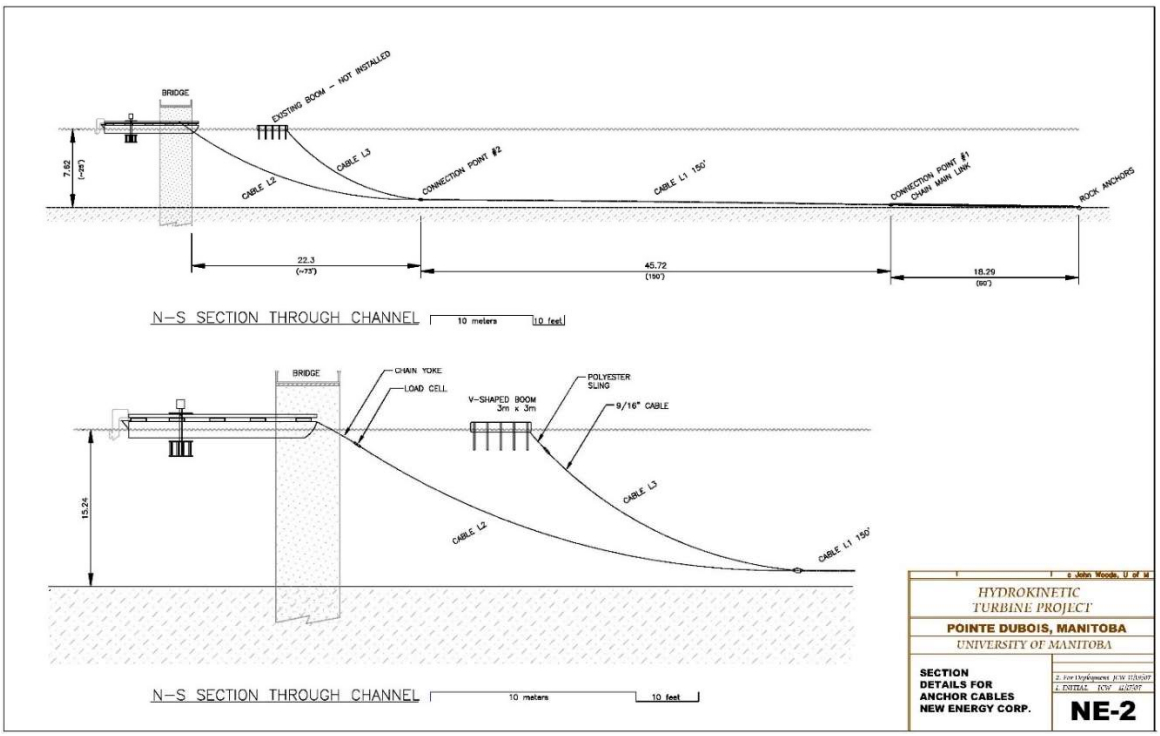

Figure 28: Two cross-section views at different scale showing the basic support-cabling plan for summer testing of New Energy Corporation 5-kW unit.

Once the vessel was in place, a 13 mm (1/2") steel safety line from shore was connected to the research vessel. The safety chain/cable CH2 is shown near the bottom of Figure 27. To install, the cable was strapped with tie-wraps to the outside of the bridge until it was fastened to the research vessel. Passing the cable from the bridge onto the research platform, it was shackled to an eyelet at the stern of the vessel. The research vessel was then secured by the main line and the downstream safety line, completing the deployment.

Figure 29: Clockwise from top left: (a) view from test platform in final location, (b) platform just prior to launch, (c) view from west shore of two people in zodiac and one on shore securing cable on Anchor 2 at Point B, (d) view from dam structure of test platform in place at first test location.

The safety line was anchored on the downstream shore of the walkway bridge. The anchor was drilled and epoxy cemented into riverbank bedrock, shown in Figure 27 and Figure 21(b). The safety line was then shackled to the anchor at one end and connected to the rear shore side of the research vessel. The safety line was not designed to withstand the full load of the research vessel in the high flow area. The line used was of a smaller diameter 13 mm (½") steel cable. Should the support main cable fail, the research vessel and turbine would be taken downstream, but the safety line connected to a shore anchor near the start of the bridge would cause it to swing radially towards the slower moving water and away from the main flow. If laid on the bottom, such cables will be caught up on rocks and may therefore be unreliable and difficult to remove. A better solution, for this site was to mount the safety cable with plastic tie-wraps to the downstream side of the bridge. If required, the force of the vessel moving downstream would easily break the plastic tie-wraps, releasing

the cable slowly and maintaining tension, keeping it off the bottom but allowing the radial motion to still water. For deployment where a bridge is not available, a floating rope submerged below the ice level, and connected to small anchors on the bottom using thin stainless steel wires or plastic ties would provide a similar break-away safety line.

Safety recommendations from the first winter deployment

- Stainless steel shackles with treaded pins bind in cold weather and the threads can foul with ice and are to be avoided.
- Shackles with treaded nut and cotter pin are more forgiving and can be assembled quickly. If necessary, the nut and pin can be installed after the connection is able to take the load. In our experience these connections had to be made as quickly as possible.
- Steel wire rope cables should not be used in cross flow situations. Where necessary, cables should be paid-out from the vessel as it moves and in line with final position. Otherwise, they are likely to jam under rocks or debris on the river bottom and may not be retrievable.
- Polyolefin ropes are resilient and float, and are recommended for temporary fastening and for safety lines. They do not absorb water and therefore do not get heavier when wet. They are also UV resistant. Three strand ropes 25 mm (1") such as those manufactured by Sampson have a breaking strength of 90 kN (20,300 lbs). However, they should be inspected regularly for any sign of abrasion, and should not be dragged over rocks.
- Floating thermal insulated suits such as those manufactured by Mustang should be worn at all times in winter conditions.
- Buoys left in the river can be damaged by ice and spring flow conditions. Where necessary for ongoing operation, they should be inspected in the fall and spring, and replaced where there are signs of wear. Tear-shaped buoys perform the best.
- Figure 30(a) shows buoys which lasted now over 10 years in-situ on the Winnipeg River.

- Cables on the boat deck can be a safety hazard if not well placed. Wire rope cables 25 mm in diameter and larger must be retained with a winch.
- A safety cable should be used to a shore mounted anchor so that in the event of main cable failure the turbine can drift towards shore and settle in an area with less flow to simplify recovery.
- A safety boat with operators should be ready to perform a rescue during any on water operations.
- Spare winches on shore and on board the vessel during deployment and retrieval are highly recommended. Spare shackles, several of every size used, must be on hand during deployment.
- The chain of command on the vessel must be planned and discussed during safety planning meetings.
- Procedures must be documented ahead of time and reviewed before every execution to minimize the risks and remain in compliance with labour codes.

Figure 30 shows a selection of the safety equipment proven to have performed well in extreme cold weather.

(a) (b) (c)

Figure 30: Items that were found to work well in cold climates: (a) a tear-shape inflatable buoy suitable for high-flow areas, (b) thermal insulated and buoyant suit for winter operations, and (c) polyolefin floating rope for temporary mooring and safety lines

4.2.2 Second deployment – Summer 5-kW turbine

After successful winter testing of the 5-kW vertical-axis turbine, discussed in Chapter 6, the testing platform was removed and moored to the shore on the downstream side of the footbridge. Recovery of the vessel is described in Section 4.3. The main anchor chains and cable were maintained in place, and a large 68 mm diameter buoy was connected to the footbridge end of the cable for reconnection in the spring. For this second deployment, again with the 5kW hydrokinetic turbine, the safety line at anchor point 3 was connected to the vessel, and the boat was moved cross-stream using the outboard motor. Once at the bridge, 12 VDC 4,535 kg (10,000 lb.) winches on the deck of the vessel were used to bring the boat near enough to the main anchor point so that the chains from the bow of each pontoon could be connected. During this test phase, the 5-kW turbine was tested with several different support arms to evaluate the overall efficiency of the unit. Using the on-board winch to provide slack, the process was reversed, and the main chains were removed from the vessel and fastened to temporary lines to the bridge.

4.2.3 Third deployment – Summer 25-kW turbine

During testing of the 5-kW unit in the winter, it was found that support of the pontoon vessel from the front of the pontoons resulted in a downward canter of the test platform. With the build-up of frazil ice at the bow, this situation worsened with time and resulted in an ice floe sliding up onto the vessel and halting the testing. Chapter 5 discusses the icing issues experienced. In order to improve the angle of the platform, and accommodate the additional weight of the 25-kW turbine and generator, a new support mechanism was developed by New Energy Corporation Inc. In the new configuration, the turbine would be self-supported below water level on both sides of the vessel using a shaft across the width of the vessel and large steel arms to connect to the mooring chains. The tubular steel shaft sits in a steel bracket on each side acting as a pivot point, allowing the arms and generator shaft to rotate 90 degrees from fully out of the water to fully in the flow. This new method of deployment and mooring are now standard for New Energy turbine systems.

(a) (b)

Figure 31: (a) Preparation for 25-kW unit testing before deployment, and (b) after final connections to the mooring system but before turbine deployment.

In Figure 31, the support chains are shown with yellow shackle connections to the blue support arm in two locations. At the bow, these chains are shackled on both ends of a spreader bar, which ensures that the main support chains do not impinge on the pontoons or the rotating turbine. Figure 31(b) shows the bow is depressed into the water by the weight of the rotor being supported by the A-frame winch and the temporary connection to the bow of the pontoon boat. Once the turbine is deployed, the downward force is moved to the center of the vessel, and the main drag of the turbine is transferred to the supported chains via the white steel shaft and blue support arms. The vessel remains connected to the main anchoring system via winch cables at the bow hooked to previously deployed chains to the main cable, as shown in Figure 31.

4.2.4 Fourth deployment – horizontal-axis turbine

After the testing of New Energy Corporation's 25-kW turbine, the test platform was retrieved, as described in Section 4.3, and moored in the slow water area near the footbridge for the winter with no damage to the pontoons. The turbine, support structure and outboard motor were removed from the site by New Energy Corporation Inc. To allow testing of the horizontal-axis shrouded turbine, a new support frame was installed to allow the turbine to be lowered into the water after the vessel was moved into place at the test area. Due to

weight considerations, the outboard motor was removed from the vessel. Therefore, a different method of deployment was necessary. In keeping with the objective of deploying hydrokinetic turbines with minimal use of infrastructure, the bridge was not used for deployment. Furthermore, Manitoba Hydro gave clear instruction that the bridge was to be used for access to the test site only and should not be relied upon for any structural support. While the shore anchors were still available upstream, the vessel was now on the downstream side of the bridge, and therefore they could not be used directly. An alternate plan was developed using a large sheave shackled to the stern of a working boat, which was itself shackled to the main support cable. In this way, that the test platform could be released into the current downstream of the bridge then pulled up to the main cable connection point using a large vehicle mounted winch on shore. The plan is shown in Figure 33, and additional details are included in Appendix 1.

For this deployment, and to facilitate future testing at the site, a large fiberglass mooring float was secured to the main cable connection upstream of the test location, Node 2 in Figure 27, and shown in Figure 32. The float had a 1.2 m diameter and was 2.5 m long.

(a) (b)

Figure 32: (a) Large 1.2 m diameter mooring float (b) installed upstream and connected to the main anchor ready for turbine platform deployment and connection.

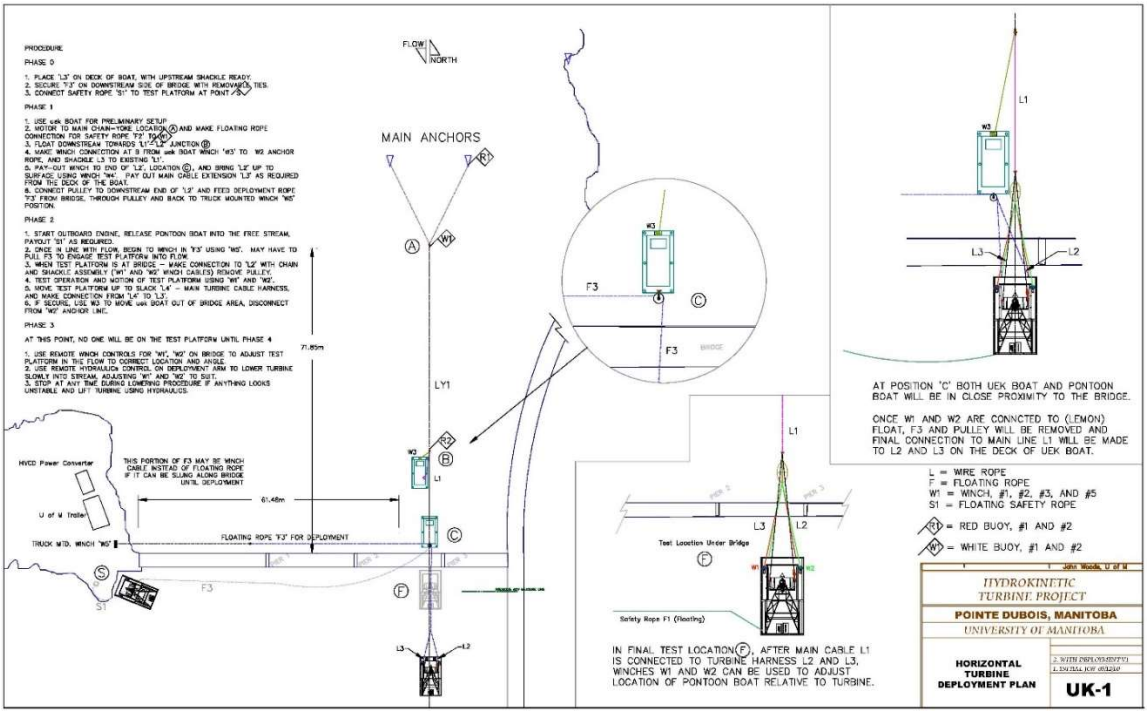

Figure 33: Plan for deployment of horizontal-axis turbine, using vessel-mounted pulley on main anchor cables and shore winch. Appendix 1 shows a full size plan.

With reference to Figure 33, a 3-strand floating rope connected at winch location S on shore was passed through pulley at point C and over to the front of the test platform while at shore. A safety cable was also attached from the normal anchor point 3 shown in Figure 27 and marked as S1 in Figure 33. The test platform was then released into the stream and eventually carried over to the downstream side of the test position by the river current. Once it had stabilized, the truck at position S was driven down the road to the west pulling the test platform north to just upstream of the test location. Then the vessel cable harness could be connected to a pulley mounted to the mooring float, as shown in Figure 34. Once this step was completed, the test platform was shackled to the mooring float and anchoring lines and the working boat was removed from the test site. Deployment of the turbine itself using the hydraulically actuated A arm is described further in Section 4.4.2. The connection through the pulley on the mooring float allowed the vessel to be pulled upstream to provide slack in the main support cables for connection directly to the turbine support flanges. Then

the winch could be released so that the turbine was supported in the in-stream direction by the direct cables only; thus simulating at least one degree of freedom for kiting support.

Before being permitted to deploy the turbine, a deployment and safety plan was prepared. A copy of the plan is included in Appendix 2 and provides additional details on the deployment. Such plans contribute to the development of standards on how to safely deploy hydrokinetic turbines on rivers.

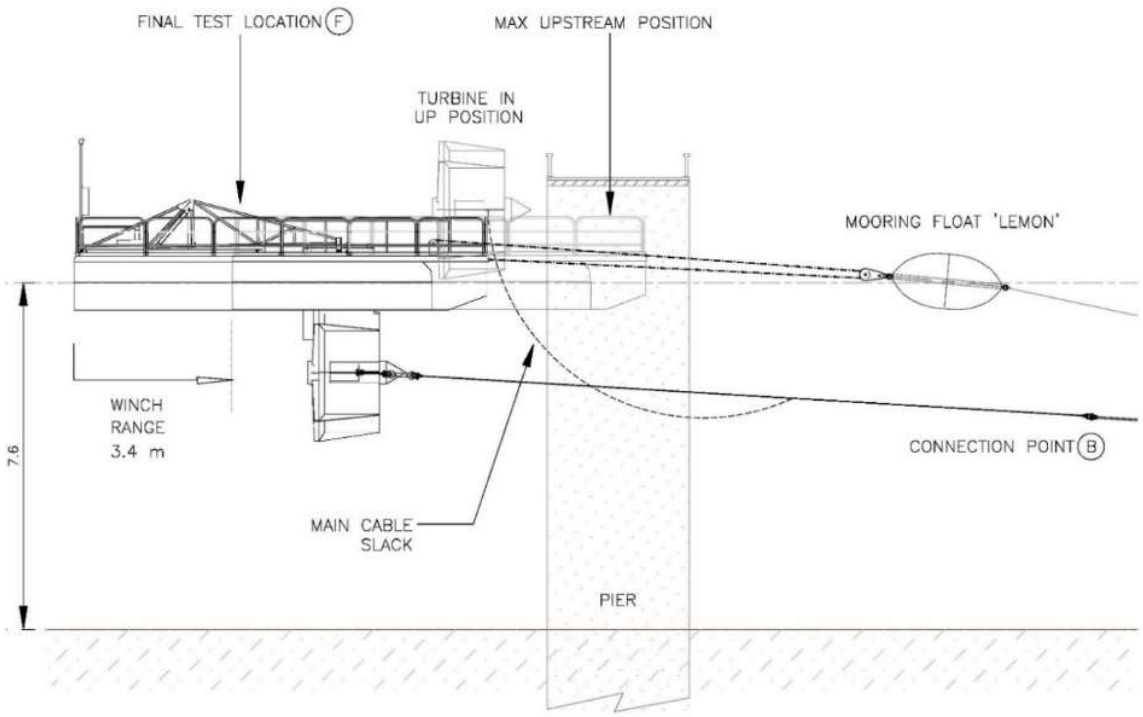

Figure 34 : Cross section of stream showing main components of deployment number 4 for the horizontal-axis shrouded turbine. Notable is the use of the mooring float or buoy, to which a sheave and winch cable, secured back to the boat, is used to move the support platform upstream to create slack for connection of main anchoring cable to the turbine.

During this deployment, the flow was in the range of 1.1 m/s due to drought conditions, significantly lower than normal levels of 2.3 m/s. However, the re-use of the main anchoring cables and mooring buoy pulley system were proven to work well. The installation of the mooring float was useful at the test site, however, as will be discussed in

detail in Chapter 5, frazil ice and floating debris likely render this more of a hazard than a help for permanent installations.

4.3 Retrieval

Retrieval of hydrokinetic systems is a necessary component of the process and must be planned from the start. A functional plan for retrieval is a typical requirement, ensuring that materials and equipment are not left in place at the end of the useful life. For example, in considering applications for tidal energy conversion testing in the Bay of Fundy, the Nova Scotia provincial guidelines require that: "… prior to installation of any device, the Province will need to be satisfied that appropriate planning and financial security arrangements are in place to decommission marine energy devices if the project is suspended/terminated at any time or at the end of the device's working life [62]."

The following describes the first retrieval, which was the most difficult due to winter conditions. The initial concept was to reverse the deployment method indicated in Figure 27 using the shore mounted rock anchors, pulleys and winches to retrieve the vessel. However, since the test platform was intended to be re-deployed in the spring, there was no reason to move it upstream of the bridge. Therefore, removal and redeployment of the research vessel took place downstream of the footbridge. Removal began with a safety meeting, outlining everyone's task and location. Those who required safety equipment such as life jackets, survival suits, harnesses, radios, etc. were so equipped. The zodiac was launched as a safety vessel. Before any mooring was disconnected, the engine was started and checked over for proper functionality and sufficient fuel. With the engine running, there were three points of control: the main support cable, the safety line, and the onboard engine.

The first step of retrieval was to remove the turbine from the water and secure it and all other equipment to the deck of the vessel for transportation. Then, the steel cable safety chain was removed and replaced by a floating rope. Earlier experience showed that steel cable, sinking to the bottom, can become wedged on large rocks and debris on the bottom

and should be avoided. Careful attention was necessary to ensure that ropes and cables were not caught up in the propeller of the outboard motor. The next step involved unfastening the main cable line. During removal, a winch line from the bow was temporarily connected to the bridge, to act as backup for the outboard motor while moving upstream toward the main cable connection point. Provision of a mooring buoy with a connection point, like the one shown in Figure 34 could be used where the bridge not available. Once disconnected, the main cables were strung up to the bridge temporarily. If the research vessel was to be removed for extended periods of time, then the free ends of the main cable were fastened to a large buoy and left to float in the water. Free of the main cable, relying on engine power, and using the safety rope for back up, the research vessel was brought as close to shore as possible, but was held up by sheet ice approximately 30 m form shore. From there, a winch on the front of a skidder easily pulled the vessel across the ice to shore. Figure 35 shows photos of the removal of the test platform.

4.4 Turbine support configurations and installation

The following sections describe the specific setup on the test platform for the different turbines tested, and their unique deployment requirements. Figure 36 shows the test platform, set up for the vertical-axis turbines.

Figure 35: Clockwise from top left: (a) View from shore with vessel at test location with floating safety blue rope ready, (b) vessel driven up on ice using outboard motor and chain connected to winch on skidder, (c) diesel fired skidder machine use to move turbine on the shore ice, and (d) vessel slid over ice to winter storage position.

4.4.1 Vertical-axis turbines

The 5-kW turbine in its mounting frame occupied the place of one of the removable surface panels. With the vessel's design, the turbine could be located anywhere along the deck in place of any of the five panels, as shown in Figure 36. The turbine, designed and manufactured by New Energy Corporation Inc., has 4 hydrofoil blades that mount to a rotor measuring 1.52 m in diameter and 0.76 m in height using eight support arms with two arms per blade. Rated for 5-kW in a water velocity of 3 m/s, the rotor rotates at approximately 90 RPM at design speed. With a gearbox ratio of 13.5:1, the nominal generator output is 200 V. Altogether, the system measures 2.25 m high and weighs 340 kg.

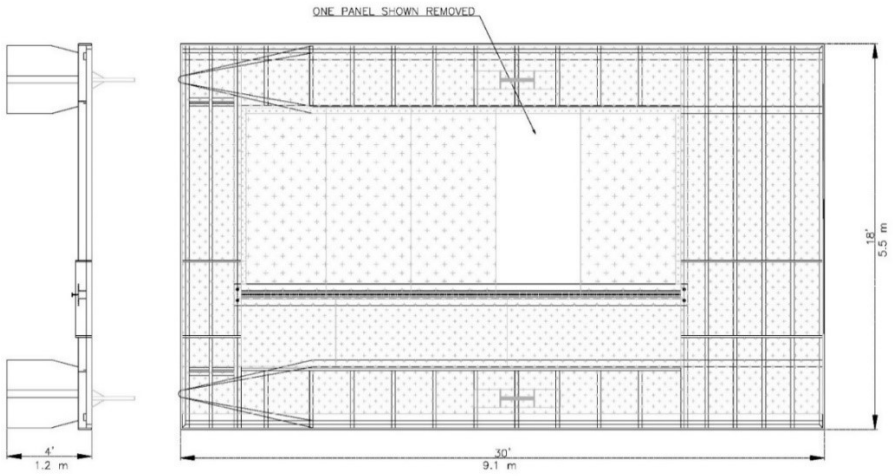

Figure 36: Test platform plan view and end view and dimensions. One of five removable panels shown removed. Pivot brackets for 25-kW unit shown on either side, near center and in grey on the end view. Longitudinal beam just off center is where the vessel's width was extended to accommodate 25-kW and larger rotors.

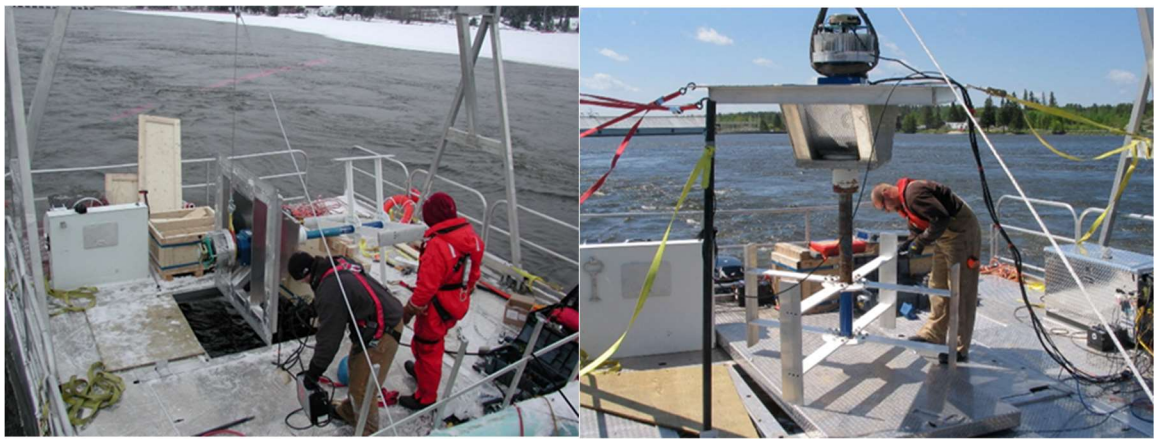

(a) (b)

Figure 37: 5-kW generator and 4-bladed Darius style turbine mounted in aluminum cradle before deployment: (a) winter installation, and (b) summer on the right. Note the wheels at the bottom of the A-frame structure allowing the A-frame to be moved to any location on the deck.

The research platform was equipped with an A-frame structure. The A-frame was erected after deployment due to limited clearance under the bridge. The A-frame supported a manual, chain driven, 1.8-tonne hoist, which was free to slide across the width of the

platform on an I-beam. The turbine and generator assembly was assembled into its aluminum support cradle on the research vessel after deployment. The hoist was used to hold the turbine upright during assembly and then lowered and fastened into place in the rear quarter of the research platform as shown in Figure 37. The A-frame was able to move along the length of the research platform on wheels integral to the unit. The turbine cradle was built to be the same width as the panels that made up the research platform deck, so that it could be moved to any suitable location along the length of the platform. The 5-kW unit was tested in the winter, and with several different support arm configurations as discussed in Chapter 6. As a result of this testing, New Energy made changes to the turbine design as well as its mounting structure for the scaled up 25-kW model.

The geometrically similar turbine rated at 25-kW had four hydrofoil blades 1.7 m high each, on a 3.4 m diameter rotor. The weight was 1,760 kg excluding the support structure, and the gearbox ratio is 61.5:1 producing a nominal voltage of 350 V. The support arms on this unit were manufactured with the same hydrofoil profile as the blades, significantly reducing the drag and improving overall efficiency. The support structure for the larger turbine was re-designed to eliminate the issues related to the bow of the platform being tilted down and to move the center of mass of the unit to mid-platform. A novel pivot arm, developed by New Energy Corporation Inc., was incorporated as described in section 4.2.3. The turbine lies horizontally during deployment and rotates ninety degrees on two pivot supports to place the turbine into the flow. Chains then connect to the mooring anchor so the axial load is on the turbine and not the vessel. This arrangement minimizes the moment onto the research platform, which is independently connected to the mooring system.

Figure 38 shows the 25-kW turbine being deployed. Note that the low solidity factor of the Darius turbine and the steep angle of the rotor shaft during deployment allows the rotor to be turned by hand into the current without loss of control. As the blades are turned into the water, the winch holding the main shaft horizontal is payed-out and the shaft is slowly rotated to a vertical position. This deployment method does not take more than 10 minutes, however a minimum of three people plus a safety boat are required. In a final design, the

cross beams between pontoons are sized to eliminate the longitudinal beam avoiding this manual rotation step. Modifications necessary to remove this main beam for horizontal turbine deployment are described in section 4.4.2.

Figure 38: (a) Rotor being deployed by slowly turning the rotor into the stream while pivoting the main shaft, (b) turbine deployed with new support system successfully eliminating forward tilt of the platform. Note water line parallel to pontoon lines during testing as per calculation of the final location of the center of mass.

During operation, at flow velocities over 2.3 m/s, the boat deck experienced significant vibration. This was found to be due to the resulting natural frequency of the boat assembly resulting from weakened welds in the pontoon frame, suspected to have been the result of ice buildups and stress during winter testing. The turbine was not left unattended during such high flows. Repairs to the welds would have resolved the vibration, however, due to the location of the suspect welds under the vessel, they could not be made in-situ and were repaired at the shore before the fourth deployment.

4.4.2 Horizontal-axis turbine

The 2.4 m diameter horizontal kinetic turbine with shroud shown in Figure 39 was also adapted for testing at the site for 2.5 m/s flow conditions. This turbine is part of a twin turbine system intended for kiting, with rotors counter-rotating to maintain position in-stream. Testing focused on deployment methods, implications of winter conditions,

verification of rotor seals and interface with the power converter. The turbine rotor is a 5-blade propeller design with a relatively high solidity. The rotor shaft torque is transferred to the generator shaft using 3 x 25 mm chains on a 2:1 gear system. A water-cooled gearbox increases the turbine speed by a ratio of 25.2:1 and connects to an air-cooled high-frequency permanent-magnet synchronous generator. Unlike the vertical-axis turbines, this turbine had no brake, as the high drag of the rotor does not permit stopping the turbine in high flow velocity without catastrophic failure. However, as a safety measure, the rotor could decouple itself from the shaft by way of a treaded connection, should a blockage halt the rotor.

(a) (b) and (c) (d)

Figure 39: (a) Rotor and shroud assembled in manufacturer's shop, (b) threaded hub for emergency release of generator shaft if rotor is blocked, (c) complete rotor, and (d) shroud with housing at top for vertical drive chain transmission and generator (photos taken with permission).

An alternative method for safety would be an electromagnetic coupling using an eddy current drive to couple the rotor to the generator shaft, as discussed in Chapter 9. The twin rotor design is intended to permit kiting on the assumption that each rotor's net torque on the support structure will cancel the other and therefore remain upright in the chosen channel location. This assumption is valid under ideal conditions only and may not be relied upon in-situ. For example, branches or floating debris might halt one rotor and not

the other. Or bearings may wear unevenly, creating different torque characteristics. The concept of using an eddy current "clutch" has recently been implemented in a small self-contained hydrokinetic turbine by Idenergie of Montreal. It was implemented as a method of transferring rotor torque accross a sealed aluminum generator housing by use of an electromagnetic field, eliminating a shaft and bearing seals. Additional discussion on this concept can be found in Chapter 9.

The horizontal-axis turbine was originally designed to be deployed using a hydraulic rotational arm powered by the onboard engine, shown in Figure 40. This method had to be abandoned due to safety concerns resulting from structural and stability issues. The fiberglass deployment arm failed during its on-shore testing before deployment. In addition, preliminary analysis of deployment indicated that even with the front ballast tank filled, the worst-case center of balance during deployment was 1.47 m high and 0.71 m outside the stern of the vessel. Deployment could not be accomplished safely without adding outrigger pontoons to stabilize the vessel. Therefore, given the success of the first three deployments, the solution was to re-fit the pontoon vessel to accommodate the horizontal-axis turbine. The first step in redesign of the platform was to remove the longitudinal beam and strengthen the cross bracing. The aluminum weld failures from winter testing were also repaired.

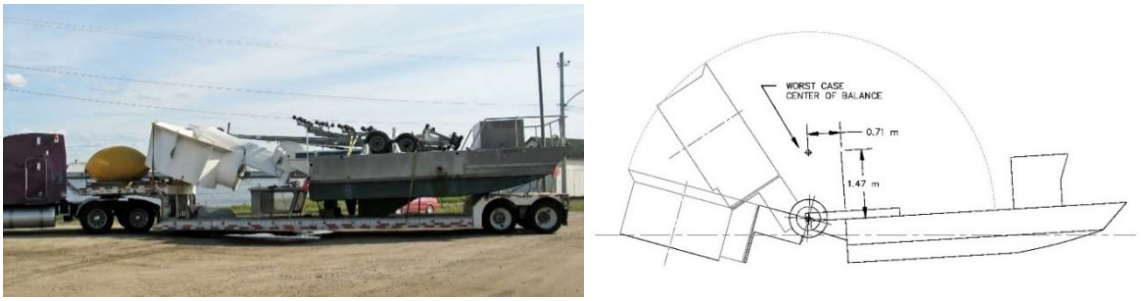

(a) (b)

Figure 40: (a) Horizontal-axis turbine and deployment vessel showing the fiberglass deployment arm and (b) a sketch showing preliminary analysis of center of balance during deployment. Photo taken with permission.

Figure 41 shows the additional steel bracing (yellow beams under the bow) and the longitudinal center beam is removed.

(a) (b)

Figure 41: New deployment structure: (a) tubular white steel support-arm for horizontal turbine deployment, and (b) yellow steel bracing under the bow, and spanning the pontoons allowed for complete opening of the deck.

The deployment arm was designed to allow the turbine to be lowered in full flow conditions and carry the rotational torque of the turbine. The in-stream thrust is carried by cables connected to the two steel support flanges, which were added to the outside of fiberglass shroud and are shown in red in Figure 42. Two hydraulic cylinders provided the necessary lifting forces to remove the turbine, as well as lower it in a controlled fashion into the flow.

In addition to the support arm, several sub-systems were designed and constructed. These included the following, and are shown in Figure 42 and Figure 43:

- Fluid (water) cooling system for speed increasing gears
- Lubrication system for vertical drive chains
- Bilge system for extracting seep water from the lower unit
- Oil water separation for bilge water and lubrication oil re-claim

The installation of the turbine and ancillary systems was completed using the on-board A-frame winch and a scaffold set up as shown in Figure 44. The test platform was deployed to the site as described in Section 4.2.4.

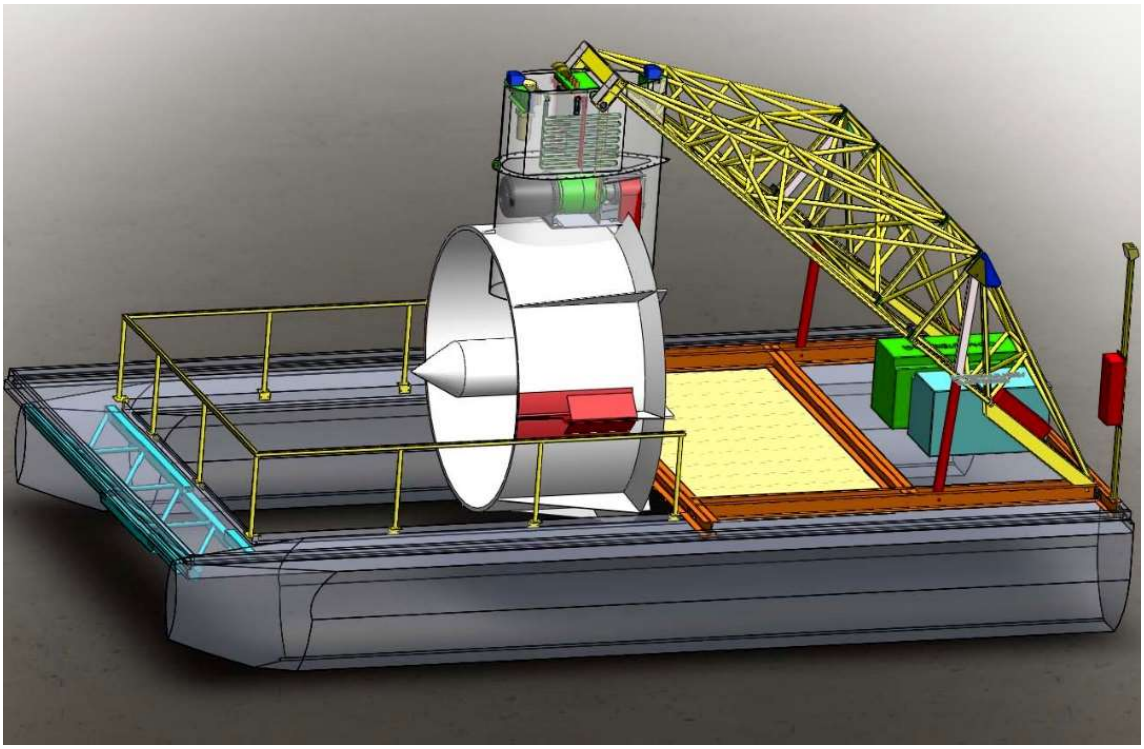

Figure 42: Solidworks® model of the test platform modified to deploy the 2.4 m horizontal-axis shrouded turbine. Tubular steel frame in yellow, re-built structure at bow in cyan (below deck) and overall steel frame in orange. Hydraulic lifting cylinders are red. At the stern, two boxes are the data acquisition equipment enclosure (green) and the Hydraulic Pump equipment and battery enclosure (cyan).

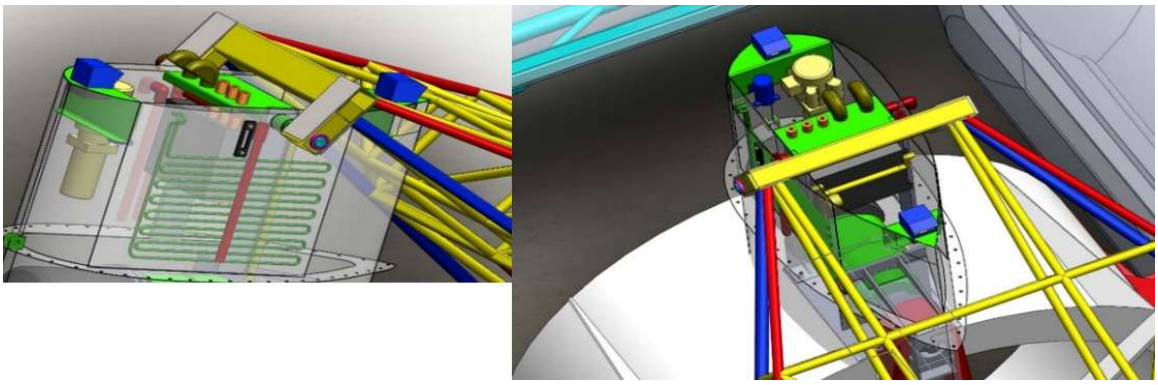

(a) (b)

Figure 43: Model of enclosure at top side of horizontal-axis turbine. (a): starboard side showing cooling water pipes (green) for gearbox water cooling system, red band is chain drive from gear on rotor shaft below, green cylinder is gear box, grey is generator. (b): view from above and rear, yellow cylindrical device is cooling water pump, blue cylinder is sump pump, blue squares front and rear are exhaust fan and vent port. Cable entries shown: three control cable ports (orange), and aux. power in / generated power out (olive green).

(a) (b)

Figure 44: (a) Turbine installation on test platform using scaffold for installations and on-board A-frame for support. (b) After installation, turbine fully raised for transit to test site. also in the right-hand photo, black cables running from pressure transducers on the shroud flange up to the top of the controls enclosure. Photos taken with permission.

Figure 45: (a) Turbine fully deployed, disconnect switch with red handle for generator output to power electronics mounted on support arm, (b) test platform in test position downstream of footbridge at Pointe du Bois, before turbine is lowered into the current. Photos taken with permission.

As shown in Figure 45, a disconnect switch was provided on the support arm in such a manner that it would open on failure of the mooring system by connecting a cord from the operating handle to the bridge. This would disconnect power from the generator to the data acquisition compartment and downstream power electronics. Figure 45(b) shows the test platform in place at the test location.

4.5 Cables, connections and data acquisition

Power from the 5-kW and 25-kW units were brought to shore using a multi-conductor 3c#8 TECK90 cable. For the larger 60 kW generator, a 4c#1/0 copper, medium voltage flexible power cable was used. Additional details on cabling are provided in this section.

4.5.1 Sensors and measurement devices

This section describes the sensors and data acquisition systems employed to gather performance data and environmental conditions for the various hydrokinetic tests. Remote sensors and data acquisition equipment include:

- Thermocouples for measurement of ambient air, water, and generator temperatures. During winter testing, the temperature within the control cabinet was also monitored.

- Vibration sensors mounted on the generator and test platform to measure vibration in-stream and cross-stream, and to monitor the test platform for collision of ice and debris.
- A load cell for measurement of tension force on the main anchor cable. However, the connecting cable failed on many occasions.
- A turbine flow meter with Hall effect sensor. A hand-held meter was also used to spot check for system flow meter accuracy, and after ice destroyed the fixed mounted sensor.
- Current transformers, one on each generated output phase. Voltage transformers were used for concurrent power measurements.
- Three phase power analyzer, Arbiter Model 930-A, calibrated for meter accuracy to 600 Hz. This device was capable of receiving the generated voltages without transformation and rated for 600 V.
- Three outdoor cameras and one underwater infrared camera.
- An Acoustic Doppler Velocimetry (ADV) device, Nortek Vectrino+ was connected to a portable computer for detailed analysis of the flow and concurrent measurement of flow, turbulence and generated power.

Figure 46 shows the on-board control cabinet, vents along the front, and exhaust fans along the rear wall with foam board insulation the sides. The weather resistant cabinet was a pre-fabricated aluminum box, approximately 600 x 600 x 1200 mm. Sensor readings were received by the DT85 dataTaker data logging device. This device was located in the control cabinet on the test platform, and can be seen in Figure 47.

Figure 46: On-board control cabinet housing instrumentation and data conditioners.

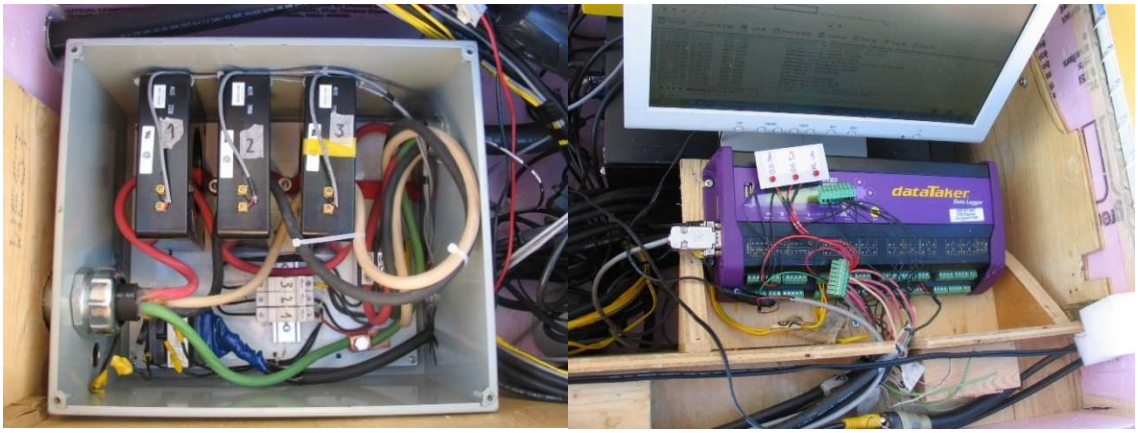

(a) (b)

Figure 47: (a) Current transducers labelled 1, 2, 3 for the main power developed by the turbine generator. Voltage is passed through finger-safe fuses to a 600:24 V transformer and to the Arbiter power measurement device (not shown). This equipment is located in a steel junction box within the equipment enclosure, providing personal safety from live electrical sources. Note the green ground wire terminating on a copper ground lug inside the junction box. (b) The dataTaker and computer monitor on top of the on-board PC.

Data acquisition was accomplished using two computers; one located in the trailer on shore, the other located on-board in the equipment enclosure on the test platform. The power analyzer Arbiter 930A was poled by the on-board computer every ten seconds. The data logger recorded sensor readings every minute. Every five minutes the log files for both the data logger and the power analyzer were copied into a common file, and these files were uploaded to the computer in the trailer located on shore. This allowed for real-time data to be recorded and viewed remotely and ensured that any failure of the platform mooring, or other environmental event, would not cause a loss of more than five minutes of data.

Fellow researcher Shamez Kassam is credited for development of the data acquisition software writing Pearl scripts, which controlled the data transfer. Details on these systems can be found in Mr. Kassam's Master's thesis [63] and our 2007 conference paper [64]. Weather-proof cable entries were provided at the box for the various sensors and cameras.

Video from the outdoor cameras was captured, stored on a computer in the control trailer, and made available over the internet via software provided with the PC-based video cards (Digimerge®). This allowed for remote monitoring of the winter ice buildup on the test platform from Winnipeg, reducing project costs. With the exception of one event, described in Chapter 5, the remote monitoring provided sufficient time to allow for driving approximately one hour and forty minutes to the site to clear the ice. Figure 48 shows an example of the video camera feed from the bridge mounted camera monitoring the bow of the test platform on January 20, 2008.

Figure 48: Example screen shots of real-time video recorded and available via the internet for remote monitoring locations in Winnipeg, Manitoba.

The vibration sensors used were unidirectional, and therefore two sensors were needed to capture vibrations within a plane: one mounted in a stream wise orientation, and one cross-stream of the flow. These were manufactured by Monitran, model MTN/1185, and have a range of 50g, with transverse sensitivity of 5%. These devices were used to collect data and monitor the status during winter testing in 2008, and is reported on by Kassam [63]. Pressure transducers were mounted to the shroud of the horizontal-axis turbine, and provided data for other researchers and is not reported here. Load cells were submersible Honeywell Sensotec RGF devices, mounted directly in line on the turbine support cables measuring the combined tension forces on the support cables from the test platform and turbines. These load cells were factory calibrated and capable of handling 222 kN of tension, consistent with the maximum expected load of 218 kN (see Section 4.1.3). The published accuracy is ±0.25% of full scale, as is the linearity. As discussed in Chapter 6, the actual force measured and reported in this work is in the range of 6 kN to 20 kN, therefore the measurement error would be in the range of 10% to 3%. Flow was measured continuously using a propeller-style counter which was calibrated in a water tunnel against an ADV probe as discussed below. The flow meter was a propeller-style located in a 50 mm diameter PVC housing, with a range of 0.1 to 6 m/s and an accuracy of ± 3 cm/s. K-type thermocouples were used to sense ambient temperature, temperature of the generator

and gearbox, as well as water temperature. These devices were inexpensive, but durable, and have an accuracy of 2.2°C or 0.75%. Underwater video was recorded using a camera with built-in infrared illuminators. Figure 49 shows a sample picture of each of these devices.

Figure 49: Clockwise from top left: 5-kW generator showing brake mounted on cyan plate and in-stream and cross-stream vibration sensors, typical pressure transducer located on shroud, tension force load cell, propeller-type flow meter, thermocouple with cable, infrared camera with built-in illuminators for underwater video.

The in-situ testing included concurrent measurement of turbulence and power output from the generator, so that a correlation between the two could be observed. An acoustic Doppler velocimeter, ADV Vectrino+ model, manufactured by Nortek was used. The manual indicates and accuracy of 0.5% or ±1 mm/s. To verify the accuracy, the ADV was tested in the water tunnel at the University of Manitoba and compared to a pitot tube device. These devices were within 3% of each other up to 1 m/s. The propeller-style velocity meter was also tested against the ADV and a calibration factor applied to the number of rotations counted by the data acquisition system brought the accuracy to within ±2% for velocity over 2 m/s, and ±4% for under 2 m/s. The propeller unit and ADV were mounted

on a 50 mm steel pipe using a custom made aluminum or steel mounting brackets which ensured that the alignment for measurements were consistent in the flow. Figure 50 shows the ADV device and mounting bracket.

During winter and early spring, there was a lack of natural particles in the water for the ADV to detect water velocity and turbulence. Milk was injected in the flow upstream of the ADV probe to improve measurement performance. Additional details can be found in a 2012 Renewable Energy journal paper [10]. Drawing M-1 in Appendix 1 shows the mounting location and details of the ADV.

(a) (b)

Figure 50: ADV: (a) device on custom mounting bracket, note small tube on upstream side of ADV for injection of milk for low particulate water during winter and spring, and (b) photo of ADV nameplate

4.5.2 Power cables

To select the appropriate power cables for each turbine generator setup, the generator output current was calculated as follows:

$$P_3 = \sqrt{3}\, V\, I \tag{16}$$

$$I = \frac{1}{\sqrt{3}} \frac{P_3}{V} \tag{17}$$

where P_3 is three phase rated power output of the generator, V is RMS voltage line-to-line and I is RMS phase current. This is based on balanced three phase loads as is the case given three-phase rectification to DC in each power converter scheme. To simplify the test setup, a common cable was used for both the 5-kW and 25-kW vertical-axis turbines. Therefore, using the larger generator and Equation (17), the maximum current is calculated to be 41.2 amps. However, the 25-kW vertical-axis hydrokinetic turbine was designed for a maximum output at flow velocities of 3 m/s. The anticipated and measured velocities at the site were in the 2.2 to 2.5 m/s range. Based on limitations of the power electronics (rectifier/inverter), and the MPPT controls, and using 2.5 m/s as a maximum operating output, the resulting peak power delivery is 12 kW and using the nominal nameplate voltage of 350 $V_{L\text{-}L}$ the resulting current is approximately 20 amps. The Canadian Electrical Code requires that conductors are sized for 125% of the calculated load; in this case 25 amps. A 3c#8 AWG TECK90 cable was selected, having an ampacity of 45 amps, which also accounts for voltage drop from the generator to the shore station.

For the horizontal-axis turbine, the power converter was designed to be capable of delivering 155 kVA of power, to accommodate future testing of two hydrokinetic turbines [9]. The cable is sized based on the generator nameplate and test data. The 60-kVA Fisher Electric Technology permanent magnet generator nameplate indicates a full load maximum current of 132 amps. At 125% of the maximum current, the minimum ampacity is of 165 amps. The cable used was Super Vu-tron 4c#1/0 medium voltage flexible portable power cable and is rated at 205 amps, 2,000 V, and is water and UV resistant. It is also suitable for use up to 90°C and down to -40°C.

A weatherproof pin-and-sleeve connector was used for connection from the test platform to the shore. It is constructed in such a way that the ground pin in the center shown in Figure 51 is slightly longer that the other connection pins, and therefore, would be the first conductor to connect and the last to disconnect. The connector was modified so that if the mooring failed, it would pull apart in a controlled fashion and drop onto the platform deck.

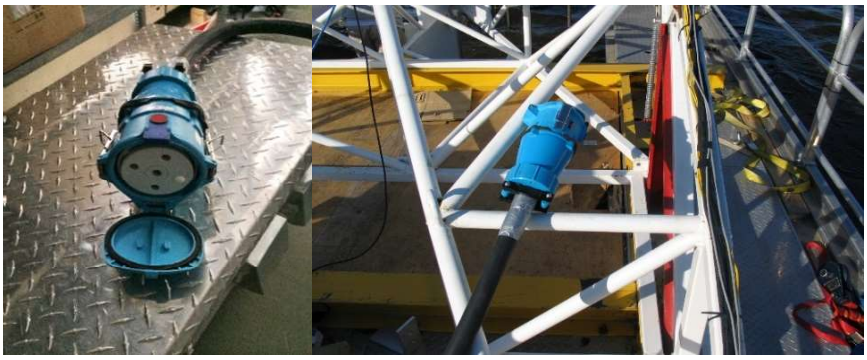

(a) (b)

Figure 51: (a) weatherproof 3 phases and ground connector for 4c#1/0 cable on turbine platform and (b) resting on "A" arm.

For a permanent deployment, a more rugged underwater cable would be used as shown in Figure 52(b) and (c). These cables are examples of those installed to test locations at Fundy Ocean Energy Research Ocean Research Center's tidal energy research site in Nova Scotia. They are 34.5 kV rated and submersible and include control cables and fiber optics cables. Using a composite cable allows for control, monitoring and video to be brought back to shore along with the power conductors. Several layers of helically-wound copper amour provide protection for use at the ocean bottom.

(a) (b) (c)

Figure 52: Power cables: (a) 2,000V 4c#1/0 cable used in this project for connection of turbine-generated power to the shore station. Cable has a rubber-based EPDM insulation with good cold weather characteristics, (b) and (c) a medium voltage cable used for bringing power to shore from tidal energy turbines at the FORCE site in the Bay of Fundy (photos courtesy of Fundy Force).

4.6 Connection to the grid

Energy produced from river hydrokinetic turbines can be grid connected, may operate stand-alone or may supply micro-grids. In the simplest form, a generator is connected directly to a load or loads, and in the case of river hydrokinetic generation, it may be sufficiently reliable to supply a base load. More than one device would always be recommended for any base-load scenario. In the first stage of this project, a stand-alone inverter/charger was connected directly to the output of the 5-kW vertical-axis hydrokinetic turbine. For testing connections to the grid, two power conversion systems were designed and constructed to supply hydrokinetic power to the Manitoba Hydro overhead lines at Pointe du Bois, Manitoba. These connections were installed in accordance with Manitoba Hydro's Technical Requirements for Connecting Distributed Resources to the Manitoba Hydro System [30]. These systems fall under a Type III Interconnection, where the distributed resource supplies their own electrical loads first, and sell the excess power generated to Manitoba Hydro at an agreed upon rate. The first system was set up to deliver power from the 5-kW and 25-kW vertical-axis hydrokinetic turbines, and was done in two

phases. A third connection was established for the horizontal-axis turbine and generator. Figure 53 shows a simplified schematic for each installation, to highlight the main equipment and identify the differences between them.

For the 5-kW system, a commercially available 6 kW rectifier/inverter system, Aurora PVI-6000 IGBT based inverter, manufactured by Power-One Renewable Energy Solutions LLC, with a matching rectifier PVI-7200 was installed in the site trailer, and connected to the 120/240V service entrance electrical panel for the trailer. The utility meter installed was a Centron bi-directional meter, manufacturer by Itron Inc., and supplied by Manitoba Hydro and shown in Figure 55. The electrical service to the trailer was connected to an existing overhead distribution line where a 7.2 kV, 120/240 V oil-filled pole top transformer provided the final water-to-wire link to the grid, as shown in Figure 53(a).

In the second phase, shown in Figure 53(b) the panel in the site trailer was upgraded to a 100 A, 120/240 V split phase service connecting to the Manitoba Hydro grid through the Centron bi-directional meter and pole-top transformer. In this test, the 25-kW turbine was installed on the test platform with a similar generator to part one, but with two stators in series and a 12 kW_e output power. To accommodate the additional power, a second Aurora PVI-6000 inverter and PVI-7200 rectifier was installed in parallel. This system required a 1:1 isolation transformer to be installed on the second inverter output to avoid ground fault detection on the first system. As the turbine rotor was oversized for the generator, surges in the river flow generated voltage above 530V and the inverter control system shut the system down on overvoltage. To address this issue, a resistive load bank was installed for each system. The overvoltage feature of the PVI-7200 rectifier was used to divert excess power away from the inverter. This bypass would continue to divert power until the incoming voltage was below 430 V. The Aurora was CSA certified for grid interconnection, having built-in anti-islanding and other protections required in IEEE Standard 1546.

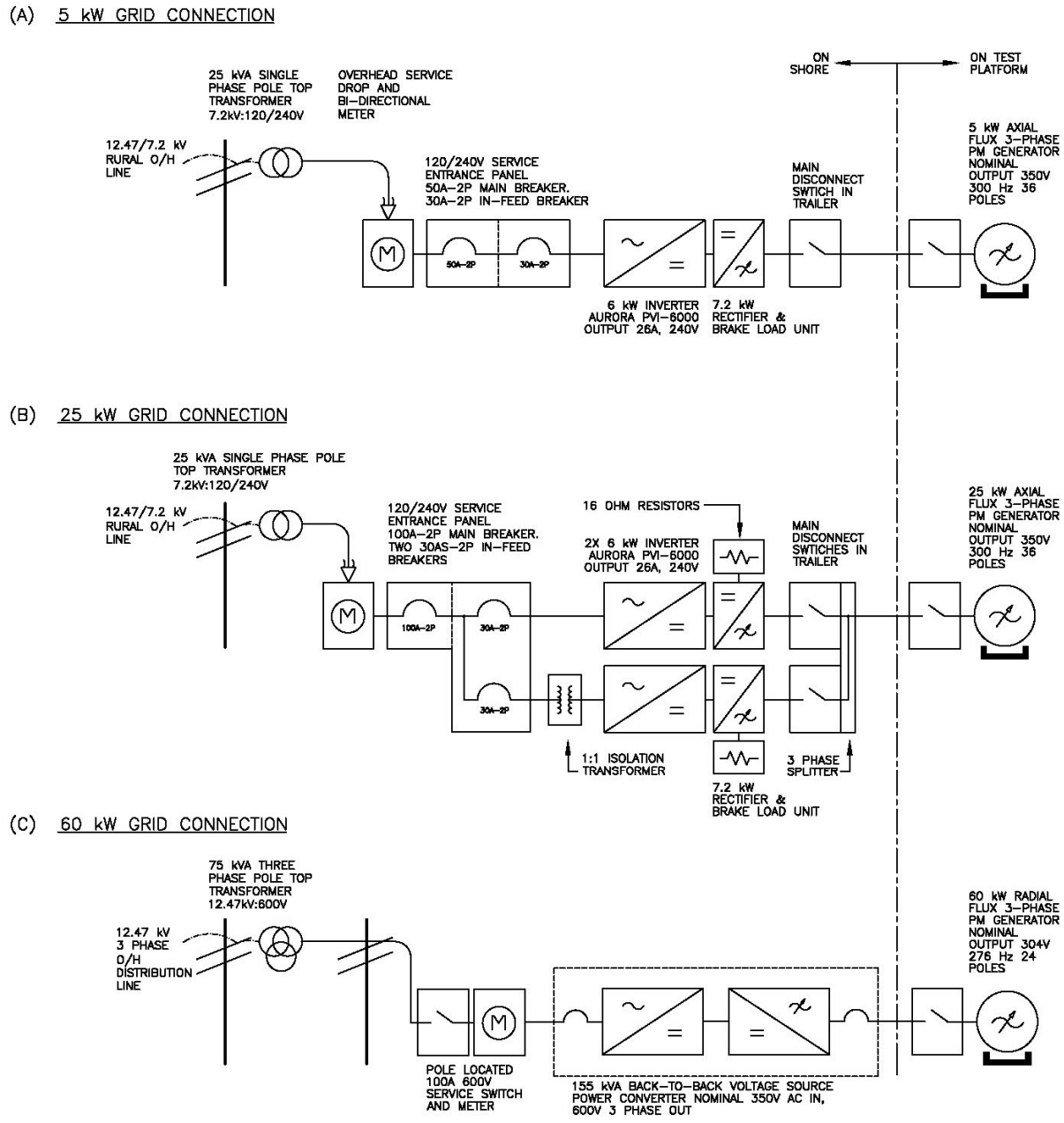

Figure 53: The three utility network grid connections implemented for testing hydrokinetic turbines: (a) split phase 50 A, 120/240 V service with bi-directional meter, (b) split phase 100 A, 120/240 V service with bi-directional meter, and (c) pole mounted, three phase 100 A, 600 V service with bi-directional utility meter.

In the third test configuration, shown in Figure 53(c), a 600 V power conversion system was designed and built for testing the horizontal-axis turbine by the University of Manitoba and Manitoba Hydro International [9]. A 75-kVA three-phase 12.5 kV, 600 V oil filled distribution transformer was provided on a pole near the trailer and connected to the 12.5-kV three-phase overhead distribution line. On a separate pole, a bi-directional meter was provided by Manitoba Hydro and a 600 V fused disconnect was installed as a service switch. From there, a 3c 1/0 cable was connected the 155-kVA solid-state power converter. This device consisted of two back-to-back IGBT voltage source converters. This device had input and output breakers which could be controlled by the system if necessary for shut down. With bold numbers indicating ANSI/IEEE protection designations, anti-islanding requirements such as under-voltage trip **27**, ground overvoltage **59g**, reverse power in non-export **32**, and interconnect disconnect device **89** were provided within this power converter. Manitoba Hydro interconnection guide DRG2003 [29] states the requirements for the power converter protections and controls. Figure 54 and Figure 55 show physical aspects of the three systems shown schematically in Figure 53.

(a) (b)

Figure 54: Power converters: (a) 5-kW vertical-axis turbine isolation switch, rectifier, 6 kW Aurora Inverter and 120/240 V panel, and (b) electrical equipment for the 25-kW vertical-axis turbine; second 6-kW Aurora (far left), disconnect switches, splitter (bottom) and rectifiers above (middle).

(a) (b)

Figure 55: (a) Bi-directional meter used for 5-kW and 25-kW grid connections to deliver hydrokinetic generated power to the Manitoba Hydro Grid, and (b) 155-kVA power converter using IGBTs designed for this project.

5. Environmental factors and impacts on hydrokinetic turbines results

Winter conditions in Canada can be extreme with respect to the rate of change in temperature and average number of cold days, providing an opportunity to evaluate installation and operation of hydrokinetic turbines in cold climates. This Chapter describes the environmental aspects and the challenges posed during the in-situ tests.

5.1 Ice conditions

The temperatures during the winter of 2008 were colder than average. During deployment, the average temperature was -15°C or below, and nighttime lows were recorded to be as cold as -36°C. The conditions of below freezing temperatures and turbulent open water create the potential for frazil ice. Areas upstream of the Pointe du Bois Powerhouse forebay are covered by stationary ice for most of the winter, preventing the formation of active frazil ice. However, the water surface in the forebay of the generating station remains open all winter due to the relatively high velocity and turbulence created by the narrowing of the river at the test site location. Open water remained, both upstream and downstream of the test site during all of the winter testing, and frazil ice was often present.

Frazil ice, consisting of filaments floating at the surface, were observed when temperatures dropped below -20°C. Frazil slush formed in the water around the vessel, as shown in Figure 56. This slush gathered on the main support system chains and within one or two days, grew into a large mass at the front of both pontoons and eventually across the entire bow of the platform; both below and above water level.

(a) (b)

Figure 56: Frazil ice: (a) inactive frazil ice flowing below the test platform, pancake ice forming on the support chains, and (b) inactive frazil ice forming large structures at the front of the test platform.

While the slush did not have significant structural cohesion, it built up on all surfaces it encountered. The presence of frazil ice and eventual adherence and build-up on the front of the vessel increases the anchor system loading and must be considered in calculations of the mooring loads. Super cooled water in the range of 0.01ºC to 0.02ºC below zero, with some nucleation seeding, is sufficient to allow frazil ice to form. However, there is no known calculation as to the amount of ice which may stick to objects in the water or the potential buildup, as the typical flows are constantly changing with respect to turbulence and waves. Furthermore, temperatures often vary 10 or 20 degrees from night to day, and in some cases as much as 40 degrees in a few days. The buildup of ice reduces the velocity of the surface water between the pontoons and creates flow stagnations, wherein the water freezes quickly to support platform surfaces. These areas of slow moving water allow more direct freezing or ice on the research vessel, and ultimately lead to a freezing of the water passage between the pontoons further restricting the water flow.

Figure 57: Five day time-lapse, clockwise from top left, showing ice formation on research vessel during a cold period. Frazil ice slush accumulates in the front of the vessel below the water line; surrounding the pontoon is the formation of rime and glaze ice. Despite reduced flow due to water passage construction, the turbine continued to generate power throughout the above sequence.

When air temperatures remain below approximately -15°C, large rime and glaze ice sections form within a day onto the aluminum pontoons and anything else placed at the water/air interface. There are two main mechanisms for this hard ice formation:

- Splashing: Water splashing up from objects at the water level and from the pontoon wakes themselves quickly add to the ice already formed, especially at the front of the pontoons.
- Water-film freezing: Wind and currents cause small periodic test platform motions. Thus, a portion of the vessel constantly moves in and out of the water-air interface. The vessel portion coming out of the water will have a thin water film adhere to the surface that will freeze immediately upon contact with the cold air (when below -15°C). As such, ice grows laterally in a relatively short time, forming an ice crust floating on the water surface. This ice crust becomes part of the vessel and is

subject to the same dynamic vessel motion. The edge of the formed ice crust also moves in and out of the water-interface and was subject to the water-film freezing mechanism.

Figure 57 shows a video capture frame taken at the same time every day for five consecutive days, giving a time laps view of rime and glaze ice growth on the research vessel. Figure 57 and Figure 58 show how passive frazil accumulated on the submerged portion of the chain as well as above the water line from splashing of both frazil ice and water due to wind and wakes. Figure 58 shows the free surface under the deck frozen from pontoon to pontoon. The thickness of the pontoon ice is shown by the segment remaining after the bulk of the ice was removed by manually removing it. Ice removal was best accomplished by using small hydraulic jacks to push the vessel upwards from the ice surface.

(a) (b) (c)

Figure 58: Ice formation examples: (a) ice formed below the vessel where bridging between pontoons occurs with the turbine still operating, (b) ice shown during deicing procedure, and (c) rime ice and frazil ice formed on anchoring chain. Ice formation was most severe for temperatures below -15°C.

Instrumentation located in or crossing the water line did not survive long. Ice growth, intentional ice removal, and unintentional natural shedding of ice pulled cables and instrument support holders from the platform. Attempts were made to protect and support the flow meter, load cell, and cameras placed under water, by incorporating rigid mounting

structures. The ice developing and its removal easily bent thick wall steel pipes 50 mm in diameter. During the coldest periods, the propeller flow meter was engulfed in ice, and could not be used. A handheld meter was used for periodic readings but froze when it was removed from the water. It required 15 minutes to thaw before subsequent readings could be taken. The added drag of the ice accumulation on the load cell wires severed the connection early on during testing and thus that sensor was lost for the remainder of that deployment.

After losing equipment to the ongoing ice and de-icing process, sensor mounts for the flow meter and underwater camera were redesigned with wires running through the inner cavity of a steel tube. All sensors were placed as deep as practical below the water level to avoid the surface ice for as long as possible. These precautions improved the life span of those sensors but generally did not last more than three or four days of -20°C conditions. The ice removed from the front of the research vessel was often pushed under the platform by the flow; impacting the sensors placed lower in the water. At one point during the 2008 winter testing, a significant accumulation of ice created a dam at the bow. The buildup of frazil at the bow, having a slush-like nature, was heavier than ice forming at the stern of the platform. Over time, and with surges of water velocity rocking the platform fore-and-aft, a large clear ice pack formed at the stern adding buoyancy, with the bow continuing to gather the heavier frazil slush. After approximately a week, this resulted in the bow of the platform having little or no freeboard. At one point, the bow of the vessel was pulled underwater with a surge wave, lifting a 275 kg boom from the deck and severely damaging the data acquisition shed and turbine enclosure. Data acquisition equipment was lost. However, the generator survived without noticeable damage. Figure 59 shows the extent of the damage.

(a) (b)

Figure 59: Damage to the test set up (a) resulting from ice buildup on bow and stern of the vessel causing the safety boom (cyan) not yet deployed to be thrown back damaging the control cabinet. Note that generator remained in operation but data instrumentation (b) was destroyed.

5.2 Materials and mitigation

Ice mitigation requires considerable attention for deployment and operation in cold climates. Figure 60 shows typical ice build-ups encountered. Electric heating solutions were ineffective or required more electrical energy than could be supported by the devices tested. Indirect heating by placing low-wattage heat trace cables within the front section of the pontoon had no effect. A hand-held propane torch took several minutes to melt the ice away from the pontoon and could only clear a small area. The presence of frazil ice and the near-freezing water continuously removing heat by conduction from the aluminum pontoons from below, caused the ice build-up to return in minutes. In an attempt to reduce ice build-up on the anchoring chains, a PVC pipe was placed around the front chains at the waterline. The concept was to put the pipe on loosely fit, allowing it to move and rotate to remove nucleation of ice. The PVC device was found a few days later inside a solid block of ice. A rubber tire inner tube was fastened to the leading edge of one of the pontoons to present an ice-phobic surface. The ice did not adhere strongly to the rubber and it was easy to detach from its surface. Ice continued to form, however, around the tube and subsequently engulfed the inner tube as shown Figure 61. Although it was embedded in ice, the ice broke loose with a minor force, as the air-filled inner tube flexed when struck.

Rubber coated pontoons have some promise as a mitigation tool, but this solution would need to be incorporated into the assembly of the support vessel. The only option that remained for this demonstration was ice removal and this took place regularly every few days.

Figure 60: Additional photos of icing during winter showing ice growth under the vessel. Although the turbine is not impacted, the ice bridge can grow thick enough to start touching the top of the blades. No ice adheres to the blades. The lower right picture shows the video cable frozen in and rendered unusable.

(a) (b)

Figure 61: Rubber inner tube tied to front of pontoon to test ice adherence. Ice did form on the inner tube, but broke off easily.

Mechanical jacks, steel picks 1.5 m long, and a rubber sledge hammer were used to de-ice the vessel. The steel pick had a flat edge on one end and a flat top on the other allowing it to be placed in a fissure or weak location and hammered with the sledge hammer. The large rubber hammer enables large sections of ice to be removed without significantly damaging the aluminum pontoons. Hydraulic and lever jacks were used to develop a force between the ice surface and the bottom of the pontoon structures as shown in Figure 62. Consecutive blows with the hammer onto the ice often broke the bond between the ice and the aluminum pontoons. After separations were created, the fast-flowing water broke off remaining bonds. Once free of the pontoon, the flowing water of the river removed large slabs of ice from the exterior of the research vessel and below it. Larger pieces of ice tumbled below the vessel, impacting on and in some cases denting the turbine blades.

Figure 62: Ice formations were broken from the bottom of the test platform using a variety of jacks. A jack is used to break ice from between the pontoons. The ice formations in this example are 300 mm to 450 mm thick.

The more solid ice build-up on the chains could be removed by striking several blows with the rubber hammer, the flexibility of the chains forcing the hard ice to break off. The submerged ice due to frazil ice process was softer and therefore harder to remove because it did not form the large crystalline structures and required more of a scraping procedure.

In general, any structure within a 30 cm of the water's free surface was susceptible to rapid ice growth; often due to splashing of waves or the wake undulating past the platform. Figure 58 and Figure 60 show the severity of the ice growth on the vessel. The photos demonstrate the thickness of the ice accumulation on and between the pontoons. The pictures were taken through the access hatches on the vessel's deck and show several stages of ice propagation and the results when ice grows across from one pontoon to the other. A pipe onto which the underwater camera was mounted is shown, entirely engulfed in thick ice. Ice grew extensively on the exterior of the pontoons as well. Clearing these sections of ice required care regarding personnel safety. Figure 62 shows the use of lanyards and safety

harnesses (red) which were mandatory during de-icing operations. Along with photos of ice buildup along and between the pontoons, this figure shows the thickness of the icebergs that break off from the ice sheets in the spring. The size of the detached ice sheets are larger than, and in many cases are estimated to have more mass than, the research vessel.

To address cold temperatures, it was necessary to change the gear oil to a synthetic oil: MOBIL SHC 626, which maintained good viscosity, even at -40°C and is shown in Figure 63(b). According to the MSDS data sheet number 6442 this oil is "not expected to be harmful to aquatic organisms and not expected to demonstrate chronic toxicity to aquatic organisms." The amount used in the 5-kW unit gearbox was in the order of 10 liters.

(a) (b)

Figure 63: The gearbox oil became viscous at low temperatures: (a) the turbine generator, gearbox (dark blue) and rigid insulation (light blue) inside an enclosure and around the support cradle, and (b) the initial gear oil was changed to synthetic oil that had better viscosity characteristics at -40°C but remained environmentally neutral.

6. Turbine testing results

This Chapter presents the results of operational testing of the four turbine-generator configurations investigated. Section 6.1 includes winter tests of the 5-kW vertical-axis turbine-generator and a stand-alone rectifier/inverter. These tests led to improvements of the power train, as well as demonstrating the viability of turbine deployment and operation in cold conditions. With additional modifications for efficiency, the 5-kW system was tested in the spring and summer, with two different power conversion systems, including grid connected modes. The results of testing the 25-kW rotor, paired with a 12-kW generator and grid connected 12-kW rectifier/inverter system are provided as well as limited testing of the horizontal-axis turbine.

6.1 Vertical-axis 5-kW system

Once the testing platform was in place, the 5-kW vertical-axis turbine, with 5-kW 36-pole axial flux permanent magnet generator and 13.5:1 geared speed increaser was placed in the water, with average flow velocities of 2.06 to 2.15 m/s. Initially, the generator was connected to a standalone MWI-5200-48 model rectifier/inverter system re-purposed from a wind application. This unit was manufactured by Magnetek, model MWI, for multi-mode wind inverter. It was built for standalone off-grid operation, and did not have the required anti-islanding or grid protection features. However, it was suitable for inputs from wind turbines, solar PV arrays as well as fuel-fired generators, and had outputs at 48 VDC and 120/240 VAC. The inverter output was connected to 120 V flood lights in the test trailer, and was also used to charge four wet-cell 12 VDC batteries connected in series for 48 VDC. The maximum power point tracking algorithm built into the MWI inverter system allowed for uploading of a voltage-power look up table with 14 points. For permanent magnet generators, voltage is proportional to rotational speed in the normal operating range. Therefore, voltage is measured and used as the table input. The matching power output from the table is used as an input to modulate the inverter output duty cycle, and therefore power output. Figure 64(a) shows a typical MPPT table for the MWI inverter.

MPPT Table MWI-5000-48				
Freq. [Hz]	**Turb. RPM**	**Gen RPM**	**MPPT [V_{DC}]**	**Revised Set [W]**
143.0	35.3	477	90	0
144.0	35.6	480	115	50
162.0	40.0	540	127	90
180.0	44.4	600	140	100
198.0	48.9	660	153	190
216.0	53.3	720	165	320
234.0	57.8	780	178	420
252.0	62.2	840	190	550
270.0	66.7	900	203	800
288.0	71.1	960	216	1080
310.0	76.5	1033	220	1700
340.0	84.0	1133	230	2900
372.0	91.9	1240	266	4400
432.0	106.7	1440	280	5000

(a)

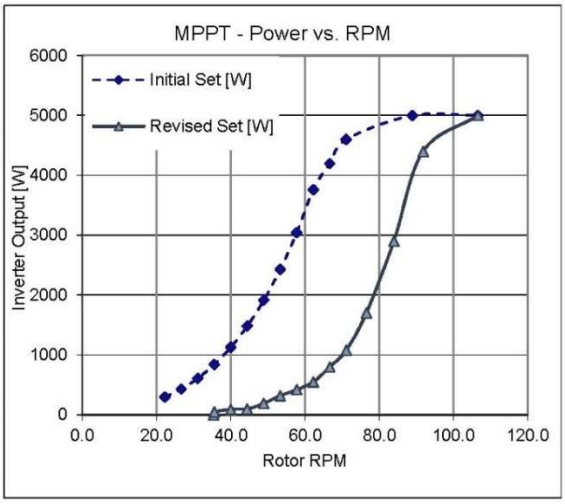

(b)

Figure 64: Maximum power point tracking input table (a) and graphical representation (b) for the 5-kW turbine. Note that the table shows the modified MPPT table, after preliminary tests using "initial set" data resulted in stalling of the turbine.

Due to the cold temperatures and hydraulically inefficient support arm geometry, the output of the generator was unexpectedly low, and the initial MPPT curve caused the turbine to stall when it applied a load greater than 500 W. The first improvement was to change the oil in the gearbox to a synthetic low-temperature oil and enclose the gearbox in an insulated enclosure. New MPPT data, shown in Figure 64, was then uploaded into the MWI controller and the unit was re-started. At the time of this test, the in-stream velocity probe had not yet been installed, but the flow was estimated to be at 2.0 m/s. For this set up, the maximum electrical load delivered, per the MWI internal recordings was approximately 420 W.

This test set up was operated for approximately two months during the coldest weather period of the year in Manitoba. During this time, night temperatures were as cold as -39°C with the average temperature remaining below -17°C for the entire test period, as shown in Figure 65. Even under these cold conditions, the turbine was operated for approximately 1,028 hours. Table 5 shows the testing times.

Table 5: 5-kW rotor and MWI inverter operation

Turbine run times - Jan 9 to Mar 5 2008			
Start	**End**	**Runtime (hrs.)**	
		Elapsed	**Running total**
2008-01-09 09:31	2008-01-16 4:10	163	163
2008-01-16 18:00	2008-01-21 5:18	107	270
2008-01-28 23:15	2008-02-04 1:30	146	416
2008-02-05 12:00	2008-02-12 3:00	159	575
2008-02-15 13:00	2008-03-05 9:33	453	1028

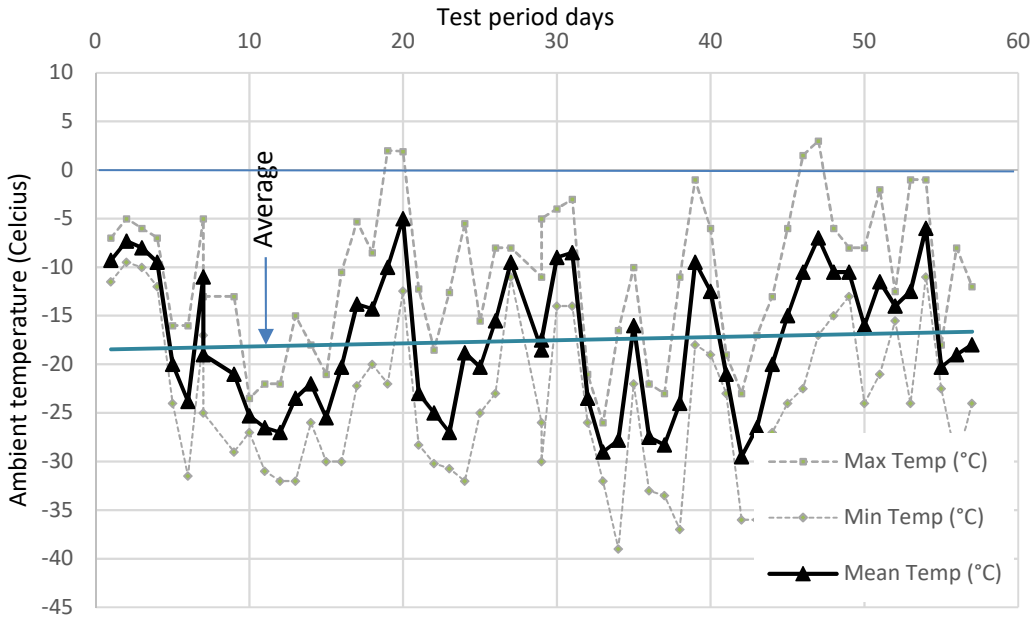

Figure 65: Local temperature in Pinawa, the nearest Environment Canada weather recording site, approximately 28-km southwest of the site, but considered equivalent with respect to this period, and for general climate data. January 9 through March 5, 2008.

These tests were dominated by icing issues on the vessel, as discussed in Sections 5.1 and 5.2. Secondary performance issues of the turbine in cold weather were addressed as noted.

Nevertheless, meaningful power and water velocity data were obtained and a sample of power and water velocity are provided in Figure 66 and Figure 67.

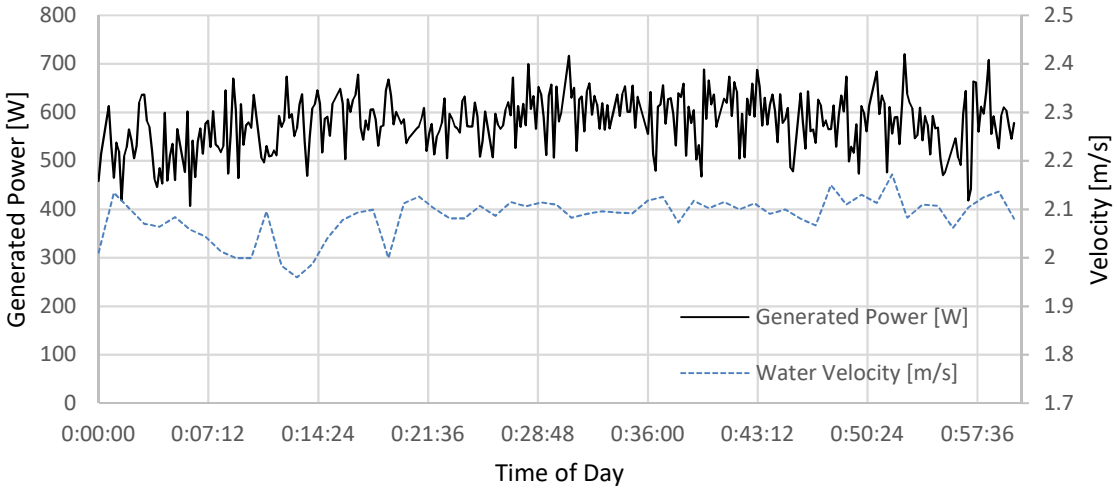

Figure 66: Generated power and velocity measurement for a representative one-hour testing starting at midnight on March 9, 2008.

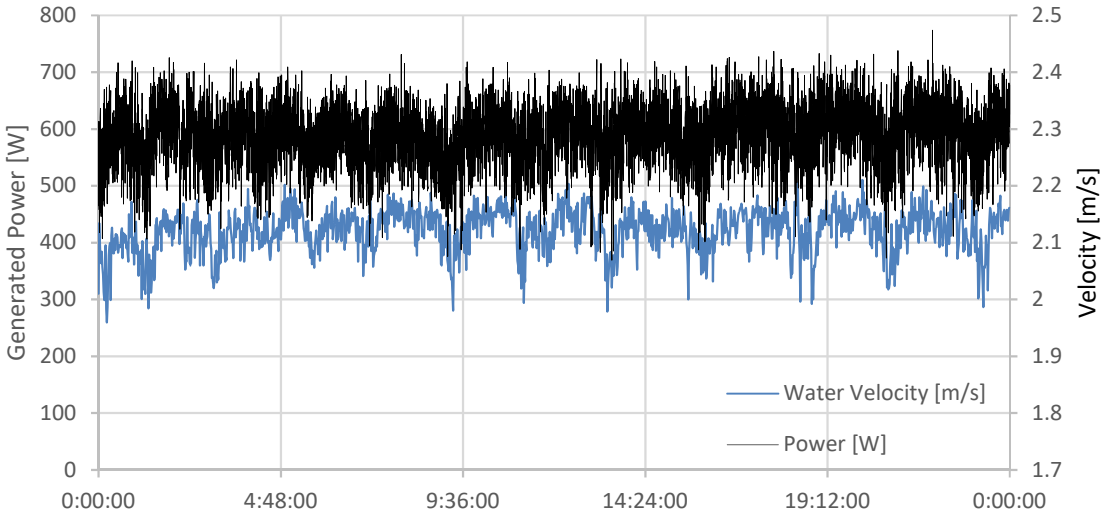

Figure 67: Generated power and concurrent water velocity measurement for 24 hours, starting midnight March 9, 2008.

Figure 67 shows how the power output tracks the overall water flow velocity. Detailed analysis of this relationship is discussed in Chapter 7.

For the test period shown as a representative period, the turbine's mean output was relatively steady. Using hourly averaged data over a day, the turbine produced 590 W with a maximum value of 774 W and a minimum of 369 W. The flow held steady with a mean velocity of 2.12 m/s, having a standard deviation of 0.03 m/s. Throughout winter testing, the turbine exhibited efficiencies around 15.9%, which is significantly less than rated performance as there was a significant source of power loss from the initial support arm design. Once corrected, the final efficiency of the turbine rotor was above 35% and the turbine self-started.

The rotor was inspected after winter operations. Slight damage to the blades, from contact with ice or debris during the winter testing was observed and is shown in Figure 68(b). Ice build-up around the rotor shaft impeded the flow. Nevertheless, even in the coldest weather, the rotor turned and kept water from freezing in place Figure 68(a).

(a) (b)

Figure 68: Winter testing: (a) rotor shaft free of ice, however, ice buildup from the pontoons of the test platform impinged water flow, and (b) hydrofoil after winter testing with slight damage to the trailing edge particularly near the water-surface end.

In March 2008, the test platform was removed from the flow, following the procedures outlined in Section 4.3, to avoid damage to the vessel and equipment during spring run-off.

6.2 5-kW hydrokinetic turbine, spring and summer testing

The following sections describe the on-site testing of the 5-kW and 25-kW vertical axis hydrokinetic turbines. For all testing at the site, grid-connection mode was used, and power was supplied to the Manitoba Hydro rural distribution line. No failures of inverters or interconnection systems were observed on any test, and Manitoba Hydro did not flag any anomalies mon the grid resulting from the delivery of power.

6.2.1 Grid connection of 5-kW turbine

Once the river was clear of ice in May, the test platform was placed back into its test location, and the 5-kW turbine was refitted with new profiled blades to reduce drag. A 6-kW rectifier/inverter was installed to grid connect the turbine, as described in Section 4.6.

Power was first delivered to the Manitoba Hydro grid on June 6, 2008 via a bi-directional meter connected to the site trailer, with power flow to and from the 12.47-kV rural distribution line through a pole-top mounted transformer.

Static Indicators	
Indicator	**Description**
888 888888	Nine digits (7 segments each) for display of alphanumeric information
EOI	End of Interval—(Registers - Dmd)
VA, VB, VC	Indicators for phase voltage (not applicable in CENTRON C12.19 meters) are present during segment check
◀■■▶	Watt Disk Emulator - scrolls right for positive; scrolls left for negative
120 240 277 480	Nominal Voltage Indicator (not applicable in CENTRON C12.19 meters) are present during segment check
Scr Loc	Scroll Lock (indicates temporary scroll lock of a display item)
SEL nor, SEL Alt	Selection of Normal or Alternate sequence
nor diSP	Entry into Normal Mode.
TEST	Entry into Test Mode.

Figure 69: Photo of Itron Centron II bidirectional meter and page from owner's manual; bi-directional meter used for 120/240 V grid connections.

The bi-directional meter shown in Figure 69 allows net-metering during a monthly billing period. When the hydrokinetic system was operating, the electrical usage in the site trailer for testing purposes was provided for by the turbine, and excess power was automatically fed to the grid. When power is supplied to the grid, the internal data storage system reduces the metered power for the billing period.

6.2.2 Turbine support arm and other losses

The power output during the winter testing was significantly less than the expected value, with a typical efficiency of 9% rather than the overall theoretical efficiency of 30%. While using suitably cold-rated gearbox oil, heating and insulating the gearbox, as well as routinely clearing ice from around the turbine made some nominal improvement, it was evident that the rotor support arms required improvement. The test platform simplified the testing of the efficiency of different rotor support configurations by allowing the turbine and generator arrangement to be removed and re-inserted into the flow, with new support arms changed in situ. Figure 70(a) shows support arms being changed while on the test platform.

(a) (b)

Figure 70: Drag reduction: (a) hydrofoil being removed while the rotor was on the test platform to change support arms, and (b) 5-kW unit on shore with hydrofoil shaped support arms which resulted in experimental efficiency values close to the calculated values.

The initial design of the turbine included eight steel plates, two per hydrofoil to support the blades from the central shaft. These plates were rectangular in cross section, slightly narrower than the hydrofoil cross-section, and are referred to as 'flat bar' support arms, as shown in Figure 70(a). The shape of these structural members effectively created eight bluff bodies, rotating with the blades, and causing significant drag that reduced the turbine efficiency. To measure and improve the turbine overall efficiency, several tests were performed.

Two new support arms designs were fabricated. The first, termed *profiled*, had machined leading edge with a rounded front and a tapered rear creating a more hydrodynamic shape. The second was constructed from the same extruded aluminum shape as the hydrofoils themselves and are shown in Figure 70(b).

To quantify the efficiency improvement, the generator output was measured with each set of support arms. The free stream water velocity and turbine rotational speed were measured continuously so that tip speed ration (TSR) could be calculated. The Aurora rectifier/inverter system was set up for each set of support arm experiments to establish the TSR power curves. Figure 71 summarizes the results of the support arms efficiency tests. Note that for these tests, the turbine was grid connected. Therefore, the load could be varied from zero to its maximum value, as controlled by the inverter through its output power versus voltage curve.

The efficiency curve shows a significant improvement, more than double, when the geometry for the support arms was changed from a flat bar to the profiled shape. As expected, the hydrofoil shape further improved the efficiency, showing a peak at 26.5% at a TSR of 2.24, an additional increase of 5.2%. In addition to improving the efficiency, the shape of the C_p vs. TSR curves also broadened, resulting in a reduced sensitivity to changes in water velocity. This is important since water velocities in a natural river flow are turbulent with large length scales in the order of meters. As noted in the winter testing results, using the flat bar configuration, the small operational range and steep loss of

efficiency when TSR is not near the optimum value caused the system to stall and generally limited the output. Note that for a given water velocity, the operating point can be shifted to the right-hand side of the efficiency curves by decreasing the load on the generator (less electrical output).

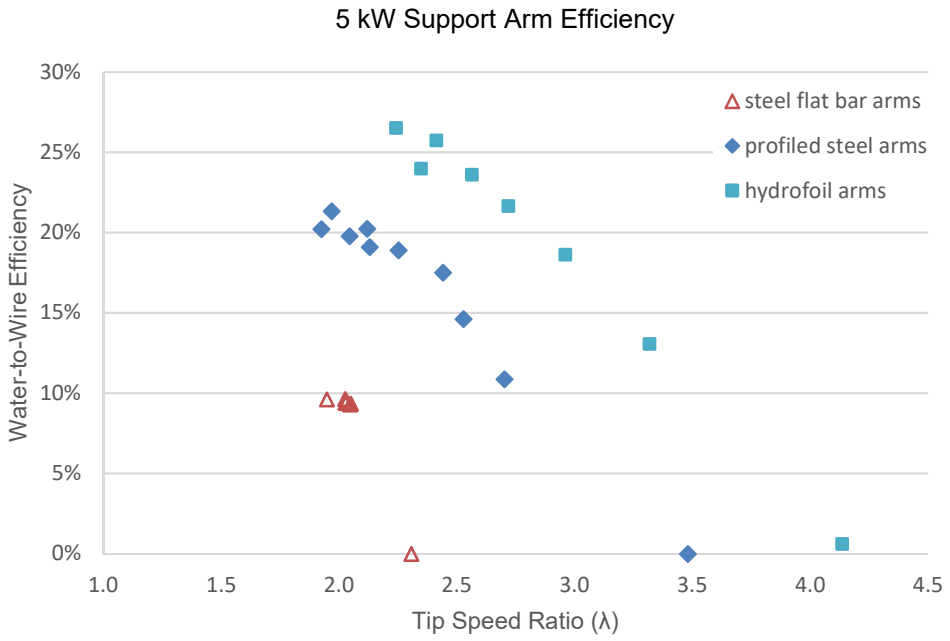

Figure 71: Results of support arm efficiency testing for the 5-kW vertical-axis turbine and generator combination.

With reference to Figure 5, the MPPT controller for the system attempts to keep the operating point on the right-hand side, or "back side", near the top of the TSR curve, to maximize power out. The MPPT avoids the steep "front" of the curve where there is potential to stall. Stalling of the rotor, particularly for vertical-axis turbines with limited self-starting characteristics is to be avoided. In addition to the losses due to the support arms and hydrofoils themselves, there are losses due to the inverter, the drivetrain gearbox and generator, and electrical line losses. Drivetrain losses include the mechanical linkages, bearings, gearbox and generator losses. These values were measured by New Energy on a

test stand. The input torque was delivered by a DC motor and the generator's AC output was used to quantify the power lost in the transfer.

The effects of the wake due to the pontoons was considered significant enough to estimate. This was done by placing the turbine in a second location on the platform, nearer to the bow, where the wakes from the two pontoons were not yet interacting. This resulted in an increase in power output of 150 W for the same velocity and support arm geometry. This value was used to estimate the loss for the other two geometries, by taking into account the difference in mass flow based on differences in mean velocity cubed for each test set up.

Table 6 summarizes the estimated losses for the peak power output for each support arm geometry. Note that the water-to-wire efficiency includes all losses. The rotor efficiency is the net efficiency of the rotor only, and is provided for comparison to other systems. Thus, the hydrofoil shape shown in photo in Figure 70(b) proved to have the best efficiency.

Table 6: Summary table of water-to-wire losses and their sources

Arm profile	Velocity (m/s)	Power (W)	Rotor (RPM)	TSR	Water -to-wire eff. (%)	Losses (W)			Rotor eff. (%)
						Pontoon	Drivetrain	Inverter	
Flat bar	2.35	727	59.6	2.03	9.6	166.53	244.7	58.2	15.9
Profile	2.27	1449	56.0	1.97	21.3	150.00	226.3	115.9	28.6
Hydrofoil	2.09	1410	58.8	2.24	26.5	117.52	240.4	112.8	35.4

During spring, rain entered the generator and the gearbox adding resistance and reducing the turbine efficiency, causing more test series to be cancelled. This issue was addressed by placing a rain cap over the generator. This issue was not found during the winter, as snow did not have that effect.

6.2.3 Main support cable tension forces

The drag force on the main anchoring line was measured using a load cell placed in-line with the turbine mooring chain, as shown in Figure 28. The load cell, Honeywell model RGF, was factory calibrated for loads of up to 222 kN. Data was recorded via the dataTaker

I/O device, sampling at 1 Hz and values were averaged each minute during testing. The load cell cable was secured to the mooring line and although several attempts to shield the connection point were attempted, the highly turbulent water passing the chains worked the cable loose limiting operation time. Nevertheless, several hours of data were recorded. Battery operated load cells that can internally store the data or broadcast the data from under the water using radiofrequency are required for such an application.

The drag force on the main cable is equal to the sum of the drag forces acting on each component of the system. Wind drag on the test platform was minimal on the test days, and was ignored. To determine the drag force on the turbine, the drag force of the system was recorded with only the pontoon (turbine out of the water), turbine with the break not on, freewheeling, and grid connected. Table 7 gives a summary of the different load forces recorded.

Table 7: Summary of load cell force measured on mooring cable for 5-kW vertical-axis turbine at a flow velocity from 2.2 to 2.3 m/s

Mooring cable loads (kN)			
		Flat bar	Profile
Base line	Research vessel only	3.65	3.80
Total drag	Turbine generating	6.12	6.56
	Turbine in, brake on	4.52	4.37
	Free wheeling	4.99	N/A

It is noted that the flat bar produces a slightly lower drag than the profiled arm while operating. However, the overall flow was lower for this test, as evidenced by the base line research platform only load. The measurement of the main support cable tension force is also useful for observing the flow dynamics and rotor/generator interaction. For the 5-kW vertical-axis turbine, sample data of the mooring cable force, average flow velocity and power generated is shown in Figure 72.

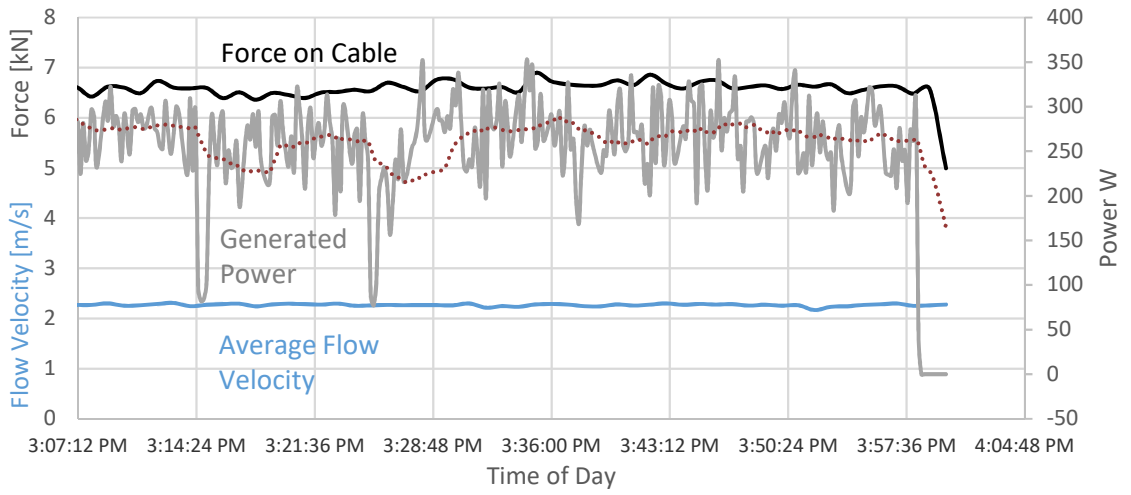

Figure 72: 50-minute sample of concurrent measurements of the tension force on the mooring cable (black line), generated power (gray line) and average water flow velocity. Also shown is a sliding average of the power signal (red dotted). At approximately 3:58, the turbine was halted by operating the brake and the cable force drops off quickly.

With respect to Figure 72, some general observations can be made. The water velocity is relatively constant, and represents an average, counting revolutions per minute from the propeller-style velocimeter located upstream of the platform. The drag force is also based on a one-minute average of the load cell readings and shows undulations relatively uncorrelated to the minor but observable flow variations. The power signal is sampled using the Arbiter Power Analyzer, sampling every ten seconds. For comparison, the figure shows a sliding average of ten power samples as a dashed line. By comparing the generator output and the cable forces to the average flow they appear to be influenced by flow structures not captured by the average water velocity value. Reaction to the generator torque pulsations due to the cross-flow rotation of the turbine blades and the complex interaction of turbulence are likely sources for this behavior. Note that the measurements for the 5-kW system are at the low end of the load cell's capability, and variations around the approximate mean value of 6.5 kN are at the threshold of the 10% accuracy of the device. The dynamic forces which the support cable and intermediate components like shackles and chains are subjected to during power generation must be considered during anchoring design. While the up and down (rocking) motions of the platform added to icing

issues, it demonstrates a potentially beneficial damping effect of the cable and chain support structure for the turbine components and the anchoring system.

The original design for the anchoring system, having the overall system rated for 218 kN based on a 3.4 safety factor on 64 kN maximum load is more than adequate. For the 25-kW system, the average peak load measured during generation was in the order of 20 kN.

6.3 25-kW turbine and generator

Following the 5-kW tests, the 25-kW New Energy turbine was tested at the same location. Chapter 4 details the turbine configuration and deployment. The velocity ranged from 1.7 to 2.5 m/s during the summer and power was delivered to the Manitoba Hydro grid by way of two rectifier/inverters installed in the shore trailer and a bi-directional meter.

6.3.1 Ancillary protection and control

The power cable was laid upon the footbridge approximately 80 m from shore and connected to the generator on the test platform. The electrical connection at the front of the platform employed a plug designed to disconnect under tension in the unlikely event of a mooring system failure. A 120 V circuit from the shore power, through a normally open relay, held the brake on the generator in the open position. If the cable were to become disconnected, or when a manual emergency stopping of the turbine was required, the break would be energized.

In the initial setup, the generator was connected to one 6-kW Aurora inverter. Due to the higher than anticipated flows, and the 25-kW oversized rotor and a 12-kW generator, over voltage situations occurred. This over voltage resulted in a shutdown of the inverter output by its internal protections. To ensure that generated voltages did not exceed safe limits for the equipment before the second stage of 6-kW inverter was delivered to the site, an overvoltage relay was added to the brake circuit such that generated voltages at the rectifier output greater than 500 VDC would cause the brake relay to open and halt the rotor.

While this improved the safety aspects in the interim, to allow continued power generation during higher flows, a braking resistor was added to the system at a designated rectifier output. The internal control of the rectifier switched in a separate IGBT inverter when the DC bus voltage was greater than 530 VDC. This inverter applied resistive load to the generator until the voltage was reduced to below 485 VDC. Then it automatically disconnected the resistor load. This significantly reduced the number of shut-downs due to over voltage. A second 6-kW inverter, with its own rectifier and braking resistor was eventually added allowing for 12 kW of generated power to be delivered to the grid. Due to changes in the river flow conditions, with the average peak of 2.4 m/s, the maximum sustained output power was approximately 9 kW at 120/240 VAC.

The Aurora inverters provided turbine speed and load control via a MPPT algorithm. The inverters were connected through an RS232 serial communications link, with one inverter's load schedule governing both outputs based on a frequency versus power output look-up table, similar to that shown in Figure 64.

6.3.2 Operation time

The 25-kW vertical-axis rotor was operational for 312 hours, between June 16 and October 23, 2008. During this time, the average output to the Manitoba Hydro rural distribution was 9.1 kW with a peak of 12.1 kW. The total energy delivered during the test period was 2,249 kWh, for an average of 7.2 kW. This includes all of the stop-start testing and testing with 6-kW inverter. The low number of operational hours was related to the induced vibration of the test platform at high velocities, as discussed below, which required operating the turbine in attended mode only for safety.

6.3.3 Output power

The Aurora rectifier and inverter combination manufactured by Power One operated within the required parameters as specified by Manitoba Hydro in their *Technical Requirements for Connecting Distributed Resources to The Manitoba Hydro Distribution System* [29]. During the testing in October 2008, generated power was supplied to the Manitoba Hydro

grid through a bi-directional meter. Figure 73 shows a representative power output for a 13-hour period.

For the sample shown, the frequency deviation was less than 0.1 Hz. The RMS output voltage had a range of ±4.5 volts, or less than 2% of the nominal rating of 250 VAC, with a standard deviation of 1.05. The input voltage, had a more considerable range of ± 28 volts or 7.5%, with an RMS value of 371.2 volts, a variance of 26.45 and a standard deviation of 5.14.

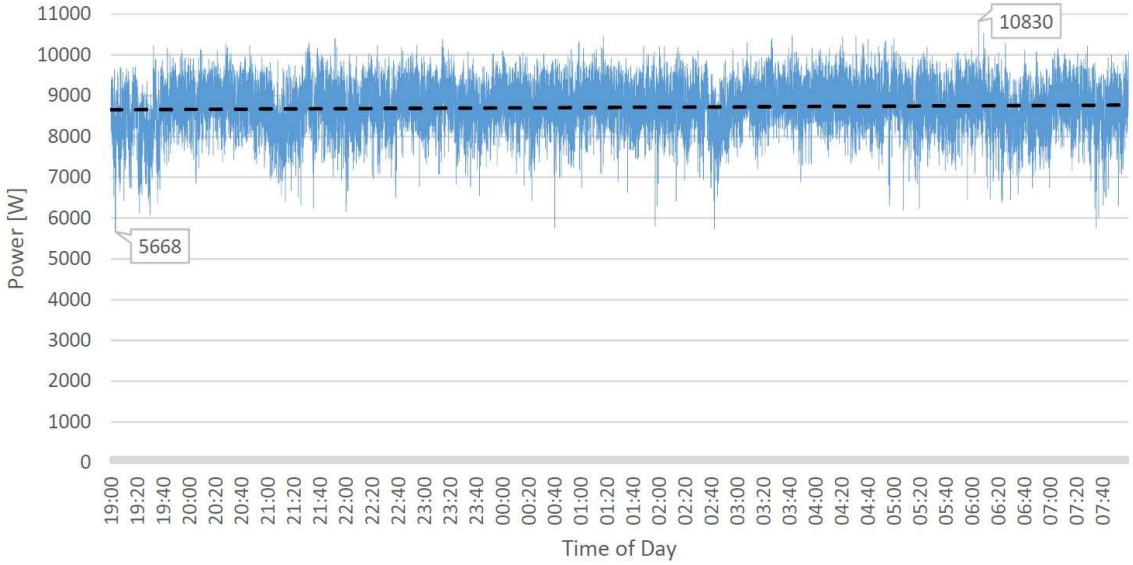

Figure 73: Representative output power from the combined Aurora inverters, one second intervals. The average power delivered in this example is 8,718 kW (dotted line), maximum 10,830 kW, minimum 5,668 kW. Power was supplied to the Manitoba Hydro rural distribution line.

Figure 73 demonstrates that power derived from the hydrokinetic turbine can supply sustained power to the grid, when operated with a MPPT control system. However, based on the fluctuations observed, if the turbine is operated as a 'stand-alone' supply, the load would have to be controlled to ensure that a peak load would remain below the minimum value produced with the constantly changing fluid velocity in the river. In the example period shown above, the total base load would not be recommended to be greater than 5

kW. In a practical scenario, more than one hydrokinetic turbine would supply a local grid or micro-grid, further averaging out flow fluctuations and increasing capacity and reliability. The addition of an energy storage facility, for example, a battery bank could be applied.

The integration of energy storage batteries into the power converter system between the rectifier and the inverter would seem to be the next reasonable evolution of this technology. Some consideration is given to this in Chapter 9.

6.4 25-kW turbine efficiency results

Figure 74 compares field measurements with theoretical values for the 25-kW turbine. For these tests, support arms with the hydrofoil geometry were used.

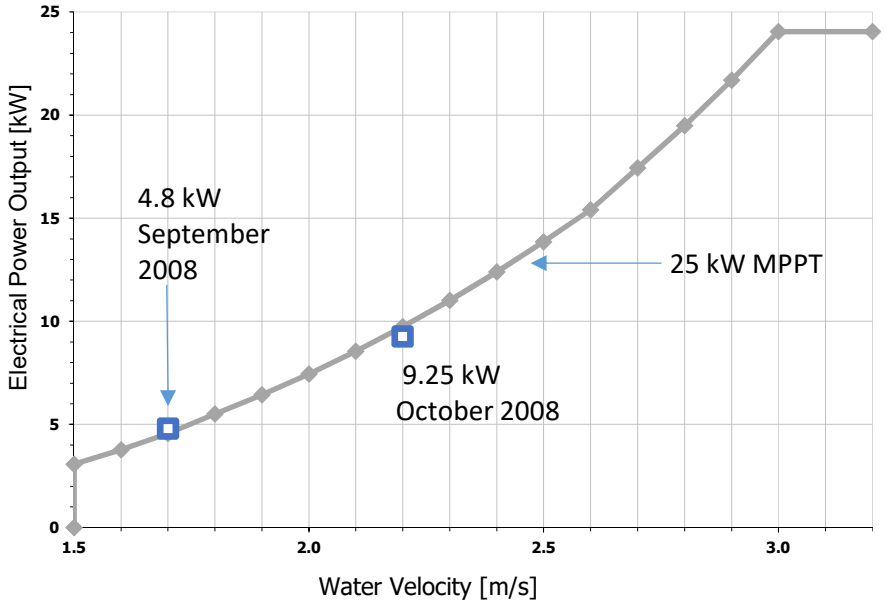

Figure 74: The peak output power for two test days relative to that expected using the 25-kW MPPT line.

Based on the efficiency measurements described in Section 6.2.2 and tested performance of the rotor, New Energy developed an MPPT curve for use in the Aurora inverters to control the system output to the grid. The actual MPPT curve used in the inverter is one

half of the output shown above, as both 6kW inverters were controlled by one inverter's control system. The testing in September was somewhat limited due to low flow conditions in the river at 1.7 m/s. For the test results shown in October, an average of 9.25 kW was generated with an average flow of 2.2 m/s. These results show that the MPPT tracking system is suitable for this system. There is good confidence that flows in the order of 2.4 m/s would result in the peak power nearing the maximum output of the two inverters of 12 kW.

6.5 Horizontal-axis turbine and 60-kW generator

In October of 2011, the horizontal-axis turbine with 60-kW radial axis permanent magnet generator was deployed in the test position after having addressed all safety concerns. Due to lower than expected rainfall in Western Ontario during the summer, the flow rate in the Winnipeg River became abnormally low. In addition, a complete test of this turbine configuration was no longer possible as the Pointe du Bois test site was scheduled for a long-term shutdown by December 31, 2011 due to a spillway reconstruction project.

At the time of deployment, the water velocity was nominally 1 m/s, which corresponded to the expected cut-in velocity of the turbine. The support "A" arm with hydraulic lowering mechanism operated as expected. The measurement and metering devices were tested and found to be operational. Figure 75 shows the test platform in place at the test position.

(a) (b)

Figure 75: Test platform in place for horizontal-axis testing. Large fiberglass mooring buoy (yellow) in the background was used for deployment, but does not support the test platform or turbine during testing. The shrouded turbine is shown fully submerged, with the housing for the generator and ancillary devices above the water line. Supports for ADV, propeller-style flow meter and underwater camera can be seen upstream of the turbine mounted to the deck of the platform (yellow and aluminum brackets).

During the first day of deployment, the average flow was approximately 1.0 m/s, and the rotor could self-start and turn. While the detailed C_p versus λ curves for the shrouded turbine remained proprietary, the 60 kW PMSG generator was tested in the lab as part of the power converter design [4]. The generator was found to have a linear voltage versus frequency relationship in the operating range. At the rotation speed anticipated for 1.0 m/s flow, the generator produced a voltage of 190 to 200 V with a frequency of 180 Hz. According to the turbine manufacturer's calculations, this should have been capable of producing approximately 5 kW of power. Under no-load conditions and 1.0 m/s velocity, the power converter could energize the line-side rectifier to charge the buffer capacitor circuit to 980 VDC. However, as soon as a load was applied, the rotor slowed down and the voltage dropped below the minimum voltage of 180 VAC, shutting down the converter on under-voltage.

The following day, the river flow at the test site had reduced to less than 1.0 m/s, which was insufficient to overcome the inertia of the rotor, drive train and generator, and therefore the unit would not rotate. Even with manual assistance, by pushing on the rotor with a bar,

the rotor would not turn. Therefore, the recommended minimum flow velocity for this turbine and generator combination is 1.5 m/s. It is noted that the specific drive train for this test configuration uses a large chain and sprocket system to transfer the power from the turbine/rotor shaft to the generator shaft. The original design anticipated that the generator would be located behind the rotor and effectively be part of a nacelle type structure. This would have eliminated the need for the drive chain and gears, which would have improved the efficiency enough to start, even under these low-flow conditions. Figure 76 shows the shrouded turbine components in the arrangement received from the manufacturer, as well as a diagram of the chain and sprocket and various components in cross-section.

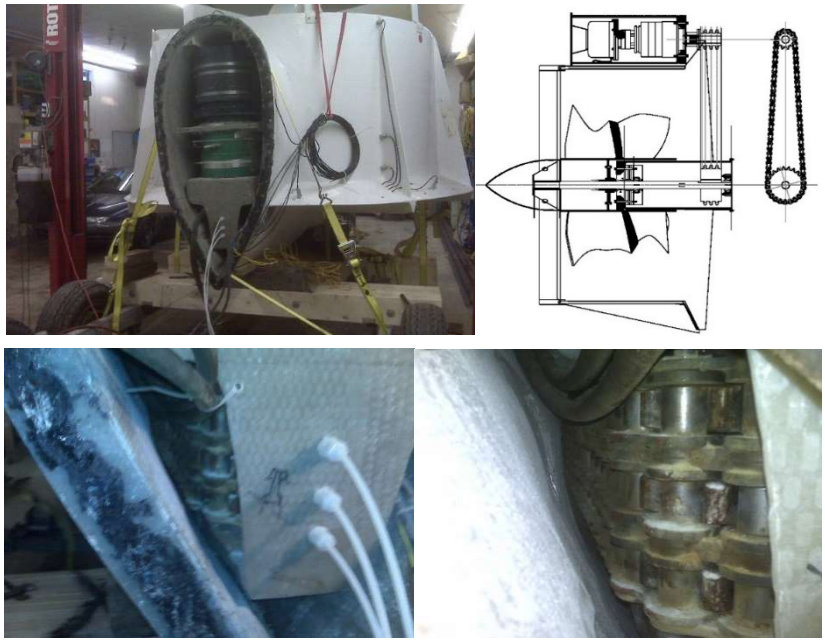

Figure 76: Clockwise from top left: end view of shrouded turbine showing generator (black) and gearbox (green). Diagram of chain and drive train arrangement. Close-up of chains on upper sprocket 3 x 19 mm wide. Fiberglass plate supporting chain-oiling tubes. Pictures and diagrams obtained by permission.

7. Water velocity and generator interaction

The interaction of natural river flows with the physical components of the hydrokinetic generator system is complex. The net torque resulting from opposing lift and drag forces of the turbine requires a minimum flow to turn the shaft, rising to a maximum value after which drag forces overtake those resulting from lift, and useable torque recedes. Flow velocities in locations of interest prove to be both highly turbulent and seasonally variable. Random events such as river water level control dams and rain can have significant affect and cannot be predicted.

7.1 Impedance and power electronics

The permanent magnet synchronous generators typically used in these systems are relatively linear in the operational range. However, the interaction between the counteracting electromagnetic forces and the non-linear rotor reactions—as well as the interaction between power flow and the cables connecting to the shore station—add to the complexity. While the power conversion devices can be suitably designed for an average flow, to make them cost effective to deploy, they need to be able to respond to a variety of situations. As a further example of the complexities arising during deployment, the commercially available rectifier/inverter combination described in Chapter 4 was used for grid connection. The rectifier circuit included a set of 4μF capacitors, delta connected, which resulted in a significant distortion of the current and voltage waveforms, as shown in Figure 77.

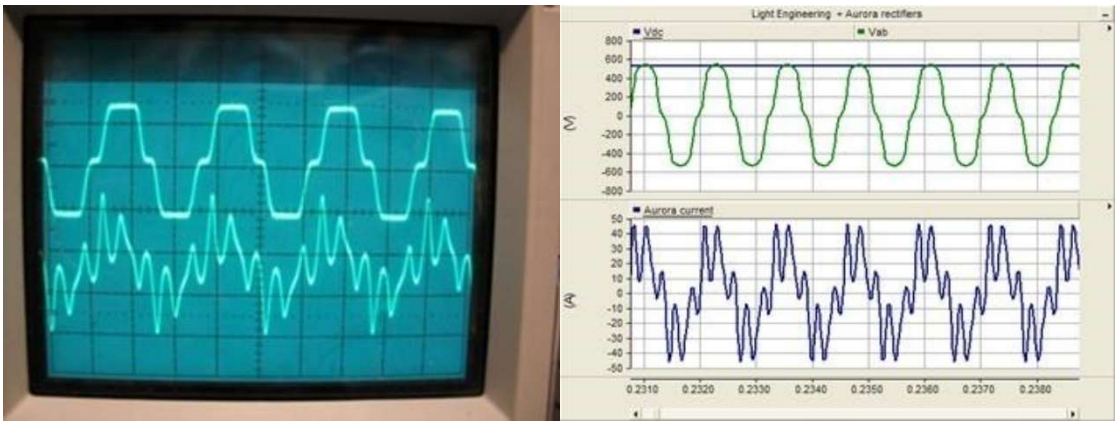

(a) (b)

Figure 77: (a) Oscilloscope capture of input voltage and current to the Aurora 6-kW rectifier, and (b) PSCAD model of 12-kW generator and rectifier modelled by Farid Mosallat.

These harmonic distortions are severe and filtering is necessary to reduce stress on the generator. Furthermore, interaction between the inductance of the lengthy shore power cable and these types of reactive loads can result, at certain frequencies, in a resonance that can be damaging. The cable inductance and necessary filtering for the 155-kVA power converter were included in the power converter design [9]. The other power converters tested used a simple look up table to adjust the output load to suit the calculated available power based on frequency or voltage. As a result, the load was observed to change on a minute-by-minute basis. Such variation obscured the relationship between flow dynamics and electrical power output.

All of the above complexities led to the development of a test setup to allow a more direct analysis of the relationship between large-scale water velocity fluctuations and small-scale turbulence on generator electrical output, as discussed in the next section.

7.2 Test setup

This testing was performed as part of the 25-kW vertical-axis turbine deployment, and just ahead of the setup for testing of the horizontal-axis turbine and 155-kVA power converter. For this testing, the rectification and active components in the system were removed, and

replaced with a series of four resistive-only electrical heaters. These were located below the trailer, with the fan circuits re-directed to a 120 VAC power supply to ensure that heat would be dissipated, and are shown in Figure 78. Given the variable nature of the electrical output, and its high frequency, the fans were not connected directly to the hydrokinetic generated power supply. A 600 V splitter was installed with four 30A-3P disconnect switches, each connected to one of the 5-kW three-phase heaters, rated for 600. This configuration allowed four purely resistive load levels to be applied to the generator by switching in heaters one at a time.

(a) (b)

Figure 78: (a) Unit heaters used as resistive loads, mounted below U of M trailer (4th unit behind not shown), and (b) splitter and switches located in trailer.

The turbine test platform was configured so that it could be moved in the cross-stream direction to a new location to subject the turbine to a different flow condition. In all cases, the ADV was setup to be located at a distance of approximately one rotor radius upstream of the rotor, as shown in Figure 79.

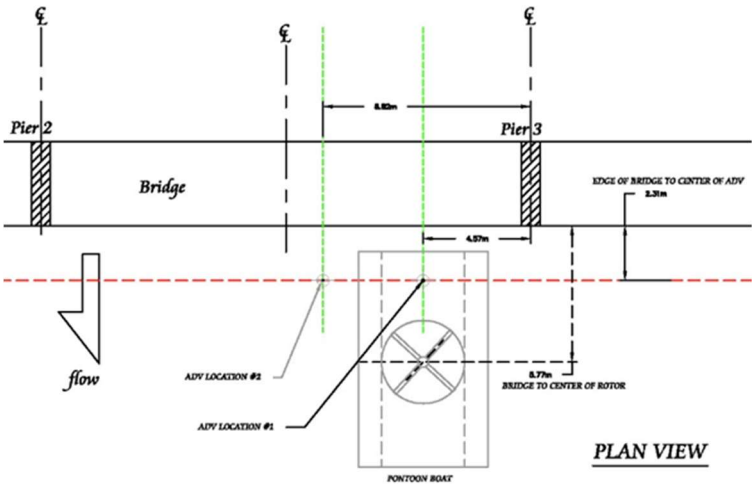

(a)

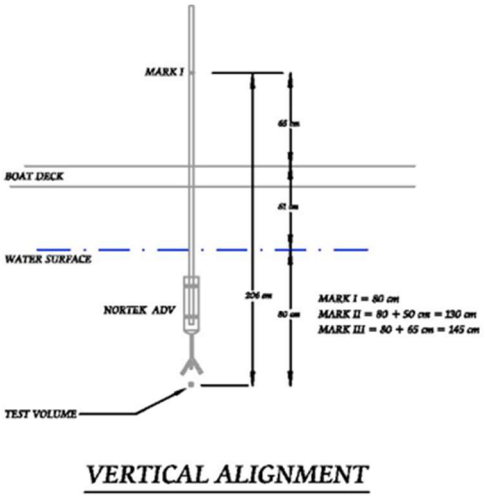

(b)

Figure 79: (a) Plan view of test set up near bridge Pier 3: test location 1 at 4.57 m west of pier, test location 2 at 8.82 m west of Pier 3, and (b) elevation view for the two test locations

Concurrent measurement of flow and generator voltage and current output were captured on the same laptop to coordinate timing of events precisely. The overall test setup is shown in Figure 80. A full-size drawing is included in Appendix 1.

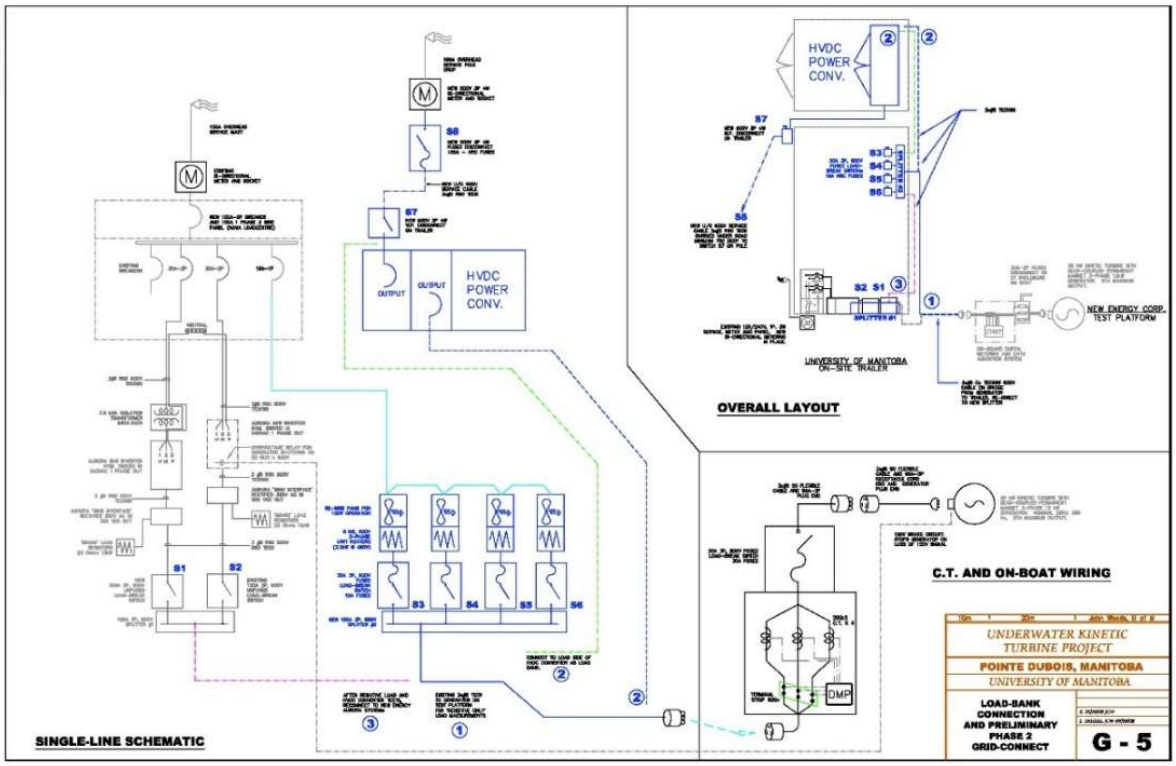

Figure 80: Schematic diagram and layout of direct load testing setup. The blue lines show the setup for testing the 25-kW vertical-axis turbine concurrent flow velocity and generator output data. The green lines show the set up for off-line (non-grid) testing of the 155-kVA solid-state power converter using the same load devices.

7.3 Test results

The individual tests described in this section are numbered as follows:

- 1R1 one resistor (heater) on, at test location 1
- 2R1 two resistors on, test location 1
- 3R1 three resistors on, test location 1
- 4R1 four resistors on, test location 1
- 4R2 four resistors on, test location 2
- 5R2 four resistors on, test location 2, with extended time.

The resulting data sets for both ADV data and power measurement are identified by this numbering scheme, and the tables and graphs to follow are identified to suit.

7.3.1 Results

The velocity measurements were taken at 200 samples per second, the maximum available for the Nortek Vectrino device. Due to the volume of data, each test was limited to 50 second duration, corresponding to approximately 10,000 velocity data points. Test labelled 5R2 was for an extended sampling duration used to analyze longer-term turbulent structures in the flow. The measurement of velocity near the surface of turbulent water, located one rotor radius upstream of the rotating turbine, had entrained air bubbles in the flow. Post processing of the data was therefore required. A new hybrid filtering method, developed by Birjandi and Bibeau [66], was applied to this data. This filter removes spurious samples which are more than three standard deviations from the average and then recalculates the average and repeats the process. Then, samples which exceed an acceleration of 3g (three times the acceleration due to gravity) are removed, as they are not physically possible. Note that this technique replaces removed data elements with an interpolated value to ensure that time-based analysis is not affected. A low-pass filter was also applied to the ADV data, with a cutoff frequency of 100 Hz, respecting the Nyquist frequency of ½ of the sampling rate.

Voltage and current were measured on the test platform at a sampling rate of 20 kHz, providing detailed waveforms for analysis and sample set of approximately 10^6 points. Evidently, this sample rate was more than adequate to capture the voltage and current waveforms which, in this case, have a nominal frequency of 700 Hz. A voltage transformer with a 600:24 turns ratio was used to reduce the voltage to a safe level for the metering equipment. Current transformers with a 1:10 turns ratio were used to enhance the signal for measurement. Table 8 and Figure 81 provide a summary of the concurrent velocity and power measurements. The sections following provide further detail on the measurements and observations of the data collected.

Table 8: Summary of concurrent generated power and velocity measurements

		Mean	RMS	Max	Min	Sdt Dev
Power (W)	1R1	1850.0	1850.8	2019.8	1658.9	55.6
	2R1	3334.0	3337.5	3706.6	2877.5	153.0
	3R1	4777.3	4781.0	5176.0	4229.3	189.7
	4R1	5618.5	5624.7	6430.5	5060.0	263.9
	4R2	6051.8	6055.9	6625.1	5527.0	221.7
Velocity (m/s)	1R1	2.121	2.123	2.447	1.793	0.100
	2R1	2.137	2.140	2.499	1.769	0.116
	3R1	2.200	2.203	2.543	1.793	0.103
	4R1	2.174	2.177	2.550	1.779	0.105
	4R2	2.288	2.288	2.482	2.086	0.065

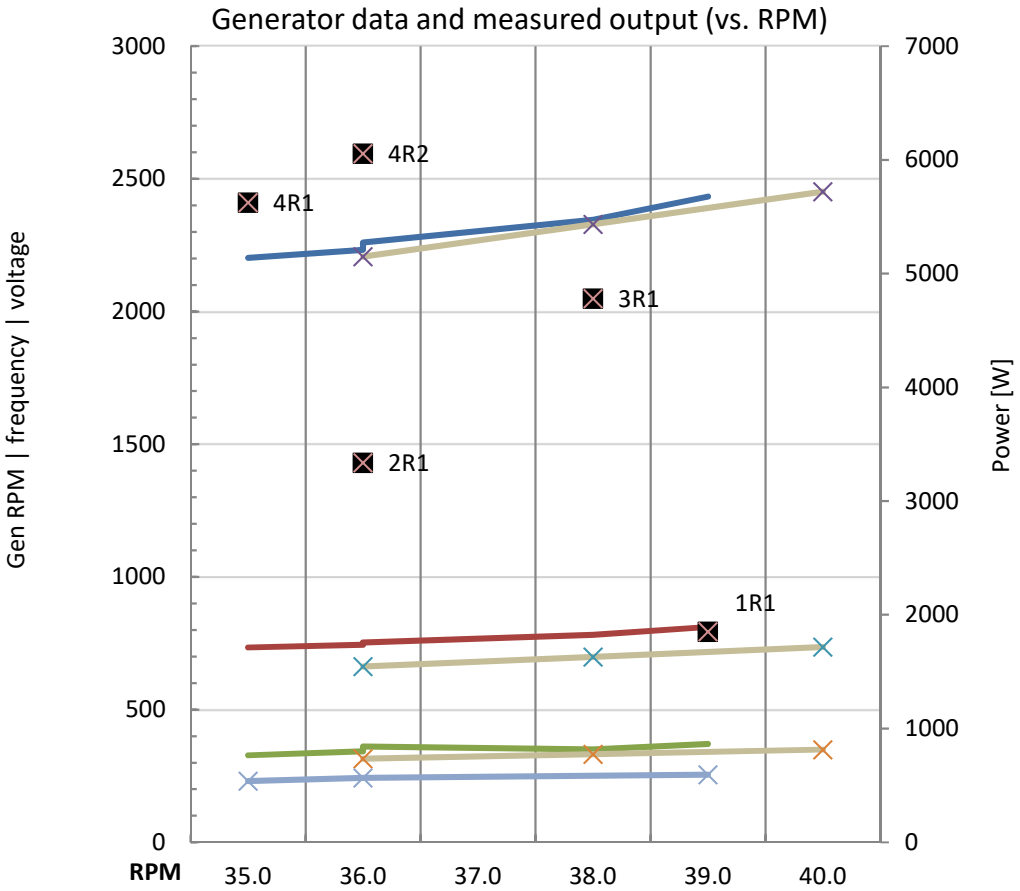

	35.9	36.0	36.4	36.9	38.0	38.3	39.7	40.0
Gen RPM (data)	2202		2232	2259.5		2345.6	2433.5	
frequency (data)	734		744	753.17		781.86	811.15	
Voltage (data)	327.7		342.93	360.99		350.09	370.28	
Gen RPM (MPPT)		2206.8			2329.4			2452
f (MPPT)		662			698.8			735.6
V no load (MPPT)		315.4			332.4			349.4
V loaded (MPPT)	230.7			242.9			255.2	
Power (data)	5625		6056	3338		4781	1851	

Figure 81: Summary of expected values and measured power output for concurrent tests

7.3.2 River velocity

This section provides additional details regarding the 3-D velocities measured during turbine flow interaction tests. Water velocity is measured using an acoustic Doppler velocimeter by transmitting an acoustic pulse, and measuring the change in frequency of signals reflecting from particles suspended in the water. It is assumed that the particles naturally found in the river are small enough to follow the turbulent structures closely. The ADV device is a Vectrino+ manufactured by Nortek and shown in Figure 50. It has four probes and a central emitter allowing for triangulation of the particle's position and relative motion. Section 2.4 describes the background of this decomposition and representation of the velocity vector.

ADV velocity measurements are calculated in real-time, within the ADV device and written to a data file. Each measurement file includes a header with device information and settings, and each line of ASCII data includes: status, sample number, in-stream velocity, cross-stream velocity, two vertical velocity measurements, and other information on signal to noise ratios beam correlations. The velocities are in m/s and are given with three decimal place accuracy.

Figure 82 shows a sample of ADV data from test measurement 1R1. This sample is indicative of the measurements observed and while the turbulence is not strictly homogeneous, the turbulent components are in the same order of magnitude. Furthermore, for our purposes, it is the time-dependent steadiness of the velocity which is important. Figure 67 shows a 24-hour sample of velocity, which remains steady within a 3.8% standard deviation of its mean. As described in Chapter 2, the analysis of turbulence by measuring velocity at a fixed point is dependent on the in-stream turbulent component u being significantly smaller than the mean flow velocity U. In this case, and in general across the data sets, the relative magnitude of each of the turbulent components remains small, and in the order of 10% of the mean. Figure 82 is a graphical representation, showing the components relative magnitude. As described in the Chapter 2, the average is removed

from the in-stream turbulence component, and each component can be analyzed as a separate signal.

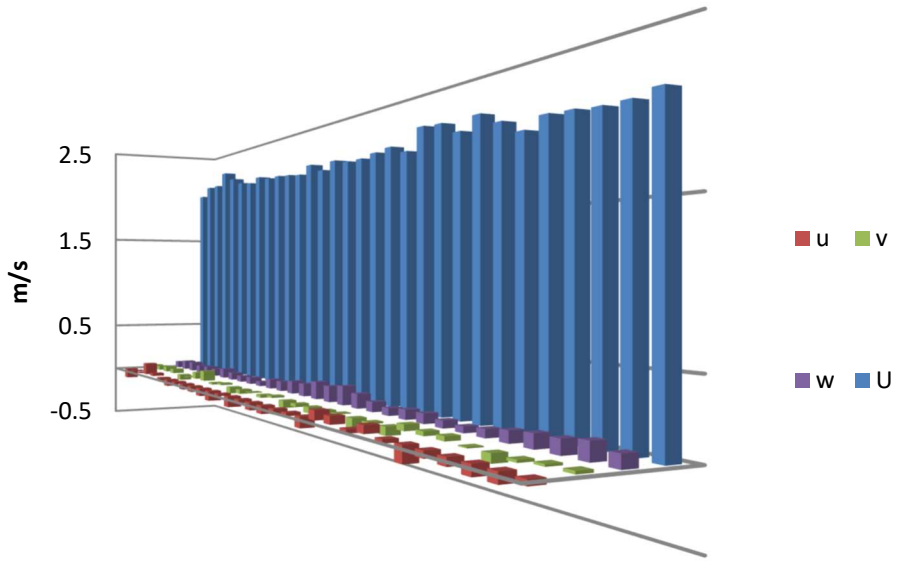

Figure 82: Sample of 1R1 of mean velocity U data and the three turbulent components, u, v and w. Each sample is 50 ms apart; the average velocity over this sample is 2.1 m/s.

The turbulence intensity as shown in Equation (6) is the RMS average of the turbulent components, and provides a single parameter for comparison of turbulence between different conditions. Figure 83 provides a visualization of the components and the turbulence intensity.

For each of the five velocity-power tests, velocity components are available and statistics were complied with respect to mean, minimum and maximums. Figure 84 provides an example of the 1R1 velocity components as an example. Note that the W1 to W4 in the chart titles indicate the window number and are features of DADiSP® signal processing software.

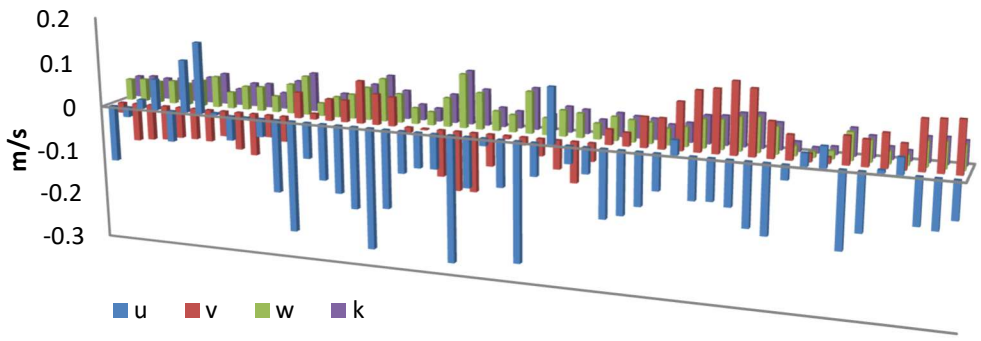

Figure 83: Visual representation of orthogonal turbulent components u, v and w and the turbulence intensity k representing the average of these components.

Note that in Figure 84 the magnitude of the turbulent components remains in the ± 0.3 m/s range with respect to the 2.1 m/s mean flow. Table 9 provides a summary of the flow data corresponding to the in-stream flow velocity direction.

Table 9: Various statistical values for in-stream velocity measurements during power and flow velocity interaction tests in m/s

Data set	Mean (m/s)	RMS (m/s)	Max (m/s)	Min (m/s)	Std Dev	u'/Uavg
1R1	2.121	2.123	2.447	1.793	0.100	4.7%
2R1	2.137	2.140	2.499	1.769	0.116	5.4%
3R1	2.200	2.203	2.543	1.793	0.103	4.7%
4R1	2.174	2.177	2.550	1.779	0.105	4.8%
4R2	2.288	2.288	2.482	2.086	0.065	2.8%

Figure 85 shows the mean flow U velocity component for the five flow interaction tests. As noted above and as can be seen on the graphs, the velocity is turbulent, but remains relatively steady on average throughout the tests, from 2.12 m/s to 2.20 m/s for Location 1 near bridge pier 3.

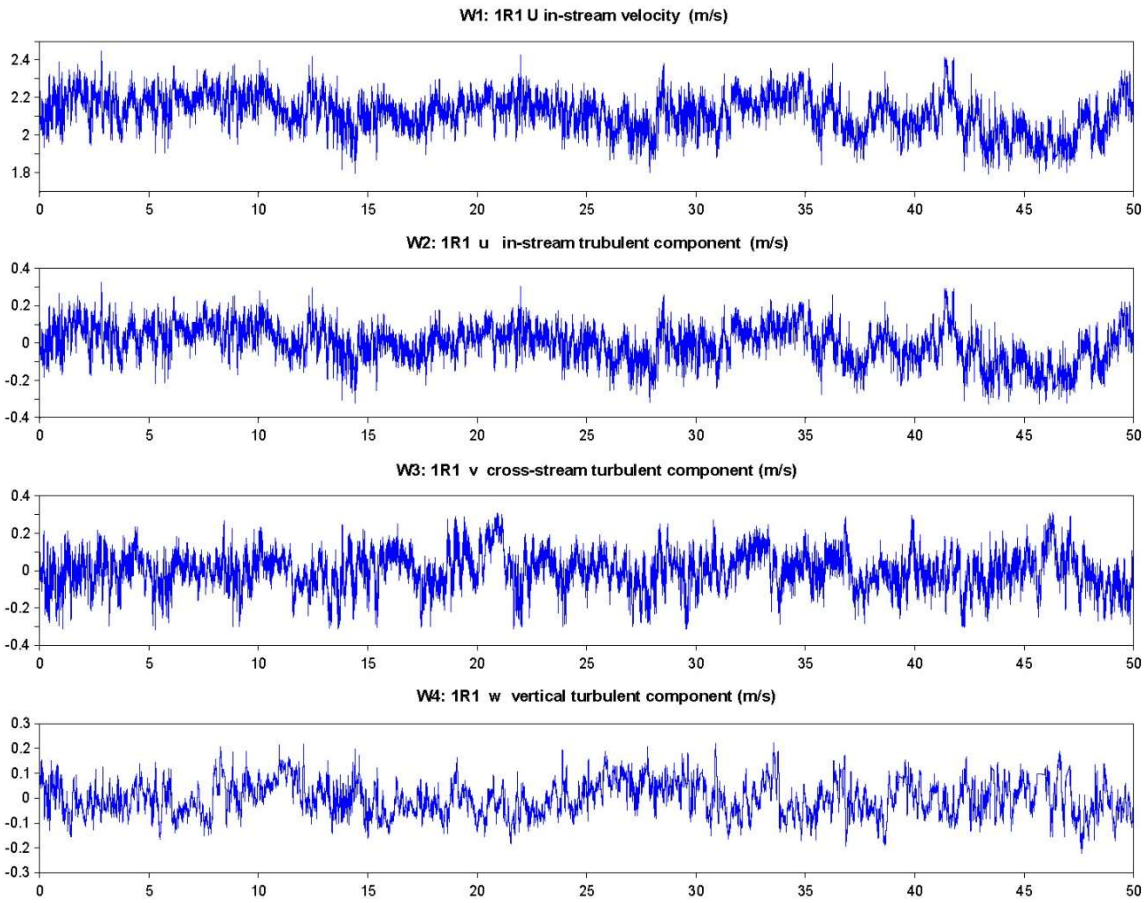

Figure 84: Test 1R1 velocity components: (a) W1 is the in-stream velocity U, (b) W2 is the u in-stream turbulent component, (c) W3 is the v cross-stream turbulent component, and (d) W4 is the vertical w turbulent component.

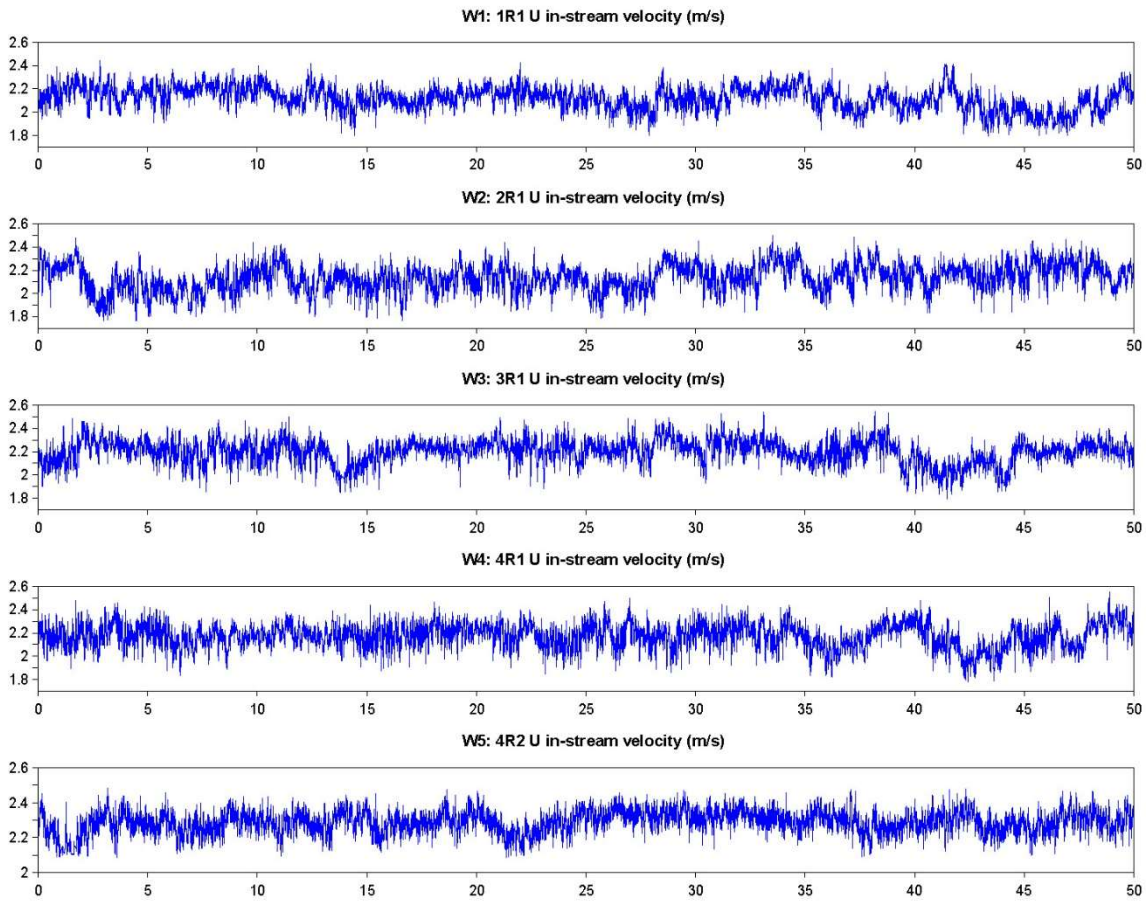

Figure 85: In-stream U velocity in m/s for each test as function of time in seconds

The signal for 4R2 appears less variable and is representative of the statistics shown in Table 9 accordance with the procedure described in Chapter 2, these velocity signals can be further analyzed to identify large-scale structures within the turbulence. Equation (13) can be used to calculate the correlation time of a given signal, which in turn can provide a magnitude for large-scale structures existing in the flow by multiplying by the mean velocity U.

Using the velocity measurements, the autocorrelation was calculated for each of the velocity measurements and is shown in Figure 86.

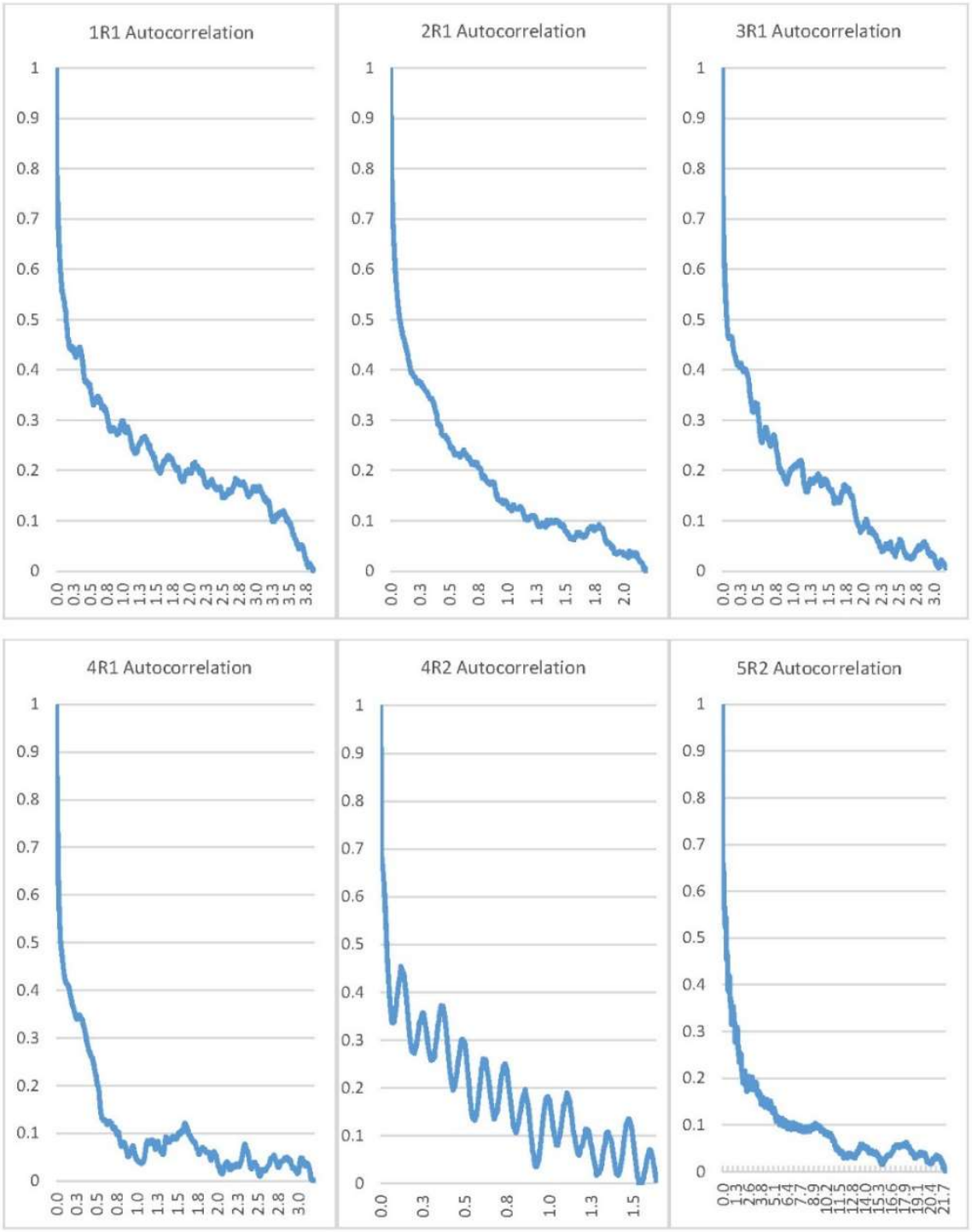

Figure 86: Normalized autocorrelation of velocity measurements for the turbine flow interaction tests with labels explained in Section 7.3.1

Using these autocorrelation functions, the correlation time is found by integrating for the area under each curve. The correlation length, is determined by multiplying the correlation time by the mean flow velocity. These calculations are summarized in Table 10.

Table 10: Correlation time and correlation lengths derived from the velocity measurements

Sample	$\bar{U}$ m/s	**time to first zero (s)**	**correlation time (s)**	**correlation length (m)**
1R1	2.12	3.88	0.882	1.872
2R1	2.14	2.20	0.393	0.841
3R1	2.20	3.17	0.551	1.213
4R1	2.17	3.20	0.357	0.778
4R2	2.29	1.64	0.309	0.709
5R2	2.25	21.93	1.101	2.475

This data indicates that the larger scale structures in the turbulence are in the order of 0.78 to 1.87 meters, and are therefore in the order of magnitude of the turbine rotor and hydrofoils. A longer sample of the same resistive load and test 2 location with 150,000 points (spanning 12.5 minutes) shown as data set 5R2 shows a correlation time of 1.1 seconds and a correlation length of 2.4 meters.

The power spectral density of each signal can also be calculated as described in Section 2.4.4. Figure 87 shows Power Spectral Density (PSD) for 4R1, 4R2 and 5R2. Comparing 4R1 and 4R2 spectrums, which are the results of the same electrical load, but different locations in the flow after the bridge, the PSD in the inertial range of 4R1 is seen to be higher than that in 4R2. However, the mean flow velocity is lower as shown in Table 10. In the dissipation range, at the right-hand side of the spectrum, 4R1 also shows higher levels indicative of the energy transported in the higher frequency, smaller wavelength turbulence, reflected also in the turbulence intensity levels shown in Table 9.

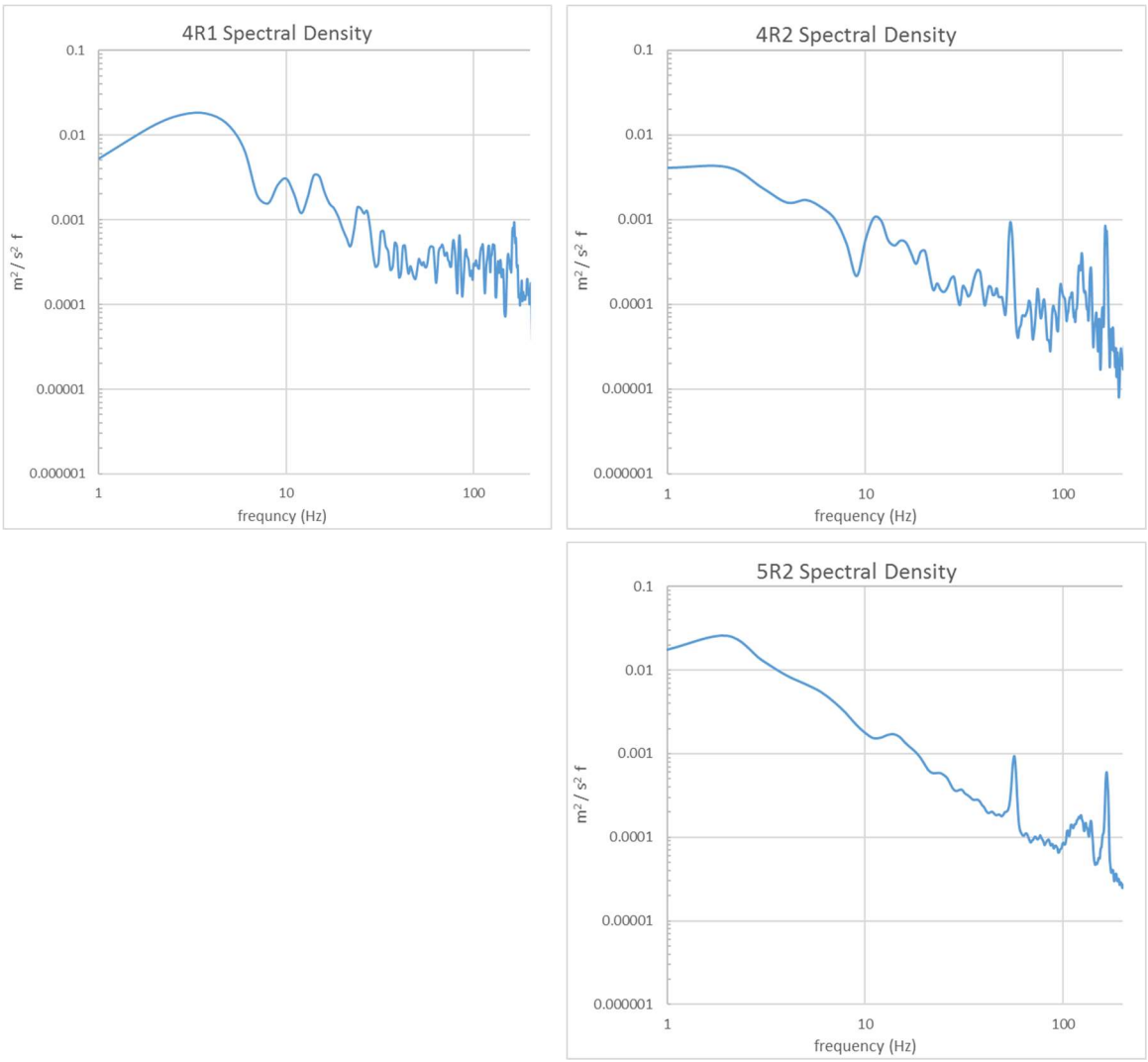

Figure 87: Power spectral density m^2/s^2 f (Hz) of velocity signals versus frequency in turbine flow interaction tests.

As a final observation, in the inertial range of 4R2 there are several significant maxima. The longer sample period of test 5R2 further clarifies these maxima as structures in the flow, showing these are not random or momentary occurrences.

7.3.3 Power measurements

Power measurements were taken concurrently with the ADV measurements using a USB based analogue to digital converter. Note that a USB optical isolator was used to eliminate common mode noise and ensure that the USB port on the computer was not subject to undue stray voltages. A single current phase and line-to-line voltage were measured, and total power calculated based on the standard relationship between three-phase voltage, current and power as per Equation (16). At a 20 kHz per second sample rate, 700 Hz (nominal) waveforms were captured with good precision. An example of measured voltage for 4R1 is provided in Appendix 4. A hand-held meter with true RMS capability was used to measure voltage and current and to verify measurements during each change in resistance level.

The hand-held meter readings were observed and written down, with an effort to capture visually the average of the voltage and current reading over approximately 10 seconds. Except for one reading, the calculated power from the hand-held meter falls within the minimum and maximum of the readings from the instruments, and is therefore considered to validate the readings. Measurements are summarized in Table 11.

Table 11: Verification of instrumentation results using hand-held meter

		Handheld			**Instrument**		
		Volts	**Curr**	**Power**	**Power (W)**		
Data Set	**Description**	**V**	**A**	**W**	**Min**	**Max**	**Mean**
1R1	1 resistor location 1	-	-	-	1658	2019	1850
2R1	2 resistors location 1	245	5.6	2386	2878	3706	3334
3R1	3 resistors location 1	327	8.4	4758	4229	5176	4777
4R1	4 resistors location 1	316	10.5	5747	5060	6430	5618
4R2	4 resistors location 2	317	10.3	5655	5527	6625	6051

To compare the 200 sample per second velocity reading with the 20k samples per second power readings, a two-step averaging process was used. First, a new signal was derived using a 100-sample sliding average. This signal was then re-sampled at 200 samples per second rate producing a new signal with approximately the same number of samples as the velocity signal. This filtering process is satisfactory for observing the relationship between velocity and average power given the relatively slower speed of velocity fluctuations compared to power. The mean power at each step of the signal averaging process was calculated to ensure that the output retained the gross features of the measured signal. For example, the initial mean value for test 4R2 was 6,066.9 W, after moving average, the mean was 6,066.7 W and in the final 200 sample per second data set, the mean was 6,066.6 W. Figure 88 shows a graphical representation of the averaging process.

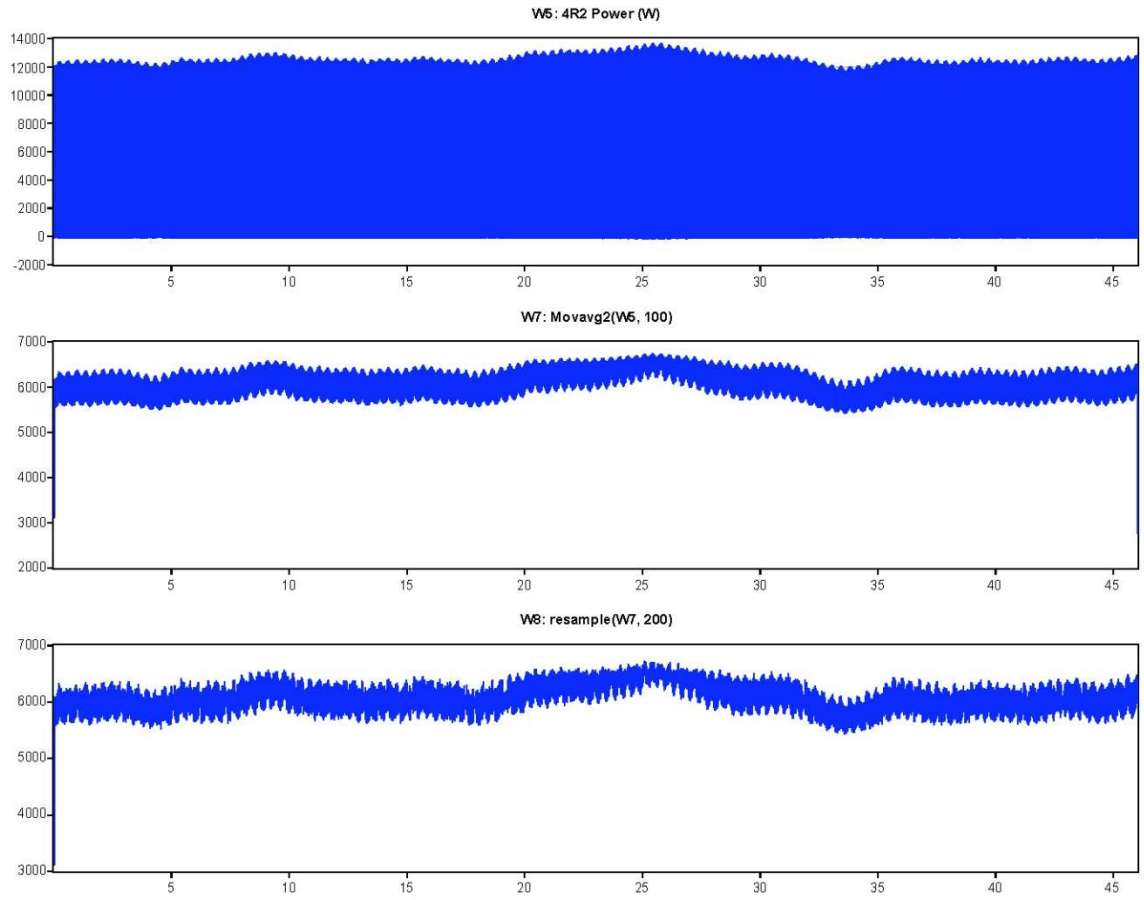

Figure 88: Power output of generator in Watts as function of time showing the averaging process for test 4R2: (a) original power signal, (b) 100 sample moving average, and (c) re-sampled signal

A visual inspection of Figure 88 shows that the sampling process does retain the general envelope of the sampled waveform, with the averaging process providing the RMS power output, consistent with the handheld readings.

7.3.4 Power and velocity

The purpose of developing the concurrent flow velocity and power output measurements was to allow for the direct observation of turbulent fluctuations on electrical power output. This provides a water-to-wire record. It is recognized that given the small velocity sample size relative to the turbine cross-sectional area, and only a single location in the flow for a

given test, that the correlation between power output and velocity may not have a simple interpretation. Furthermore, this concept parts with traditional analysis of turbulence using statistics only, and not treating it as a signal. Nevertheless, the test set up and data obtained are considered valid, and correlations between signals exist.

The removal of the power electronic effect provides a more direct insight into the interaction by applying a purely resistive load. Using the velocity signals and power signals developed in the previous sections, a cross correlation is developed to determine if there is a measurable statistical relationship between turbulent flow elements and electrical power output. A cross correlation was obtained with an equal number of points (9205) from each signal.

Figure 89 shows an example of the cross-correlation for Test 1R1. A correlation is identifiable at -3.79 seconds, with the power signal lagging the velocity. Note that there is no significant correlation between the cross-stream 'v' or vertical 'w' velocities with respect to the power. If the correlation were a result of direct vibration, it is expected that the cross-stream velocity component would show some similar correlation since the rotation is in the x-y plane.

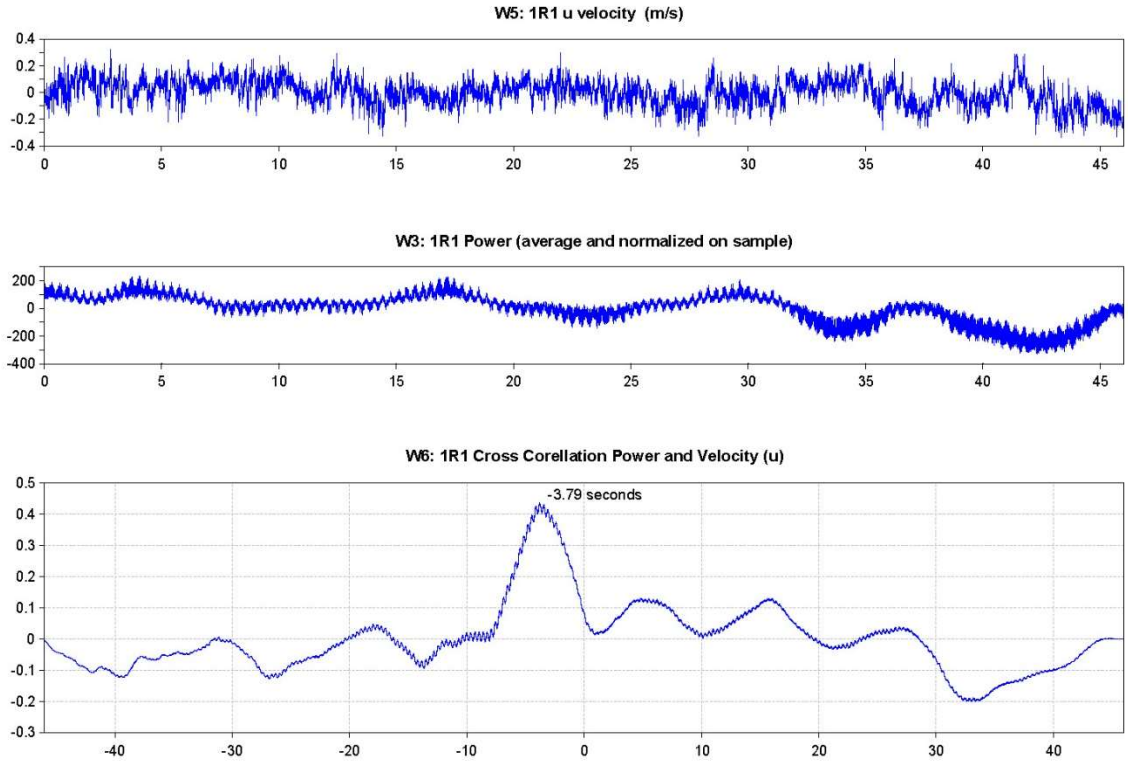

Figure 89: Power and velocity cross-correlation for 1R1, instream u velocity and normalized power signal

A similar averaging and resampling process was performed on the 4R2 data, and a correlation is found at 5.15 seconds.

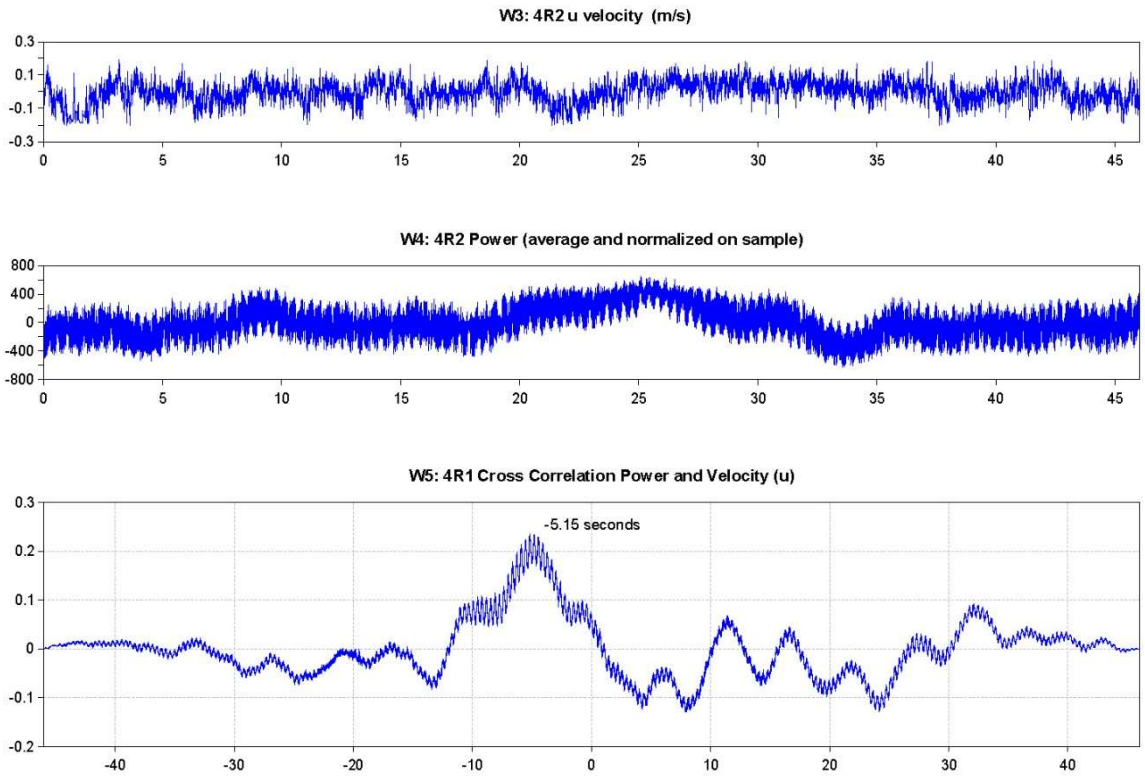

Figure 90: Power and velocity cross-correlation for 4R2, instream u velocity and normalized power signal.

The above two correlations are based on a 50 second sample set and a measurement at only one location ahead of the turbine. However, the following can be observed:

- ADV sampling within one turbine radius ahead of a rotating hydrokinetic turbine can detect interaction between the turbine and the flow.
- The turbulence is affected by changes in loading on the turbine.
- Correlation between the two signals can be calculated.

It is conceivable that such signals may be used to provide a control for the loading of the turbine to avoid stalling and allow a reverse current to be brought into the generator from the shore power converter; in order to advance the rotor into an optimum range. For example to shift the operating point, momentarily, the right hand side of the MPPT curve to optimize performance.

As a final comparison of the concurrent velocity and power data, the data sets were compared using an X-Y graph format. Figure 91 provides a view of the locus of power and velocity, and allows for a comparison of data sets 4R1 and 4R2. These represent the highest power delivered and were obtained from the two different test positions near Pier 3.

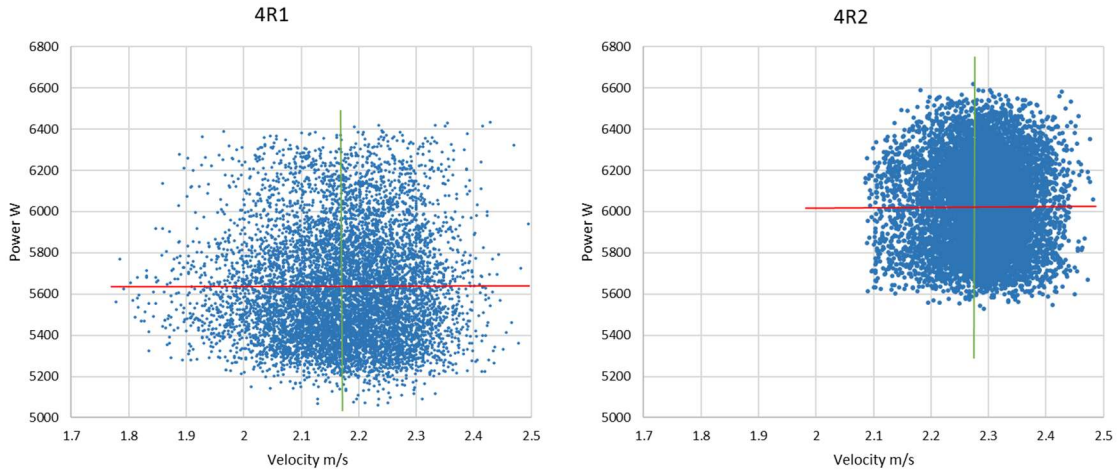

(a) (b)

Figure 91: (a) X-Y graph of power delivered with y-axis in watts versus in-stream velocity U with x-axis in m/s for 4R1 sample, and (b) same parameters for 4R2. The average power is noted by a red line and the mean velocity noted by a green line.

From these figures, it can be observed that the velocity in the 4R1 sample has a more variable nature, and reflects a more turbulent flow. The mean velocity is evidently less than the 4R2 sample, and the average power reflects this. A more detailed account of power output and flow is summarized in Table 12.

Table 12: Power data from tests 4R1 and 4R2

		4R1	**4R2**	Delta	Delta/4R1 %
Power	min	5,060	5,527	467	9.2%
	max	6,430	6,625	195	3.0%
	mean	5,618	6,051	433	7.7%
Flow	min	1.779	2.086	0.307	17.3%
	max	2.55	2.482	-0.068	-2.7%
	mean	2.174	2.288	0.114	5.2%
	u’	0.105	0.065	-0.04	
	u’/U	4.8%	2.8%	-2.0	-41.2%
Theoretical Power	min	24,049	38,772	14,723	61.2%
	max	70,826	65,309	-5,516	-7.8%
	mean	43,888	51,161	7,273	16.6%
measured/theory		12.8%	11.8%		

With reference to the change in velocity, there is a 5.2% increase in mean flow from location 1 to location 2, and a reduction in relative turbulence intensity from 4.8% to 2.8%. The increase in output average power is 7.7%. Given that the electrical load was identical for both measurements, and the generator performance is almost linear in the 6 kW to 8 kW range: the differences found here are a result of changes in the turbine-flow interaction. Referring back to Figure 5 as a representative Tip Speed Ratio curve, all of the above test are clearly on the right hand side of the TSR curve, where 1R1 represents $\lambda = 12.3$ and for 4R1, $\lambda = 9.9$. The TSR curve for this rotor was not obtained from the manufacturer.

While there is limited data, a theoretical conclusion is that the turbine’s performance was better in the higher turbulence location.

8. Conclusions

Testing hydrokinetic turbines in-situ in cold weather provided the means to achieve research objectives. First, hydrokinetic turbines were safely deployed and operated in stand-alone and grid-connected modes in a cold climate. Second, concurrent measurements of turbulent velocity and electrical power output were obtained, and new observations were made on the interaction between flow velocity and electrical power generated by the turbines. These tests in winter are the only documented tests of the influence of ice on a floating hydrokinetic turbine ever recorded and were only made possible because of a foot bridge providing access to the turbine in cold climates.

A significant amount of work was dedicated to the design and building of the test structures and developing safe testing and deployment methods in harsh climates. Unique measurements of power and velocity with and without an intervening power electronic device provide additional insight into the interaction of the generator with the turbulent velocity. These tests are a unique contribution to the field of hydrokinetic power generation and have not been duplicated.

More specific conclusions reached are as follows.

1. Potential river hydrokinetic turbine generation sites were investigated and the following outlines the minimum requirements and considerations.

    - Proximity to (a) the electrical load to be serviced or (b) an existing and suitable distribution line is a nominal consideration. This potentially reduces line losses and simplifies interconnection requirements. Costs for maintenance, crew safety and monitoring are also expected to be reduced with proximity.

    - Water depth limits the turbine dimensions, and therefore has a direct impact on how much power a device, or array of devices can deliver. The generated power is proportional to the cube of the flow velocity, and for sites of interest, the maximum flow will be near the surface.

- Flow velocities of 2.5 m/s were found to be suitable for consistent power production from vertical axis devices in the 5 kW to 25 kW device range. The devices tested were designed for a 3 m/s peak flow. Flow velocities of 1.5 m/s may be accommodated by adding more or larger blades/hydrofoils to ensure self-starting, but less that 1.5 m/s is not considered economically feasible for turbines in this size range (2.4 to 3.2 m diameter).
- An understanding of ice floes, ice thickness and frazil ice conditions are essential to determining site feasibility for specific turbine technology. Where frazil ice is prevalent, surface mounting of a turbine from a pontoon or barge is limited to post ice-out to late fall operation only, therefore limiting yield. In some cases, for example in remote communities, this may be satisfactory, as liquid fuel supply is often by winter-road.
- Frazil ice was encountered consistently at the test site in the winter months of December through March. This is due to turbulent flow in sustained contact with below freezing air temperature due to open water conditions. Frazil ice, travelling with the flow, was encountered when air temperature was -20°C and below.
- Bathymetric and ADCP measurements from a boat are suitable for evaluation of three-dimensional flow profiles. However, observation of areas of open-water during dead-of-winter conditions are indicative of flows in the order of 1.5 m/s and therefore may narrow the selection set. Satellite imaging in the winter can assist in locating such potential sites.
- Understanding the velocity profile is essential for the design of larger rotors. In the case of horizontal turbines, the thrust bearing will be affected where velocity gradient from top to bottom is significant. For vertical axis turbines, with the generator above water level, there is less concern since the end of the rotor farthest from the bearing, and therefore with the longest moment of force, is in the lower velocity zone.

- Turbulent channel flow is considered to be beneficial in this regard, as the closer a flow is to fully-turbulent, the more vertical the velocity profile over the turbine cross section.
- An understanding of season flow variations is essential to ensure that the design of the devices can accommodate the minimum and peak flows. Some options are (a) seasonal removal (b) physical adjustment of rotor or gearing, (c) oversizing of generator, (d) switchable load resistors to dampen speed, and (e) MPPT adjustment.
- As with other forms of distributed generation, best practices require a full understanding of the site, and its seasonal variances. Nevertheless, unlike traditional hydroelectric plant design, understanding these variables does not mean that one device can be fully optimized. Some flexibility and a range of acceptable operation conditions is necessary (since the flow is uncontrolled).

2. Hydrokinetic turbine support structures can be deployed and retrieved in fast moving rivers, without significant equipment and infrastructure, even in winter.
   - The installation of 25.4 mm diameter epoxy grouted stainless steel treaded rod anchors into rock on opposite shorelines (allowable shear strength of 55 kN) were suitable for mooring and maneuvering a barge to river-bottom anchor locations. Several of these can be installed in one day, using a hand-held electric hammer-drill.
   - Drum-type winches, powered by an on-board diesel fired compressor and outboard directional sheaves can be used to maneuver to nearly any cross-stream position, even in flow velocities up to 2.5 m/s.
   - Rock anchors can be drilled into the river bottom using a track-mounted compressed air drill rig (suitable for drilling blasting holes in rock) where a suitable jig is lowered with the drill to hold the drill bit in place at the bottom. The compressor and drill rig can be supported using a simple flat-top barge.

- Rock anchors, 38 mm in diameter and grouted into the river bottom using pressurized grout from the barge, make a suitable anchoring method for mid-stream turbine locations.
- A minimum of two rock anchors per device or platform, using a "Y" chain configuration at the rock anchor end and wire-rope cable to the platform; together sized for at least three times the calculated load is recommended. In the tested case, the overall anchoring system, sized for 3.4 times the calculated peak load have remained in place and viable for more than eight years.
- The combined use of chains at the "rock" end and wire-rope cables for support of the mid-stream turbine platform was found to be suitable. Advantages of this setup are: superior wear capability of chains, where they may by in contact with rocks or boulders; an anticipated ability of the cable to absorb momentary peak tension from impulses in the flow, and simple self-correcting of seasonal changes to water levels.
- Large pear-shaped buoys are suitable for holding the platform-end of the cable at the surface – for later connection of the platform. In addition, these connection points can be re-used for temporary mooring during maintenance or unit retrieval and re-deployment.

3. Deployment and retrieval of surface mounted platforms for turbine deployment mid-stream can be performed in winter months and cold weather: nominally -20°C and below.
    - Significant safety precautions must be planned and executed. Including exposure suits, fall-arrest lanyards, safety boats and above all a well-developed safety plan; understood and fully supported by all participants.
    - Rock anchors at shore locations placed for mooring anchor installation can be re-used to deploy the turbine platform, using a similar process as the drilling barge, or to act as attachment points for safety lines for access.
    - Anchors should also be installed downstream to support back-up and safety lines. Where arrays of turbines are considered, anchors could be installed at various

intervals, with each anchor acting as support for installation, back-up and safety and even allowing relocation of the device in different seasons to accommodate changes in the flow.

- Where possible, safety lines and ropes used in deployment should be floating-type. Polyolefin ropes with UV resistance and breaking strength of 90 kN were used in this project, and no failure was experienced. Note, however, that dragging the ropes on rock surfaces can cause abrasion and degradation, therefore regular inspection and over-sizing is necessary.

4. Surface mounted platforms can successfully support hydrokinetic turbines in fast flowing water. While turbines can continue to generate power in cold weather, even with sustained temperatures below -15°C and lows of -30°C, operation of the system can be quickly compromised.

    - With respect to year-round operation, the water temperature does not fluctuate more than 18°C. However, the water air interface can fluctuate by nearly 40°C in one week.

    - In winter a thin film of water freezes upon exposure to the air. Due to platform motion, waves and wakes, this film forms accumulative layers of ice which change the platform balance and buoyancy in uncontrolled ways. Significant growth can occur over night, or after several hours during extreme cold.

    - Vertical-axis turbines, located on surface platforms are therefore not recommended for winter use in extreme cold climates. Operation for a total of 1,040 hours was achieved in winter in off-grid and grid-connected modes. However, it is not economically feasible; due to the level of maintenance and/or ancillary heating required to maintain reliable winter operation.

    - Several ice-mitigation methods were attempted, but none were found to be effective. The use of inflatable rubber bumpers at the upstream side of the platform were capable of shedding ice due to the flexing of the surface. However, it is likely

that the impact of larger ice floes, branches or other floating debris would penetrate the rubber and degrade this capability.

- The use of bottom anchors and the chain/cable mooring is considered suitable for fully submerged systems as well as surface mounted, where additional buoys and mooring points are integrated into the support system for maintenance or retrieval.
- Submersible power cables for off-take of generated power and monitoring of the system requires additional consideration, additional comments on this are provided in Chapter 9.

5. Electrical interconnections to a utility-run power grid were designed and successfully implemented.
   - Power was successfully delivered to the Manitoba Hydro grid, for the first time in June 2008. This was previously achieved only once in Canada by NRC and Nova Energy in 1986.
   - Interconnections were made to a 12.47kV rural distribution grid at both 120/240V and 600V levels, through bi-directional metering. This was found to be a suitable connection method, by both the utility and the energy provider, and is relatively commonplace in Canada for generation up to 100 kW.
   - Interconnection requirements described in IEEE Standard 1547 and CAN/CSA C22.2 No. 257 such as: disconnecting means, anti-islanding, under-voltage trip, over-voltage trip, instantaneous overcurrent, under-frequency trip and over-frequency trip are routine and built-in to commercially available inverters.
   - For larger and custom-built power conversion devices, these protections can be integrated using commercially available electronic protection relays.
6. For vertical-axis Darius H-style turbines, significant improvement to rotor efficiency can be made by using hydrofoil shaped support arms.
   - Improvements of nearly 50% were found over support arms of rectangular cross-section.

- The use of the same cross-sectional extrusion for both the hydrofoil blades and the support arms, constructed by New Energy Corporation Inc. and tested as part of this project, improved both performance and the economics of constructing hydrokinetic turbines.

7. The efficiency of the system is important for power production. Other efficiency findings and considerations include the following.

    - The hydrokinetic turbines developed in this work are intended to be installed in natural flowing rivers and are subject to debris and unexpected changes in flow. Therefore, it is essential that a stalled or stopped turbine can be self-starting.

    - For vertical axis turbines, due to their low solidity ratio and the position-dependent torque of each blade, other losses need to be minimized. The use of low-temperature synthetic oil for gear boxes is a minimum. A better solution is the elimination of the gearbox entirely.

    - In some low-flow cases, vertical axis turbines with additional blades can be used.

    - Depending on the seasonal flows, the ability to modify the MPPT system may be necessary. Some options are considered in Chapter 9.

8. A welded tube-steel support arm was successfully constructed and used to deploy a 2.4 m diameter horizontal-axis fiberglass shrouded turbine with a 60-kVA permanent magnet generator.

    - The deployment system was operated using hydraulic pistons powered by multiple 12 VDC lead-acid batteries, suitable for remote deployment.

    - The generator for the test device was located in a projection above water level, and therefore would be subject to the same icing conditions as the tested vertical axis unit. For sustained operation in cold climates the turbine, with generator, would have to be located below the surface and below the level of spring ice floes.

9. Long term measurements of water velocity and power output, lasting several weeks at a time were obtained in both winter and summer operation.

    - Power generation fluctuated significantly and generally followed changes to average flow velocities, as would be expected. Since power is proportional to the cube of the velocity, this larger range of output must be considered when determining load capability and potential over-speed of the generator during high flows.

    - As an example, for a 24-hour winter day, the standard deviation of the flow velocity, as measured on a 1 minute averaging of a propeller type flow meter, was 2% on a 2.1 m/s mean. The standard deviation of the power output of the 5-kW vertical axis H-style Darius hydrokinetic turbine during this period was 9%.

    - Regarding capability and loading, the power production should not be overstated, particularly for off-grid electrical production. Variances in production are, in general, impossible to predict. For the larger 25-kW turbine in the same location and similar flow; while the average power production was 8.7 kw, the range of power output was 5.7 kW to 10.8 kW over 12 hours, and therefore would not support a base load of over 5 kW. Energy storage may extend this base load, and an array would provide additional capacity. These concepts are described further in Chapter 9.

10. Concurrent measurements of turbulent velocity using acoustic Doppler velocimetry, sampled at 200 Hz, with instantaneous power measurements sampled at 20 kHz produced a unique data set. Four resistive only loads were applied to the generator, and two locations with different turbulence levels.

    - It was found that an increase in moderate levels of turbulence intensity, from 2.8% to 4.8% improved power conversion by 7.6% relative to calculated Betz limit for the mean velocity at the location. This is consistent with the theory that increased levels of turbulence improve conversion by reducing separation of the flow from the rotor.

- The velocity measurements in two platform locations and under four generator load conditions were used to generate autocorrelation plots, and to calculate the correlation length of the flow. These lengths varied from 0.709 m to 1.8 m, indicating eddy lengths comparable to the rotor dimensions.
- This also demonstrates that the loading of the generator affects the upstream flow in a measurable way, opening the potential for direct measurement feedback for load control and importantly for stall avoidance.
- The elimination of the grid-connected power converter allowed for variances in power output to be measured as a more direct function of the natural flow variations.
- A power signal, with a 200 Hz sampling rate was derived by averaging of the instantaneous power measurement and resampling. A cross-correlation of the derived power signal with the velocity measurement produced a significant correlation at a delay of approximately 3 seconds in one case and 5 seconds in another.

9. Recommendations for further work

Research in hydrokinetic turbines continues in Canada and elsewhere in the world. The development of reliable hydrokinetic systems for river systems is necessary to provide electrical power to remote communities and operations, which may not benefit from local electrical grid and are moving towards low-impact energy sources.

1. Further analysis of the long-term power and flow data will be of interest to researchers considering commercial applications. Arrays of turbines are expected to be deployed and the number of devices necessary to supply a known and measured base load in a remote community and the number of redundant devices must be determined.
2. The deployment of local energy storage facilities to improve the economics of renewable energy are applicable to hydrokinetic turbine-generated power and should be investigated. The associated power conversion devices have an inherent capability to include a DC to DC battery charging stage before inverting. This can also allow for the reversing of power flow, to clear debris and more importantly, during times of highly variable flow, allow the rotor to be advanced to the optimum side of the power curve to avoiding stalling of the unit, and further stabilizing the output power.
3. The concurrent power-velocity (ADV) data sets are unique to this work and contain information with respect to generator reaction to ever-changing flow conditions in a natural river flow. Some work relating these natural flow interactions to scaled devices in a laboratory flume would be of value to confirm such modeling for predictive control system testing.
4. Power control systems which can optimize output power and learn from and predict output from changes in incoming flows should be advanced. This will be necessary for hydrokinetic turbines to act as a 'prime power' supply for a community.
5. The use of an electromagnetic eddy current device, already effectively used in pumping applications to provide variable speed without power electronics, can be located between the rotor and the generator. It would provide a method of disconnecting the rotor from the generator when necessary for safety, and for deployment purposes. It

would also provide another tool to smooth out power flow – reducing stress on the generator in highly turbulent flow conditions. Methods for controlling the engagement of the device, are necessary, and DC power could be drawn from the energy storage system proposed above.

6. Robust cables, including both power and control cables or fiber optic communications are required for river hydrokinetic turbine connections. Those already designed and manufactured for tidal energy capture are of suitable construction, but are generally too large and expensive for river use.

References

1. Glickman J., Herrera S., Kline K., Warwick M., "Planning for the Next Blackout: Optimizing the Use of Distributed Energy Resource," Proceedings of the ACEEE 2004 Summer Study on Energy Efficiency in Buildings, Pacific Grove, California, Paper No. 5, 2004.

2. Energy, Mines and Resources Canada, Surveys and Mapping Branch, "Canada - Drainage Basins," Ottawa, 1985.

3. Marine Renewable Energy Technology Roadmap Steering Committee, "Charting the Course, Canada's Marine Renewable Energy Technology Roadmap," ISBN M154-56/2011E - 978-1-100-19522-3, 2011.

4. Kolekar N., Hu Z., Banerjee A., Du X., "Hydrodynamic Design and Optimization of Hydro-kinetic Turbines using a Robust Design Method," Proceedings of the 1st Marine Energy Technology Symposium, April 10-11, 2013, Washington, D.C.

5. Lazauskas L., Kirke B. K., "Modeling Passive Variable Pitch Cross Flow Hydrokinetic Turbines to Maximize Performance and Smooth Operation," Elsevier Renewable Energy 45, 2012.

6. Jonkman J., Musial W., "Hydrodynamic Optimization Method and Design Code for Stall-Regulated Hydrokinetic Turbine Rotors," National Renewable Energy Laboratory, ASME 28th International Conference on Ocean, Offshore, and Arctic Engineering, Honolulu, Hawaii, May 31–June 5, 2009.

7. Hobson, M., "A Renewable Energy Success Story Above the Arctic Circle," Energywire E & E Publishing, October 20, 2015.

8. Cherniak D., Dufresne V., Keyte L., Mallet A., Schott S., "Report on the State of Alternative Energy in the Arctic," School of Public Policy and Administration, Carleton University, Ottawa, September 21, 2015.

9. Mosallat F., "Specialized Power-Electronic Apparatus for Harnessing Electrical Power from Kinetic Hydropower Plants," PhD Thesis, University of Manitoba, Winnipeg, MB, 2012.

10. Birjandi A., Woods J., Bibeau E., “Investigation of Macro-Turbulent Flow Structures Interaction with a Vertical Hydrokinetic River Turbine,” Elsevier Renewable Energy 48 p. 183-192, 2012.

11. Betz A., “Das Maximum der Theoretisch Möglichen Ausnutzung des Windes Durch Windmotoren,” Gesamte Turbinenwesen, 1920.

12. Vennell R., “Exceeding the Betz Limit with Tidal Turbines,” Elsevier Renewable Energy 55, p. 277 – 185, 2013.

13. Birjandi A., “Effect of Flow and Fluid Structures on the Performance of Vertical River Hydrokinetic Turbines,” PhD Thesis, University of Manitoba, Winnipeg, MB, 2012.

14. Ferrer E., Willden R., “Blade–Wake Interactions in Cross-Flow Turbines,” Elsevier International Journal of Marine Energy 11, 2015.

15. Birjandi A.H., Chatoorgoon V. and Bibeau E.L. (2015), “Marine Kinetic Turbine Operation in the Wake Zone,” Ocean Engineering, vol. 97**,** 15, p. 145-155.

16. Stallard T., Collings R., Feng T., Whelan J., “Interactions Between Tidal Turbine Wakes: Experimental Study of a Group of Three Bladed Rotors,” Philosophical Transactions of the Royal Society A 371: 20120159 October 2015.

17. Mathieu J., Scott J., An introduction to Turbulent Flow, Cambridge University Press, The Edinburgh Building, Cambridge CB2 2U, UK, 2000.

18. Canadian Hydraulics Centre National Research Council of Canada, “Assessment of Canada’s Hydrokinetic Power Potential,” Natural Resources Canada Canmet ENERGY- Ottawa 580 Booth Street Ottawa, ON, Canada, K1A 0E4, 2010.

19. U.S. Energy Information Administration (EIA), under the direction of John J. Conti, “Annual Energy Outlook 2013,” Office of Communications, EI-40 Forrestal Building, Room 1E-210 1000 Independence Avenue, Washington, DC 20585, 2013.

20. Poste J., “Open Hydro: Bay of Fundy,” Presentation ICOE 2014, Halifax, Nova Scotia, 2014.

21. National Energy Board, “Canada’s Energy Future 2016 Energy Supply and Demand Projections to 2040”, Cat. No. NE2-12/2025E-PDF ISSN 2292-1710, 2016.

22. Jenkinson W., “Canada's Hydrokinetic Power Potential,” Presentation for Marine Renewables Canada, Ottawa, ON, 2013.

23. Khan M. J., Bhuyan G., Iqbal M. T., Quaicoe J. E., “Hydrokinetic Energy Conversion Systems and Assessment of Horizontal and Vertical-Axis Turbines for River and Tidal Applications: A Technology Status Review,” Elsevier Applied Energy 86, p. 1823 – 1835, 2009.

24. Ginter V., “Robust Gain Scheduled Control of a Hydrokinetic Turbine,” Master’s Thesis, University of Calgary, Calgary AB, 2009.

25. Gorban, A.N., Gorolov A. M., Silantyev V. M., “Limits of the Turbine Efficiency for Free Fluid Flow,” Energy Resource Technology 123(4), 311-317, Aug 14, 2001, doi:10.1115/1.1414137.

26. Jacob, A., “Tidal Turbine Features Composite Rotors,” Materials Today Journal, Elsevier, Amsterdam, 2008.

27. Frost C., Evans P., Morris C., Mason-Jones A., O’Doherty T., O’Doherty D., "The Effect of Axial Flow Misalignment on Tidal Turbine Performance," Cardiff Marine Energy Research Group, School of Engineering, Cardiff University, Cardiff, UK.

28. Gaden D., “An Investigation of River Kinetic Turbines: Performance Enhancements, Turbine Modelling Techniques and an Assessment of Turbulence Models,” Master’s Thesis, University of Manitoba, Winnipeg, MB, 2007.

29. Manitoba Hydro-Electric Board, “Technical Requirements for Connecting Distributed Resources to The Manitoba Hydro Distribution System,” DRG2003, Revision 2.1, 2011.

30. NERC, “Special Assessment Interconnection Requirements for Variable Generation,” IV GTF Task Force 1-3 Chair Richard Piwko, Lead Authors for Report Chapters Abraham Ellis, Reigh Walling, Bob Zavadil, David Jacobson, Richard Piwko, 2012.

31. Canadian Electricity Association, “Vision 2050 - The Future of Canada's Electricity System,” Canadian Electricity Association (CEA) April 2014 Edition.

32. Slemon G. R., Straughen A., “Electric Machines,” Addison-Wesley Publishing Company, Reading, Massachusetts, 1980.

33. Open Hydro Group Limited, “US Patent US 20100026002 A1 Hydroelectric Turbine,” PCT/EP2007/006258, 2006.

34. Wikander O., “Handbook of Ancient Water Technology, Technology and Change in History 2,” Leiden: Brill, pp. 371–400, ISBN 90-04-11123-9, 2007.

35. Wisner R., Bolinger M., US Department of Energy, “2012 Wind Technologies Market Report,” U.S. Department of Energy Office of Scientific and Technical Information P.O. Box 62 Oak Ridge, TN 37831-0062, 2012.

36. Environment Canada, “Canadian Wind Atlas,” Gatineau, QC: Environment Canada, 2003.

37. Adegas F. D., Villar Alé J. A., dos Reis F. S., da Silva Simioni G. C., Tonkoski R., “Maximum Power Point Tracker for Small Wind Turbines Including Harmonic Mitigation,” Proceedings European Wind Energy Conference & Exhibition, 2006.

38. Neary V. S., “Reference Inflow Characterization for River Resource Reference Model: Reference Model 2 (RM2),” Oak Ridge National Laboratory Oak Ridge, Tennessee 37831-6283, Ut Battelle, LLC for the U.S. Department of Energy under contract DE-AC05-00OR22725, 2011.

39. St. George S., “Streamflow in the Winnipeg River Basin, Canada: Trends, Extremes and Climate Linkages,” Elsevier Journal of Hydrology (2007) 332, 396– 411, 2007.

40. Lucas-Picher P., Arora V. K., Caya D., Laprise R., “Implementation of a Large-Scale Variable Velocity River Flow Routing Algorithm in the Canadian Regional Climate Model (CRCM),” Canadian Meteorological and Oceanographic Society, Atmosphere-Ocean 41, pp. 139–153, 2003.

41. Henderson F. M., Open Channel Flow, McMillan Publishing Company, New York, 1966.

42. Ruopp A., Ruprecht A., Riedelbauch S., Arnaud G., Hamad I., “Development of a Hydro Kinetic River Turbine with Simulation and Operational Measurement Results in Comparison,” 27th IAHR Symposium on Hydraulic Machinery and Systems (IAHR 2014), IOP Conf. Series: Earth and Environmental Science 22 (2014) 062002.

43. Neary A.S., “Field Measurements at River and Tidal Current Sites for Hydrokinetic Energy Development: Best Practices Manual,” Oak Ridge National Laboratory, Oak Ridge Tennessee 37831-6283 for the US Department of Energy under contract DE-AC05-00OR22725.

44. Grabbe M., Yuen K., Goude A., Lalander E., Leijon M., "Design of an Experimental Setup for Hydro-Kinetic Energy Conversion," The International Journal on Hydropower & Dams, 2009, Vol. 16, Issue 5.

45. Qu J., “Pointe du Bois Powerhouse Forebay CFD Model,” report prepared for Manitoba Hydro by KGS Group, 2014.

46. Previsic M. and Bedard R., “System Level Design, Performance, Cost and Economic Assessment – Alaska River In-Stream Power Plants,” EPRI RP 006 Alaska, 2008.

47. Marine Current Turbines, Presentation International Conference on Ocean Energy 2014, Proceedings ICOE, 2014.

48. Daly S. F., “Ice Formation and Ice Cover Hydraulics,” 2004 Cold Regions Workshop, ERC/CRREL US Army Corps of Engineers Engineer Research and Development Center, 2004.

49. Lake of the Woods Control Board, “Historical and Present Water Level Data,” Lake of the Woods Control Board, Block E1, 373 Sussex Dr. Ottawa ON K1A 0H3.

50. Taylor, G. I., “Spectrum of Turbulence,” Proceedings of the Royal Society, London UK, 164, 10.1098/rspa.1938.0032, 1938.

51. O'Neill P., Nicolades D., Honnery D., Soria J., “Autocorrelation Functions and the Determination of Integral Length with Reference to Experimental and Numerical Data,” 15th Australasian Fluid Mechanics Conference, The University of Sydney, Sydney, Australia, p.13-17, December 2004.

52. Johnson J. B., Pride D. J., “River, Tidal, and Ocean Current Hydrokinetic Energy Technologies: Status and Future Opportunities in Alaska,” Alaska Center for Energy and Power Report, 2010.

53. Walsh C., Fochesatto J., Toniolo H., “The Importance of Flow and Turbulence Characteristics for Hydrokinetic Energy Development on the Tanana River at Nenana, Alaska,” Journal of Power and Energy, Vol. 226 Issue A2 p. 283 – 299, 2012.

54. Kaimal J., Finnigan, J., “Atmospheric Boundary Layer Flows: Their Structure and Measurement,” Oxford University Press, New York, p. 289, 1994.

55. Ives J., “Ocean Energy in Ireland: Challenges and Opportunities,” Presentation by Open Hydro at Conference by Institute of International and European Affairs, The Institute of International and European Affairs, 8 North Great Georges Street, Dublin 1, Ireland, 2014.

56. US Army Corps of Engineers, “Ice Engineering,” EM-1110-2-1621, U.S. Army Corps of Engineers Washington, DC 20314-1000, 2002.

57. Schmaltz J. (image), MRIS Image St. Lawrence River, NASA Earth Observatory, EOS Project Science Office, Nasa Goddard Flight Center, Mail Code 130, Greenbelt, MD 20771, USA, 2014.

58. Bear C., Wessener C., “Vertical Axis Hydrokinetic Turbines: Practical and Operating Experience at Pointe du Bois, Manitoba,” New Energy Corporation Inc., Calgary, Alberta, Canada, 2011

59. Bastedo, J., “The Canadian Encyclopedia”, Toronto: Historica Canada, 2006. Web. 8 Feb 2006.

60. Weber-Shirk M., “Open Channel Flow,” School of Civil and Environmental Engineering, Cornell University, 2014.

61. Blake A., “Handbook of Mechanics, Materials, and Structures,” John Wiley & Sons Inc., US and Canada, 1985.

62. Nova Scotia Department of Energy, “Guidelines for Permitting of a Pre-Commercial Demonstration Phase for Offshore Renewable Energy Devices

(Marine Renewables) in Nova Scotia," Farwell S., Acting Manager Regulatory Innovation Strategic Policy, Planning and Services Nova Scotia Department of Energy, 2007.

63. Kassam S., "In-Situ Testing of a Darrieus Hydro Kinetic Turbine in Cold Climates," Master's Thesis, University of Manitoba, Winnipeg, MB, 2009.

64. Bibeau E., Kassam S., Woods J., Gole, A., Mosallat F., Vautier P., Molinski T., "Design of In-Situ River Kinetic Turbines Test Facility in Cold Weather," Canadian Engineering Design Network Conference, University of Manitoba, Winnipeg, MB, 2007.

65. Faure T., Pratte B., Swan D., "Darrieus Hydraulic Turbine Model and Field Experiments," ASME Fluids Engineering Division Conference FED Proceedings, Anaheim, CA, USA, vol. 43, 1986.

66. Birjandi A., Bibeau E., "Improvement of Acoustic Doppler Velocimetry in Bubbly Flow Measurements as Applied to River Characterization for Kinetic Turbines," International Journal of Multiphase Flow, 2011: 37(8).